NATIONAL HURRICANE RESEARCH PROJECT

PART II

REPORT NO. 50

Proceedings of the Second Technical Conference on Hurricanes

June 27-30, 1961 Miami Beach, Fla.

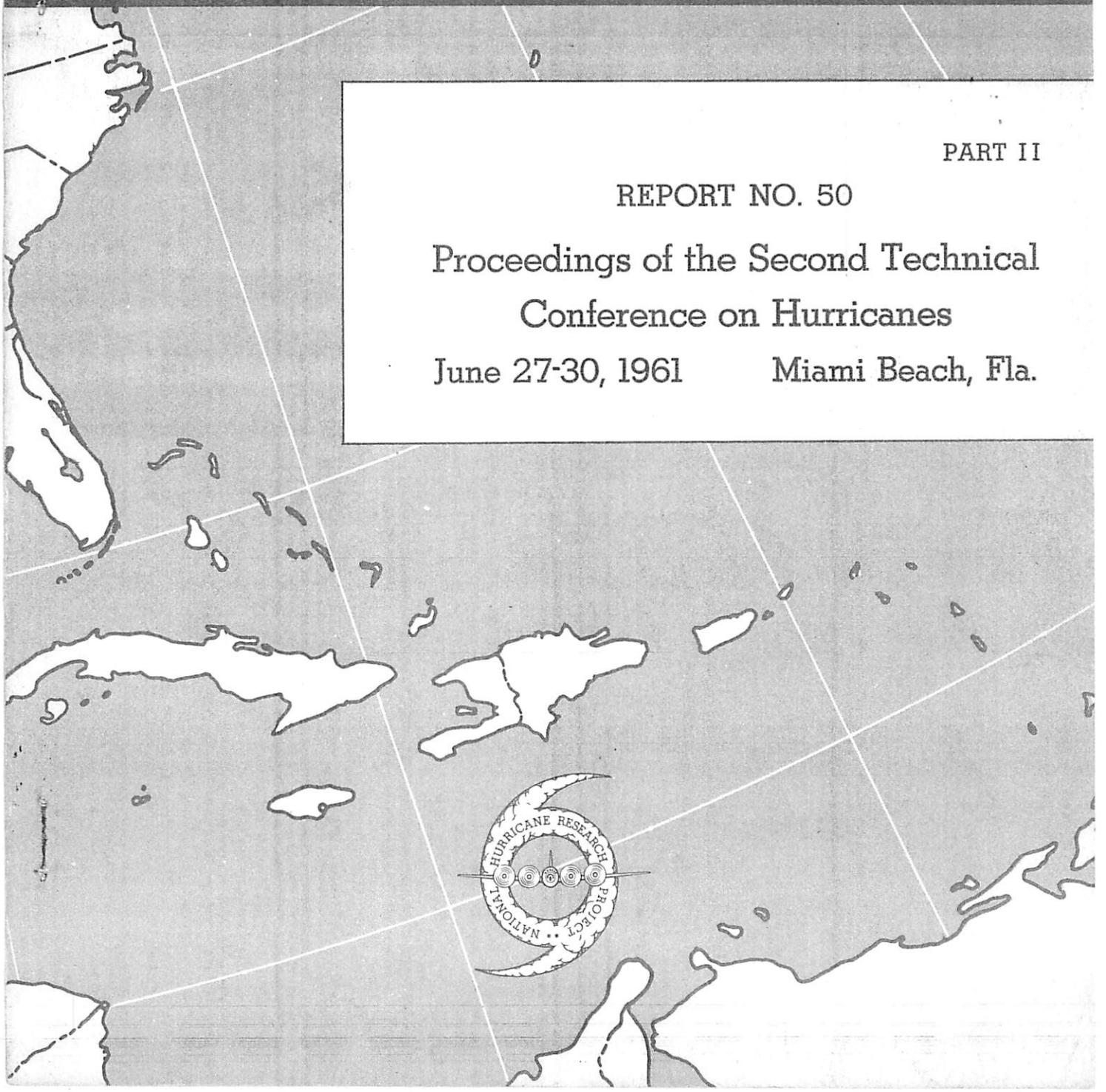

U. S. DEPARTMENT OF COMMERCE
Luther H. Hodges, Secretary
WEATHER BUREAU
F. W. Reichelderfer, Chief

NATIONAL HURRICANE RESEARCH PROJECT

REPORT NO. 50

— PART II —

Proceedings of the Second Technical Conference on Hurricanes

June 27-30, 1961 Miami Beach, Fla.

Under the Joint Sponsorship of the American Meteorological Society
and the Greater Miami Branch, AMS

Edited by
M. A. Alaka
National Hurricane Research Project, Miami, Fla.

Washington, D. C.
March 1962

NATIONAL HURRICANE RESEARCH PROJECT REPORTS

Reports by Weather Bureau units, contractors, and cooperators working on the hurricane problem are preprinted in this series to facilitate immediate distribution of the information among the workers and other interested units. As this limited reproduction and distribution in this form do not constitute formal scientific publication, reference to a paper in the series should identify it as a preprinted report.

No. 1. Objectives and basic design of the NHRP. March 1956.
No. 2. Numerical weather prediction of hurricane motion. July 1956.
Supplement: Error analysis of prognostic 500-mb. maps made for numerical weather prediction of hurricane motion. March 1957.
No. 3. Rainfall associated with hurricanes. July 1956.
No. 4. Some problems involved in the study of storm surges. December 1956.
No. 5. Survey of meteorological factors pertinent to reduction of loss of life and property in hurricane situations. March 1957.
No. 6. A mean atmosphere for the West Indies area. May 1957.
No. 7. An index of tide gages and tide gage records for the Atlantic and Gulf coasts of the United States. May 1957.
No. 8. Part I. Hurricanes and the sea surface temperature field. Part II. The exchange of energy between the sea and the atmosphere in relation to hurricane behavior. June 1957.
No. 9. Seasonal variations in the frequency of North Atlantic tropical cyclones related to the general circulation. July 1957.
No. 10. Estimating central pressure of tropical cyclones from aircraft data. August 1957.
No. 11. Instrumentation of National Hurricane Research Project aircraft. August 1957.
No. 12. Studies of hurricane spiral bands as observed on radar. September 1957.
No. 13. Mean soundings for the hurricane eye. September 1957.
No. 14. On the maximum intensity of hurricanes. December 1957.
No. 15. The three-dimensional wind structure around a tropical cyclone. January 1958.
No. 16. Modification of hurricanes through cloud seeding. May 1958.
No. 17. Analysis of tropical storm Frieda 1957. A preliminary report. June 1958.
No. 18. The use of mean layer winds as a hurricane steering mechanism. June 1958.
No. 19. Further examination of the balance of angular momentum in the mature hurricane. July 1958.
No. 20. On the energetics of the mature hurricane and other rotating wind systems. July 1958.
No. 21. Formation of tropical storms related to anomalies of the long-period mean circulation. September 1958.
No. 22. On production of kinetic energy from condensation heating. October 1958.
No. 23. Hurricane Audrey storm tide. October 1958.
No. 24. Details of circulation in the high energy core of hurricane Carrie. November 1958.
No. 25. Distribution of surface friction in hurricanes. November 1958.
No. 26. A note on the origin of hurricane radar spiral bands and the echoes which form them. February 1959.
No. 27. Proceedings of the Board of Review and Conference on Research Progress. March 1959.
No. 28. A model hurricane plan for a coastal community. March 1959.
No. 29. Exchange of heat, moisture, and momentum between hurricane Ella (1958) and its environment. April 1959.
No. 30. Mean soundings for the Gulf of Mexico area. April 1959.
No. 31. On the dynamics and energy transformations in steady-state hurricanes. August 1959.
No. 32. An interim hurricane storm surge forecasting guide. August 1959.
No. 33. Meteorological considerations pertinent to standard project hurricane, Atlantic and Gulf coasts of the United States. November 1959.
No. 34. Filling and intensity changes in hurricanes over land. November 1959.
No. 35. Wind and pressure fields in the stratosphere over the West Indies region in August 1958. December 1959.
No. 36. Climatological aspects of intensity of typhoons. February 1960.
No. 37. Unrest in the upper stratosphere over the Caribbean Sea during January 1960. April 1960.
No. 38. On quantitative precipitation forecasting. August 1960.
No. 39. Surface winds near the center of hurricanes (and other cyclones). September 1960.
No. 40. On initiation of tropical depressions and convection in a conditionally unstable atmosphere. October 1960.
No. 41. On the heat balance of the troposphere and water body of the Caribbean Sea. December 1960.
No. 42. Climatology of 24-hour North Atlantic tropical cyclone movements. January 1961.
No. 43. Prediction of movements and surface pressures of typhoon centers in the Far East by statistical methods. May 1961.
No. 44. Marked changes in the characteristics of the eye of intense typhoons between the deepening and filling states. May 1961.
No. 45. The occurrence of anomalous winds and their significance. June 1961.
No. 46. Some aspects of hurricane Daisy, 1958. July 1961.
No. 47. Concerning the mechanics and thermodynamics of the inflow layer of the mature hurricane. September 1961.
No. 48. On the structure of hurricane Daisy (1958). October 1961.
No. 49. Some properties of hurricane wind fields as deduced from trajectories. November 1961.

USCOMM-WB-DC

TABLE OF CONTENTS

CYCLOGENESIS - CURRENT OPERATIONAL NEEDS AND EFFORTS AND A FEW PROPOSALS FOR THE FUTURE

Arnold L. Sugg
U. S. Weather Bureau, Miami, Fla.

INTRODUCTION

The most vexing and perhaps the most urgent problem that the hurricane forecaster must deal with is the formation of the tropical cyclone. This forecast is a time consuming job and one that is not very productive. Our position is not firm and we can only improve it if, periodically, we survey our operational needs regarding cyclogenesis, take a good look at our current efforts, and then try to decide on the avenues and procedures to apply to future research. This paper will try to assess the problem from the forecaster's point of view.

Those who are or have been engaged in the business of warnings have, at times, found it most difficult to arrive at a professional decision on where and when cyclogenesis will occur. Our forecast rules for deepening and formation of extratropical storms are certainly more rewarding than those which we apply to incipient conditions in the Tropics. This, of course, is due in part to the greater amount of data in northern latitudes. What is most disturbing to many of us is the knowledge that we can forecast a 10-mb. drop in pressure in a baroclinic atmosphere, but find it most difficult in the Tropics, and the realization at the same time that this amount of change could mean the difference between a weak easterly wave and a potentially dangerous tropical storm.

To place the problem in its proper perspective, we can say bluntly that we are not doing a good enough job in forecasting hurricane formation. It is true that over the past decades there have been very few disasters, if any, that could be attributed to this deficiency. Probably the record has been good, or at least satisfactory, because there is a never-ending alert on the incipient conditions and aircraft and radar surveillance have been improved and increased. It is doubtful if there is a forecaster in the business that ever leaves a tour of duty without a very uneasy feeling about the moderate to strong easterly wave which he left, status quo. This is not to say that forecasters are floundering with this problem, but it is to say that we should be doing better and that research along these lines deserves the highest priority.

From time to time the Weather Bureau publishes various kinds of forecasting guides. One, dealing with hurricane forecasting, came off the press in 1959. In this particular one, in which the foremost hurricane forecasters were consultants and editors, there appears this statement: "The problem of determining precisely when and where a tropical storm will form in a five-day forecast period (or even in 24 hours for that matter) is of a high order of difficulty and is presently done on a very subjective basis" [1]. This statement is as true today as it was two years ago.

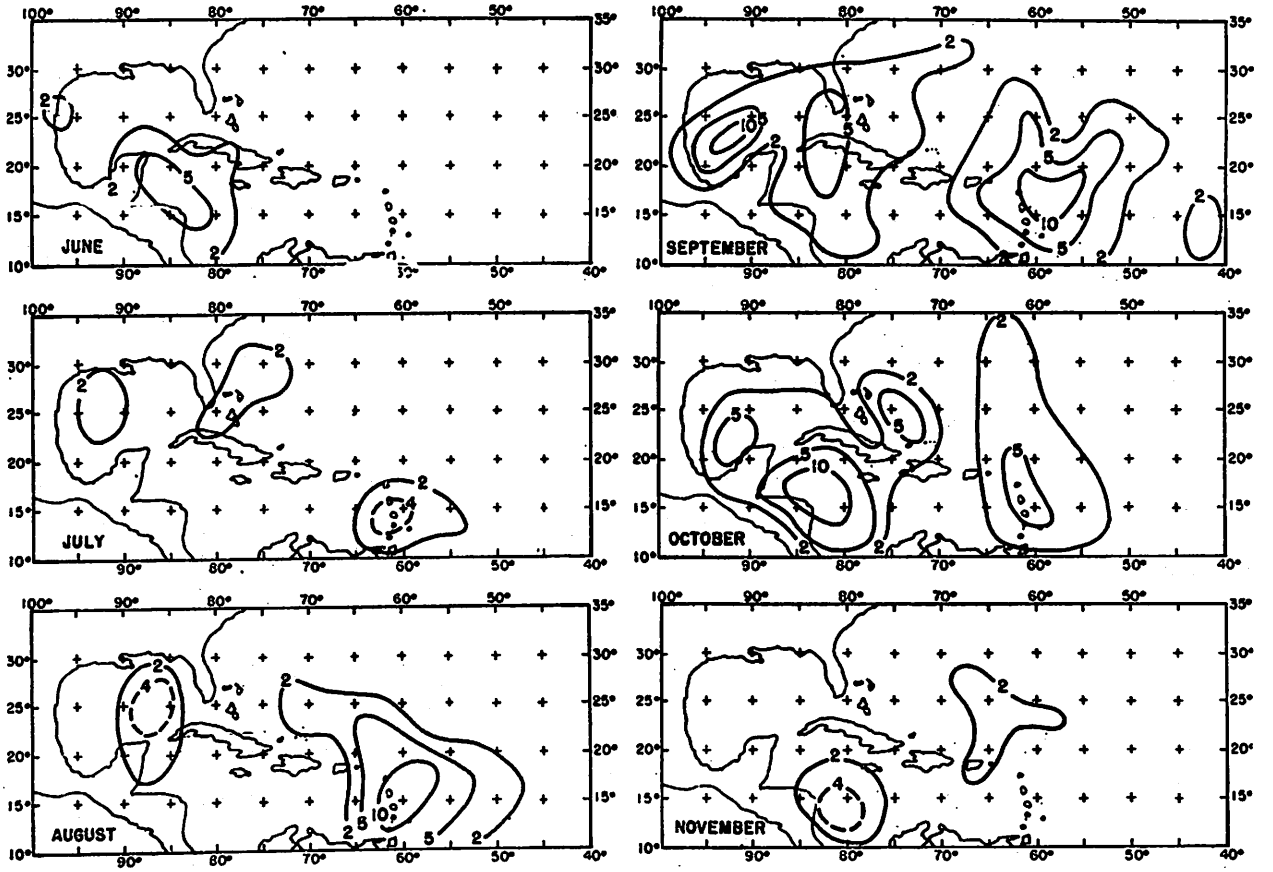

Figure 1. - Total frequency of tropical cyclones with track starting at each 5° square during the period 1887-1950. (From Colón [2].)

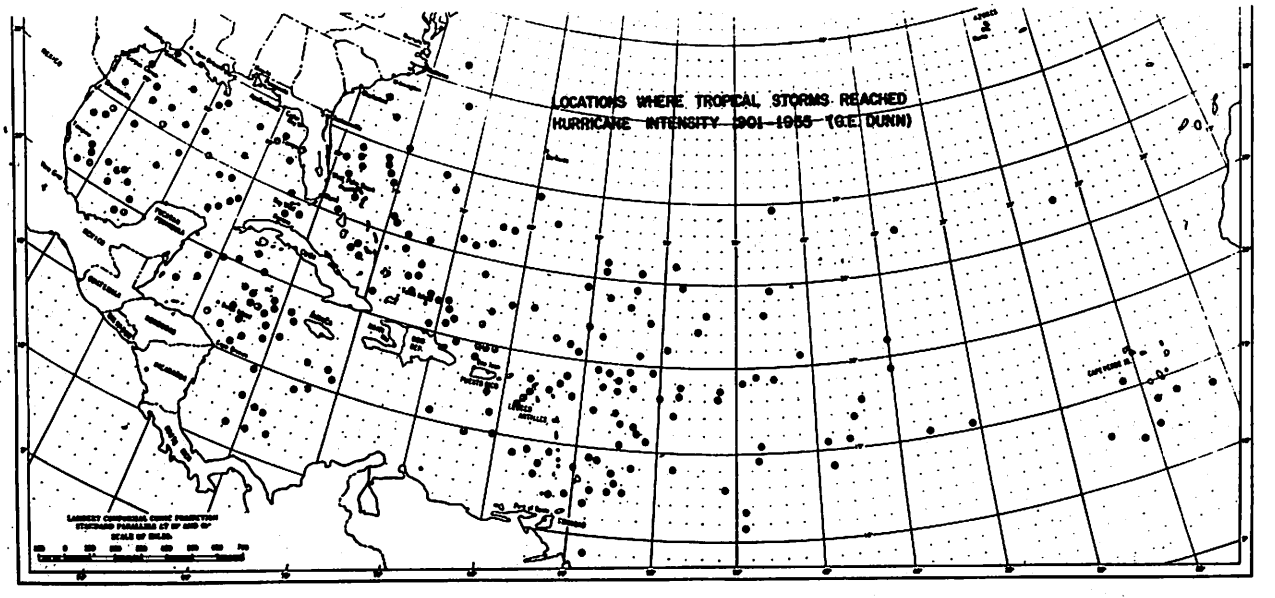

Figure 2. - Locations where tropical storms reached hurricane intensity 1901-1955. (From Dunn [3].)

OUR OPERATIONAL NEEDS

It would be very easy to be complacent and ignore our dilemma using the argument that formation takes place so far at sea that there is always sufficient time to warn people of any dangerous winds or tides, one might say that we should not be too concerned about formation but that we should apply our efforts toward better forecasts of movement after the storm has been located. The truth of the matter is that a great many of our storms form rather close to land. Here are illustrations (fig. 1 and 2)taken from papers by Colón [2] and Dunn [3]. These figures are a reminder that some of the main areas of cyclogenesis appear near the continent or near some insular group - locations which are too close for comfort for the duty forecaster.

Figure 3 depicts the tracks of the storms which formed during 1959. We note that hurricane Debra (No. 5 on the figure) formed and intensified only a short distance off the Texas coast. Comparatively speaking, one might say that this was a minor storm; yet at Dickinson, Tex., the barometer reached

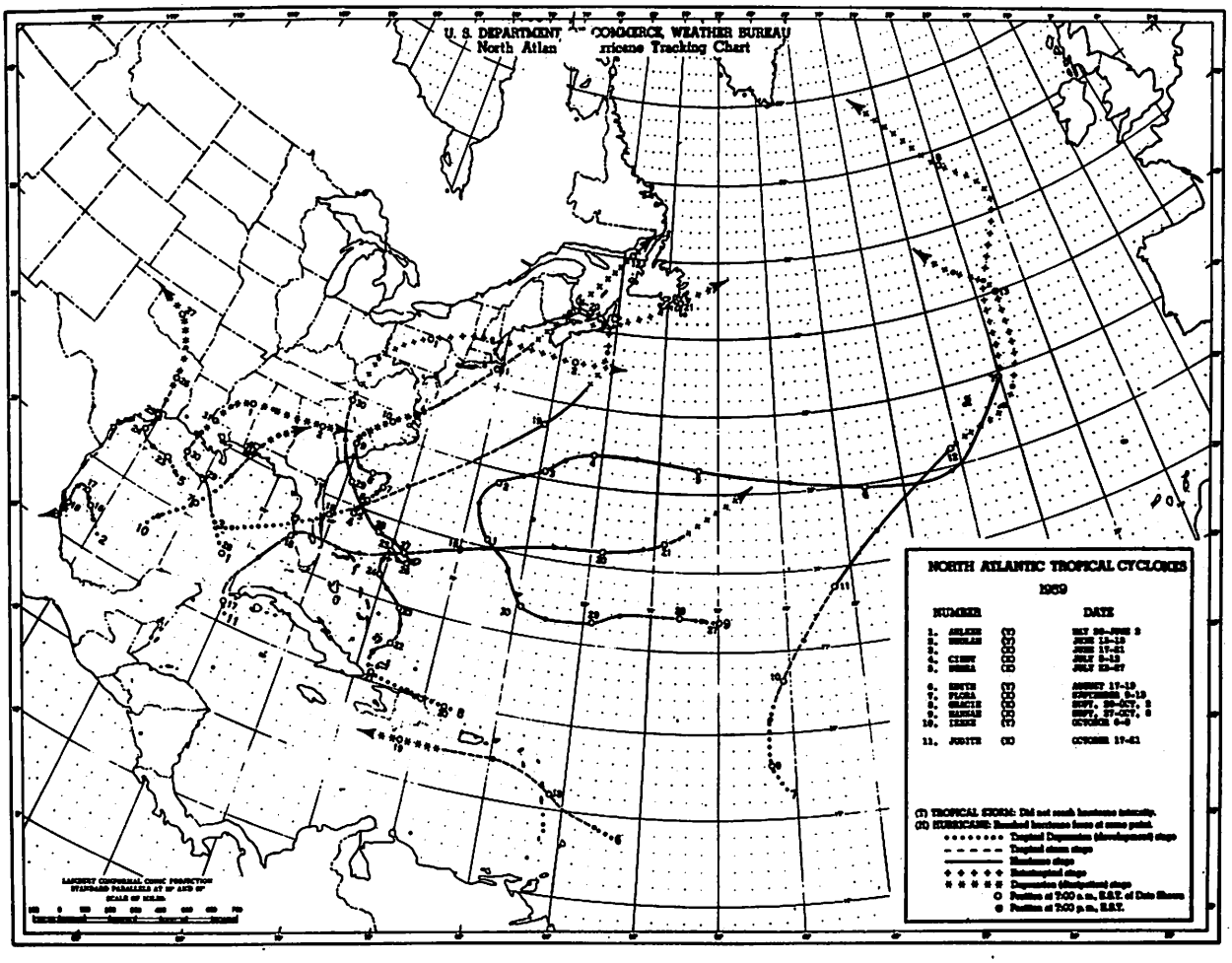

Figure 3. - Tracks of North Atlantic tropical cyclones of 1959.

29.13 in., there were wind gusts to 105 m.p.h., and rainfall totaling 13.40 in. The seriousness of such a situation is best described by a statement by Mr. Ernest Carson, MIC at our Galveston office. "Since Debra developed only a short distance off the Texas coast, which naturally limited the time period for issuance of warnings, it was noted that people and interests taking immediate action had no complaint. It was noted, however, many other people procrastinated and lost valuable time in making their preparations for protection of property."

Even if the suspicious area is far at sea, the argument (that we should not be too concerned until after the storm is formed) is weak simply because the Weather Bureau and Navy do have various marine responsibilities to military craft and to the merchant marine. Demands are increasing. Missile and satellite firings and recovery operations by the Air Force and other military and civilian agencies are bringing about more and more requests for spot forecasts throughout the marine areas. These things are mentioned to show that we do have real needs, aside from the academic interest, and that we must move ahead toward a better understanding of tropical storm formation.

Just what does the forecaster do at various stages of development of a suspicious area? Each day there is a regularly scheduled tropical weather summary which locates and briefly describes all areas of suspicion. This is the only course of action taken when it appears that there is less than a 50 percent chance for development. If the situation seems more favorable than this, but not enough to warrant naming the storm, the forecaster issues a bulletin on the existing conditions and then takes every course of action that he has available, through radar, aircraft, ships, and special land observations to determine the first possible clue to intensification. Although some reconnaissance into suspicious areas has been curtailed in recent years, we have had sufficient flights in most cases. There have been times when a huge amount of various types of data has been supplied over a period of several days prior to the development or dissipation. At other times we have barely had time to get some data, much less sufficient data, before the initial formal advisory. Most of us have relied heavily upon aircraft reconnaissance during the formative stages, and have taken the attitude that this is the best procedure to firm and direct our thinking, at least for the next 24 hours. But this is hardly enough because many times it means that we are merely reporting weather rather than forecasting. Again, this points up the need for better forecast rules on tropical cyclogenesis.

There are other reasons why we must improve the cyclogenesis forecast. One conclusion which seems fairly obvious, although it might not necessarily be true, is that we should expect improvements in forecast movement, decay, rainfall amounts, etc., if and when we solve the issue being considered here.

OPERATIONAL PROBLEMS

It is probably true that very few formations have actually and scientifically been forecast. In every given situation and in every group one will find the usual variety of conclusions based upon the usual variety of reasons. Our present knowledge requires that operations lean toward the conservative side. This must be true, otherwise we would wind up most hurricane seasons with a number of named easterly waves. This simply means that the inadequacy

of our forecast rules forces us into a waiting game of calculated risk. We would like to be able to eliminate this risk with good solid reasons, rather than wait until conditions worsen to the point where the observational technique is no longer tenable.

The next problem which should be mentioned is always present although really not difficult after the decision has been made that a storm is developing. Our machinery for finding and tracking storms and every facet of operations which goes into the forecast and the dissemination of the warning are not in complete operation for the five months or so which is normally designated the hurricane season. Planes of the Air Force, Navy, and Weather Bureau are on various degrees of Alertness and this involves a great number of men at various locations. Extra teletypewriter circuits need to be placed into operation while work schedules are revised to take care of the additional work load. Special reports from ships are requested and accelerated observational procedures are activated throughout the West Indies, Central America, and the States. Here, then, are some time-consuming chores that could be done in a more leisurely manner if we were able to determine that there would be an advisory 3, 6, or 12 hours hence.

Forecasting for the plan of the day poses another operational problem. This plan is a joint Weather Bureau, Air Force, Navy plan which outlines the area to be reconnoitered by aircraft on the following day. If these suspicious areas cannot be forecast with some degree of accuracy, then many valuable and expensive flying hours are lost searching for the unknown. The better our initial effort, the better the planes can be directed to coordinates with greater confidence and the time that will be saved in search can be used to meet specific data requirements. Any improvement in the forecast will automatically lead to smoother operations which will in turn relieve the forecaster of some duties which time could presumably be used to improve the warning.

Here, as in other areas of research and operations, we have the difficulty of securing data. This seems to be an age-old problem and one that can never improve materially unless the observation and communication systems are overhauled. We have too many dual circuits with a variety of traffic with different priorities. Some bottlenecks are the result of air, land, and sea surface information of a variety of kinds, in a variety of codes, arriving at one place or another over different communication channels from various foreign countries. There are, of course, other restrictions which depend upon the priority. Some of these are necessary so that normal commercial traffic can continue. In recent years, some of our requests have been challenged by the authorities directing missile and satellite operations. Undoubtedly, the fact that our business is seasonal and that the tempo increases greatly with the first clue to cyclogenesis, contributes to compounding a knotty problem.

So far, it might seem that the remarks here are anything but complimentary for the hurricane warning service. This was not intended; it is intended that these general remarks describe some of our activities prior to, during, and immediately after tropical storm formation.

CURRENT OPERATIONAL TECHNIQUES

Just what is being done to improve forecasting cyclogenesis? The following list briefly describes some of the work on cyclogenesis which is currently being tested and checked at the National Hurricane Center. Most of this is done on a daily basis with the results available to the forecaster during the daily map discussion. Again, this is a joint effort with the military, the National Hurricane Research Project, and the operations unit of the Weather Bureau. The objective here is short range forecasting; that is, determining if an incipient situation will intensify in 12 to 24 hours.

1. 24-hr. pressure changes are plotted. The importance of this was first pointed out by Dunn [4]. He later indicated that these changes should be watched very closely in the vicinity of an easterly wave, since about 80 percent of our hurricanes originate in this particular synoptic feature.

2. Nephanalysis. This is used to delineate areas of above normal cloudiness and serves to direct our attention to specific danger areas.

3. Our low-level isotach analysis continues in somewhat of an experimental stage. Here we try to pick up areas where low-level convergence is occurring. This is also a subjective attempt to define the vorticity fields.

4. Using sea surface temperatures, computations are made on heat flux.

5. An attempt is made to classify the easterly wave as stable or unstable. This is done in a very subjective way using the weather and clouds on either side of the wave.

6. The strength and trend of the zonal westerlies are noted each day. While Riehl [5] never intended that this type of analysis would pin-point the formation, it is regarded as most important by practicing forecasters today.

7. Thickness charts were analyzed during the last two seasons. It is too early to report on this technique from the practical stand point, however, our theory would imply that this analysis will be rewarding.

8. Recently, Riehl has been doing computational work on the divergence field in the vicinity of the high-level anticyclone and on the mean radial inflow in the very low levels. This latter computation makes use of ship observations.

9. An attempt is made to follow all high-level vortices.

10. Current charts are checked against composites constructed by Miller [6]. These composites are for selected situations. They are constructed at the 200-mb. level and represent times up to 2 days prior to maximum intensity.

11. Current 700-mb. height anomalies are checked against Ballenzweig's [7] height anomaly charts.

12. Using the IBM computer, Colón has been doing some work on high and

low level divergence and convergence patterns. The Bellamy triangle method is utilized. This has helped some in routine air mass shower forecasts and, data permitting, has promise for the problem of cyclogenesis.

13. Landers has been working with the 500-mb. charts. Using streamlines, he subjectively determines and follows, from day to day, centers of action, the depth of the easterlies and westerlies, and the vorticity maxima.

14. Rosenthal is working on numerical prediction. The objective here is a model which can be used to forecast the field of motion in the Tropics. A usable prognostic chart would certainly be an important step in solving the formation problem.

15. Alaka is doing work on dynamic instability above the incipient area.

16. The forecaster places a great deal of faith in climatology especially where data are sparse or where other methods appear weak or conflicting. There seems to be no question that climatology will play an even more important role in the future.

17. Various check sheets are used. These contain practically all of the above-mentioned techniques in one form or another, weighted in a number of ways. So far, this has not been too successful. It seems that there are too many results too close to the 50 percent probability figure, which is usually known prior to completing the check sheet.

It is not my purpose here to evaluate the above analyses and techniques. But, considering the number of items listed above, a large part of our manpower is diverted to this effort since there seems to be a suspicious area every day of the hurricane season. Our data indicate that more than 50 percent of our days are non-storm days, and this means that most of our time is spent trying to locate where and when the next storm will occur. During the 1960 season, we had the first of what seemed to be an organized system in our map discussion. This is a start toward streamlining our procedures; perhaps it can be improved.

PROPOSALS

There have been many theories of tropical storm cyclogenesis. None is considered completely satisfactory, although all have contributed something, directly or otherwise. Riehl [8] has done more in recent years to evaluate the various aspects of the theories and, of course, has added his own concepts. Forecasters feel that his basic ideas are firm and that we need to move ahead along the lines of his theory.

It is obvious that tropical storm formation requires a unique combination of parameters. It has often been stated that the question may not be why we have hurricanes but why we have so few of them. Since there may be various factors involved and the meshing of these is so intricate, there is some doubt that we may ever be able to evaluate the parameters objectively. At least this is a reasonable conclusion if one considers the amount of data at hand. This attitude then leads to the need for a statistical method utilizing multiple regression equations as in the Veigas-Miller [9] technique for motion

forecasting. One would then start with the first indication of a surface disturbance, then search for predictors, surface and aloft, which would make a significant contribution to the deepening process.

Once more data are available, there is no reason why a rather simple methodical approach cannot be applied. In general terms, this may take on the form of the determination of the mechanism for the well organized ascent of the air which is necessary to release latent heat. Secondly, the mean radial inflow in the lower levels must be found. Thirdly, we should assign some measure of strength to the existing surface perturbation. We can do this objectively. Computations can be made on the divergence field at high levels, the mean radial inflow near the gradient level, and, through a vorticity analysis, the strength of the system can be noted. It would seem that a vorticity analysis would have some advantage over the streamline analysis. In the past we have probably concerned ourselves too much with the various singular points in the streamline pattern and overlooked, at least to some extent, the speed field. More frequently than not, the latter represents a greater vorticity concentration than the singular point. The importance of the speed maxima is noted in tornado and precipitation forecasting. The analyses and forecast positions of the high and low level jet stream maxima are current operating procedures in severe weather forecasting. There is no reason why a similar technique cannot be utilized in the tropical atmosphere. There is every reason to believe that the meso-low so frequently observed in the homogeneous air mass in tornado situations will be observed during the initial stages of the tropical storm and that the causes for this depression in the pressure pattern are the same in both cases.

Perhaps the above is too simple and we shall find that the whole basic theory must be improved. Perhaps there is a missing link, although it is more likely that current data deficiencies prevent any breakthrough to a logical operating procedure. There is every reason to believe that we will have sufficient data in the next few years. We have recently seen a highly successful Marine Automatic Meteorological Observation Station (MAMOS). It is my understanding that there will be three such stations during the coming season. Considering what is at stake here and the amount of money being spent elsewhere around the world, we should urge that this number of automatic stations be doubled each year during the next four or five years. More observations will mean better research and definitely better forecasts for Latin America. The latter would seem to be a cheap and good way to establish goodwill in that community.

Let us proceed one step further and collect our MAMOS into a close network over a well-known spawning area such as the northwestern Caribbean Sea. Apparently these stations offer no particular hazard to marine navigation, not even if we place them 60 n.mi. apart. With adjacent land reports we would then be able to compute two of our unknowns - the low level inflow and the vorticity field. We would need frequent flights of just a few aircraft operating at high levels and a WSR-57 radar on an island in the center of the network. Small precipitation area winds (SPAWINDS) computed from the radar along with the MAMOS net and the flight data would produce the amount of data necessary for the research. The quality of the forecasts and the fruits of research would depend upon the density of the network up to a certain point, however, at

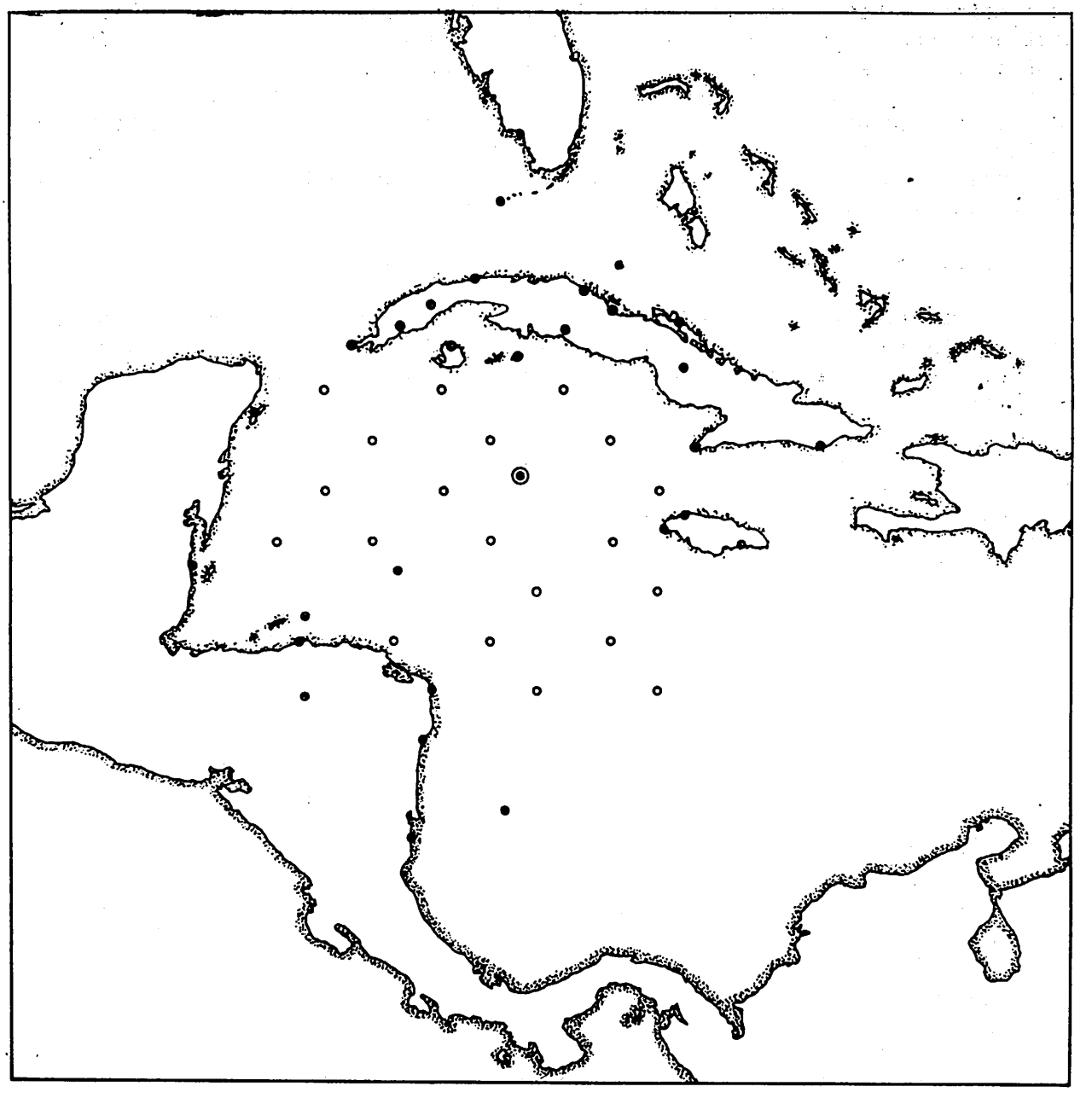

Figure 4. - Optimum MAMOS grid over the Northwestern Caribbean.

some place along the line the law of diminishing returns would take over. After the first storm, it would seem that a decision could be made on the optimum density - one that does the job and is economically feasible.

Figure 4 represents what is initially thought to be an optimum grid. Twenty automatic stations plus existing land stations are indicated in a cyclogenetic area.

There is a remote possibility that an economical network does not exist. However, this seems very unlikely in view of the advancements being made in

automation. Instrument specialists believe that very shortly our automatic stations will be operated without a power source at the installation. The station would be activated by energy from a remote location, such as a radar beam. If one considers installation on buoys, ships, aircraft and free balloons, along with land and airborne radar, the dream of sufficient data may be coming true. It is just about a reality then, that our observational program will undergo major changes and that there will be an unlimited amount of data at all elevations and at a relatively low cost.

Summarizing these remarks, I would like to say:

1. There is a real need for an objective technique to forecast tropical storm cyclogenesis. Warnings will be better and more timely if we can erase some of the uncertainty that currently prevails, especially during near-shore developments.

2. Serious operational problems with data and communications do exist; however we seem to be coming into an era where automation and computers will eliminate most of the difficulties.

3. Most forecasters feel that researchers have, to some extent, neglected the problem of tropical cyclogenesis. It should enjoy a higher priority position and more attention. The time appears right for an accelerated research program.

REFERENCES

1. U.S.Weather Bureau, "Hurricane Forecasting," Forecasting Guide No.3, April 1959, 108 pp.
2. J.A.Colón, "A Study of Hurricane Tracks for Forecasting Purposes," Monthly Weather Review, vol.81, No.3, Mar. 1953, pp. 53-66.
3. G.E.Dunn, "Areas of Hurricane Development," Monthly Weather Review, vol.84, No.2, Feb.1956, pp. 47-51.
4. G.E.Dunn, "Cyclogenesis in the Tropical Atlantic," Bulletin of the American Meteorological Society, vol. 21, 1940; pp. 215-229.
5. H. Riehl, "On the Formation of West Atlantic Hurricanes," Miscellaneous Report No.24, Dept. of Meteorology, University of Chicago, 1948, pp. 1-67.
6. B.I.Miller, "On the Maximum Intensity of Hurricanes;" Journal of Meteorology vol. 15, No.2, Apr. 1958, pp.184-195.
7. E.M.Ballenzweig, "Formation of Tropical Storms Related to Anomalies of the Long-Period Mean Circulation," National Hurricane Research Project Report, No. 21, 1958, 16 pp.
8. H. Riehl, Tropical Meteorology, McGraw-Hill Book co.,Inc.,New York, 1954, 392 pp.
9. K.Veigas and R. G. Miller, " Probabilistic Prediction of Hurricane Movements by Synoptic Climatology," Occasional Papers in Meteorology, No. 2, The Travelers Insurance Co., Hartford, Conn., 1959.

MECHANISM LEADING TO HURRICANE FORMATION

(A Condensed Version*)

H. -L. Kuo
Massachusetts Institute of Technology,
Cambridge, Mass.

1. INTRODUCTION

The formulation of a satisfactory theory on hurricane formation depends on finding the proper initial atmospheric conditions and the necessary energy supply for the atmosphere which, in accordance with the appropriate dynamic and thermodynamic equations, will lead to the development of a tropical storm. In order that such a development shall occur, the initial condtion must have the following properties: (i) It must be unstable with regard to some perturbations, in the sense that it tends to change, and (ii), the combined system of the initial state plus the perturbation must tend to evolve into a system which has the characteristics of the tropical storms.

The aim of this paper is to find such initial conditions by the application of linearized dynamic and thermodynamic equations. Because of this simplification, the verification of the theory or the model must await integration of the nonlinear equations.

2. PERTURBATION EQUATIONS

Since we are interested in the formation of the hurricane, which is rather symmetric in its fully developed stage, we shall adopt a cylindrical coordinate system (r, λ, z) and use u, v, and w to denote the corresponding velocity components. Dependence of the variables on the polar angle λ is assumed to have been eliminated by integration.

In order to find the proper initial conditions leading to hurricane formation, we assume the averaged initial state to be characterized by v_o, p_o, ρ_o, and T_o, each being a function of r and z, which satisfy the following equations

$$\frac{1}{\rho_o}\frac{\partial p_o}{\partial r} = \frac{M_o^2}{r^3} - \frac{f^2 r}{4}, \qquad \frac{\partial p_o}{\partial z} = -g\rho_o \tag{2.1}$$

$$g\frac{\partial s_o}{\partial r} \doteq \frac{1}{r^3}\frac{\partial M_o^2}{\partial z} \tag{2.2}$$

where $M_o = v_o r + \frac{1}{2} f r^2$, $s_o = \log \theta_o$, θ being the potential temperature.

---

*The complete version of this paper will be published elsewhere.

Putting $\vec{V} = \vec{v'} + v_o j$, $p/\rho = (p_o + p')/\rho_o$, $s = s_o + s'$, the linearized dynamic and thermodynamic equations are given by

$$E\,(ru) = -\,r\,\frac{\partial \pi}{\partial r} + \frac{2M_o}{r^2}\,M' - rJ_1 \tag{2.3}$$

$$E\,M' + u\,\frac{\partial M_o}{\partial r} + w\,\frac{\partial M_o}{\partial z} = -\,r\,J_2 \tag{2.4}$$

$$E\,w = -\,\frac{\partial \pi}{\partial z} + gs' - J_3 \tag{2.5}$$

$$E\,s' + u\,\frac{\partial s_o}{\partial r} + w\,\frac{\partial s_o}{\partial z} = \frac{Q}{c_p T_o} - J_4 \tag{2.6}$$

where $E = \partial/\partial t - \nu \nabla^2$, $\pi = p'/\rho_o$, and ν is the eddy coefficient of viscosity and eddy conductivity.

Introducting a Stokes stream function ψ for the meridional velocity components u and v, and a related function ω, defined by

$$\rho_o ru = -\,\frac{\partial \psi}{\partial z}, \qquad \rho_o rw = \frac{\partial \psi}{\partial r}, \qquad \omega = \psi e^{\sigma z/2} \tag{2.7}$$

where $\sigma = -\,\rho_o^{-1}\partial p_o/\partial z$, a partial differential equation in ω is obtained by eliminating M' and s' from the equations (2.3) to (2.6),

$$E^2\left(D^2\omega - \frac{\sigma^2}{4}\omega\right) + g\,\frac{\partial s_E}{\partial z}\,D_1^2\,\omega + \frac{1}{r^3}\,\frac{\partial M_o^2}{\partial r}\left(\frac{\partial^2 \omega}{\partial z^2} - \frac{\sigma^2}{4}\omega\right) - 2g\,\frac{\partial s_o}{\partial r}\,\frac{\partial^2 \omega}{\partial r \partial z} = N \tag{2.8}$$

where $D_1^2 = r\,\frac{\partial}{\partial r}\,\frac{1}{r}\,\frac{\partial}{\partial r}$, $D^2 = D_1^2 + \partial^2/\partial z^2$, and $\frac{\partial s_E}{\partial z} = \frac{\partial s_o}{\partial z} + \frac{L}{c_p T_o}\,\frac{\partial M_s}{\partial z}$ for saturated ascending motion and $\frac{\partial s_E}{\partial z} = \frac{\partial s_o}{\partial z}$ for unsaturated or descending motion, and N denotes the contribution by the asymmetric nonlinear terms and is independent of ω.

According to this equation, there are three different kinds of instability which may serve to drive the meridional circulation:

(i) unstable stratification, $\frac{\partial s_E}{\partial z} < 0$

(ii) rotational instability, $\frac{\partial M_o^2}{\partial r} < 0$

(iii) instability due to radial temperature gradient, requiring

$$\left(\frac{\partial s_o}{\partial r}\right)^2 > \frac{f^2}{g}\frac{\partial s_o}{\partial z}$$

We note that when $\partial s_o/\partial z$ is small, a small radial temperature gradient will be able to initiate a meridional circulation. However, observations show that the traveling disturbances in the Tropics, out of which tropical cyclones develop, are cold core rather than warm core systems, therefore type (iii) instability is absent at the initial stage of the development, although the radial temperature gradient may become the main driving force later. Thus if the initiation of the tropical storms can be attributed to the instability of a simple state for small perturbations, it must be due to either type (i) or type (ii) instability.

3. PERTURBATIONS PRODUCED BY UNSTABLE STRATIFICATION

When $\frac{\partial s_o}{\partial r} = 0$ and $r^{-3}\frac{\partial M_o^2}{\partial r} \equiv f_o^2 > 0$, eq. (2.8) permits solutions of the form

$$\omega = A\, e^{qt} \sin\frac{k\pi z}{h}\, r\, J_1\left(\alpha\frac{\pi r}{h}\right) \tag{3.1}$$

Substitution of (3.1) in (2.8) yields

$$q = \left\{\frac{gS\alpha^2 - f_o^2(k^2+\lambda^2)}{k^2+\lambda^2+\alpha^2}\right\}^{1/2} - \frac{\pi^2}{h^2}(\alpha^2\nu_h + k^2\nu_z) \tag{3.2}$$

where $S = -\frac{\partial s_E}{\partial z}$ and $\lambda = \sigma h/\pi$. Maximum q corresponds to $k = 1$, $\alpha \geq 1.6$, therefore the resulting motion is cumulus-scale convection. (See fig. 1 and Kuo [4].)

The effect of a stable descending region is to narrow the ascending region further [4]. Therefore simple convection theory cannot explain the hurricane formation. The limiting perturbation as explained by Haque [2] and Syōno [8] seems to be of no particular significance unless a nonlinear mechanism can be found for the intensification of this scale of motion.

However, the temperature perturbation given by the solution dictates that if an organizing mechanism is present to promote the large-scale circulation, the small-scale convections can contribute directly to the maintenance of the large-scale circulation (see fig. 2).

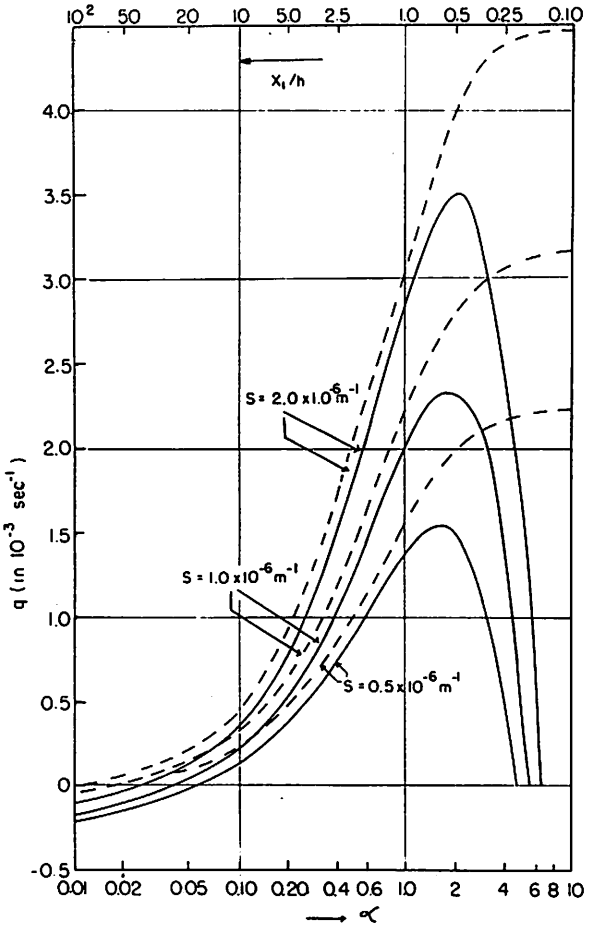

Figure 1. - The growth rate q as a function of the horizontal wave number α (below) or reduced horizontal wavelength x_1/h (top) for three different values of S. Dashed curves given by inviscid approximation, solid curves given by viscous equation for $\nu = 10^3$ m^2 sec^{-1}

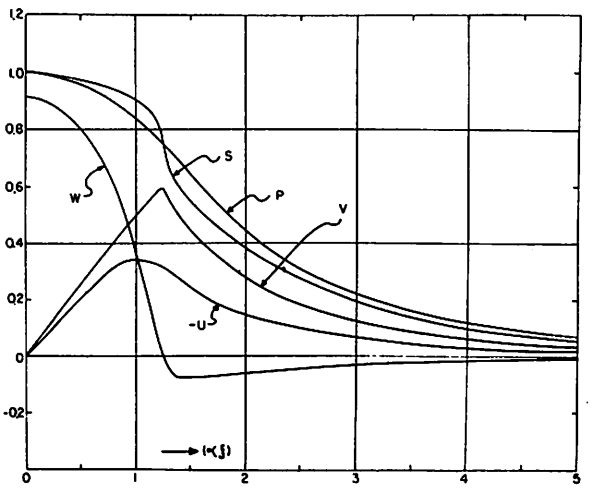

Figure 2. - Radial variations of the mid-level vertical velocity (w), the surface tangential wind (v), the surface radial wind (-u), the mid-level entropy (S) and the surface pressure (p) perturbations for a disturbance in supercritical stratification

4. PERTURBATION INITIATED BY ROTATIONAL INSTABILITY

Assuming $\frac{\partial s_o}{\partial r} = 0$, $Q = 0$,

$$s_z = \frac{\partial s_o}{\partial z} > 0, \text{ and } -r^{-3}\frac{\partial M_o^2}{\partial r} \equiv R > 0,$$

the amplification factor q of the solution (3.1) is then given by

$$q = \left\{ \frac{R(k^2 + \lambda^2) - g s_z \alpha^2}{k^2 + \lambda^2 + \alpha^2} \right\}^{1/2} - \frac{\pi^2}{h^2}(\alpha^2 \nu_h + k^2 \nu_z) \qquad (4.1a)$$

The maximum growth rate is associated with perturbations of large horizontal dimension ($\alpha \to 0$) and k = 1, and is given by

$$q_m \doteq R^{1/2} - \frac{\pi^2}{h^2}\nu_z \qquad (4.1b)$$

Thus rotational instability favors large-scale circulation. In addition, it tends to create horizontal divergence in the region of $\partial M_o^2 / \partial r < 0$, which is

important for the initiation of the proper large-scale circulation if it occurs in upper levels.

Initiation of tropical cyclones by this mechanism has been proposed by Sawyer [7] and by Kleinschmidt [3].

However, this instability cannot supply the energy for tropical storms because R is rather small, of the order of f^2. Its importance is solely to organize a large-scale flow, which will derive its energy from the heat of condensation.

5. A COMBINED INITIAL STATE FOR HURRICANE FORMATION

The following model is proposed:

(i) A deep layer of moist but unsaturated conditionally unstable tropical atmosphere ($r_m < r < r_d$), which is stable for small perturbations but possesses enormous amounts of energy which can be released by organized finite amplitude disturbances,

(ii) A warm ocean with a temperature higher than the sea level air temperature, so as to give a continuous flux of heat and water vapor from ocean to air. However, the low-level atmosphere should be unsaturated unless it has traveled a long journey over the ocean. This factor will insure the growth of large-scale circulation and prevent cumulus-scale convection from developing spontaneously. The heat and water vapor flux are apt to keep the surface temperature uniform even when horizontal pressure difference is present, a seemingly efficient state stressed by Riehl [6].

(iii) A pre-existing wave disturbance, such as an easterly wave, which has organized large-scale convergence and divergence regions and associated small vertical motion. This system is stable by itself.

(iv) The superposition of an upper-level anticyclonic circulation, with rotational instability, over the convergence region of the wave disturbance. This factor serves as a trigger action to set up a large-scale horizontal mass divergence aloft and to intensify the convergence below, and thereby helps to transform the wave motion into a symmetric motion.

While (i) and (ii) are necessary for both the development and maintenance of the tropical cyclones, (iii) and (iv) are important only for the initial stage of the development, and may possibly be replaced by other synoptic situations if they can produce the same effect.

If this model is to be tested by a numerical integration, cumulus-scale convection must be controlled so as not to give rise to unbounded amplification. Entrainment of dry air into the ascending current and strong lateral diffusion are important factors for controlling small-scale convection. A preliminary study shows that it is necessary to take a nonlinear diffusion in order to control the cumulus convection. However, it seems that nature's more effective way of controlling small-scale convection is through the exhausting of the moist air supply by precipitation and the drying of the descending branch of the circulation. This will make the small-scale convective motion

stop after the dry air from the top has reached the bottom. Further, continuous upward transports of heat and water vapor by both large- and small-scale motions in the general ascending area make the lapse rate in this region nearly equal to the saturated adiabatic, after which the sporadic cumulus-scale convection will stop growing too rapidly, whereas the large-scale motion will be maintained by the horizontal temperature gradient set up through the upward transports of heat and moisture in the general ascending region.

6. DIFFERENT STAGES OF DEVELOPMENT

In discussing the development of low pressure systems, meteorologists often like to discuss the removal of air by considering a single equation. Thus, Durst and Sutcliffe [1] and Palmén [5] discussed the radial flow by an application of the tangential equation of motion, which is written as

$$u = -\frac{\frac{\partial v}{\partial t} + w\frac{\partial v}{\partial z} - \frac{1}{\rho}\frac{\partial \tau_{\lambda z}}{\partial z}}{\zeta_a} \tag{6.1}$$

Assuming $\zeta_a \equiv f + \frac{\partial vr}{r\partial r}$ to be positive, Durst and Sutcliffe attributed the outflow aloft to the association of positive w with a negative $\partial v/\partial z$, while Palmén included all three terms in the numerator and differentiated into different stages.

However, even though these descriptions may be correct, it will be very hard to derive the radial velocity from the tangential equation of motion. Since energy is being released directly through the vertical motion, it seems much easier to deduce the changes of u from the continuity equation, by first assessing the change of the vertical motion. The radial equation of motion can also be used to assess the change of radial velocity, particularly in upper levels during the time when cyclonic circulation is gradually expanding upward. Thus we may visualize the development as going through the following stages:

(1) Beginning of upper-level anticyclone and outflow and central ascending motion.

(2) Establishment of low-level low pressure, cyclonic motion, and inflow and continuation of high-level anticyclonic motion.

(3) Cyclonic motion extends upward.

(4) Cyclonic motion occupies whole depth (or nearly so) in central region. Upper outflow driven by large centrifugal force.

REFERENCES

1. C. S. Durst and R. C. Sutcliffe, "The Importance of Vertical Motion in the Development of Tropical Revolving Storms," Quarterly Journal of the Royal Meteorological Society, vol. 64, 1938, pp. 75-84.
2. S. M. A. Haque, "The Initiation of Cyclonic Circulation in a Vertically Unstable Air Mass," Quarterly Journal of the Royal Meteorological Society, vol. 78, No. 337, July 1952, pp. 394-406.
3. E. Kleinschmidt, "Grundlagen einer Theorie der Tropischen Zyklonen", Archiv für Meteorologie, Geophysik, und Bioklimatologie, Ser. A, vol. 4, 1951, pp. 53-72.
4. H. -L. Kuo,"On Initiation of Tropical Depressions and Convection in a Conditionally Unstable Atmosphere," National Hurricane Research Project Report No. 40, 1960, 46 pp.
5. E. Palmén, "Formation and Development of Tropical Cyclones," Proceedings, Tropical Cyclone Symposium, Brisbane Dec. 10-14, 1956, (Paper No. 13), Melbourne, 1956.
6. H. Riehl, Tropical Meteorology, McGraw-Hill Book Co., Inc., New York, 1954.
7. J. S. Sawyer, "Notes on the Theory of Tropical Cyclones," Quarterly Journal of the Royal Meteorological Society, vol. 73, Nos. 315-316, Jan.-Apr. 1947, pp. 101-126.
8. S. Syōno, "On the Formation of Tropical Cyclones," Tellus, vol. 5, No. 2, May 1953, pp. 179-185.

PREDICTION OF TROPICAL CYCLOGENESIS BY STATISTICAL-SYNOPTIC METHODS

(Extended Abstract)

Keith W. Veigas
The Travelers Research Center, Inc.

INTRODUCTION

Prediction of the initial development and subsequent changes in intensity of tropical cyclones is plagued by many problems. One of the most serious of these problems is that of specifying the state of the atmosphere at a given time. This is especially true over the areas of frequent tropical cyclogenesis.

This difficulty indicates that one should systematically incorporate into the prediction not only the observational data that are available at the initial time in the immediate area of interest but also observations that are somewhat removed, either in space or time.

It also seems likely that one must attempt to increase the practical value of the predictions by obtaining a quantitative measure of the uncertainty associated with each prediction. Statistical techniques may be of considerable value in accomplishing both of these aims.

STATISTICAL PREDICTION MODELS

In developing a statistical prediction model one is faced with two major problems. First the form of the assumed predictor-predictand functional relationship must approximate the predictor-predictand relationships in the real world and secondly as Lorenz [1] has pointed out the number of predictors that can be employed is only a small subset of a large array of possible predictors.

Two techniques which assume more realistic predictor-predictand relationships have yielded results of practical value.

The first is the application of linear regression in a moving coordinate system. Examples of such prediction experiments are to be found in Veigas, Miller, and Howe [5], Ostby and Veigas [3], and Veigas [6]. Here the behavior of cyclones (motion, change in central pressure and intensity) was related to predictors measured at locations relative to the center of the cyclone.

Here if we examine for example the prediction equation for the change in central pressure of the cyclone and rewrite the assumed form of the predictor-predictand relationships in terms of predictors and predictands defined at fixed locations it is easy to see that it is assumed in the moving coordinate prediction model that the pressure change at a fixed location is a function of predictors measured at varying locations depending on the location of the

cyclone or in other words of the synoptic situation. Certainly this model is more in agreement with synoptic experience than a fixed coordinate regression prediction model where we must assume that the predictand (say pressure change) is a function of predictors measured at the same location regardless of the synoptic situation.

Another statistical technique that has been adapted to meteorological problems and is capable of capturing a type of non-linear predictor-predictand relationship is multiple discriminant analysis. This technique has been applied to the terminal forecast problem by Miller [2]. Although it grossly oversimplifies the mathematics involved, the general aim of this type of analysis can be visualized by considering the problem geometrically. For this analysis the predictand is divided into n mutually exclusive and exhaustive categories. As an example consider the subsequent temperature at a station as the predictand. The predictand might be divided into three categories corresponding to above normal, below normal, and "near" normal temperatures. For each category let us assign a color say red for above normal, blue for below normal, and green for near normal temperatures. Now visualize a three-dimensional predictor space where the first predictor is measured along the x axis, the second along the y axis, and the third along the z axis of a Cartesian coordinate system.

Now for each set of predictor-predictand observations we can locate the coordinates of the set in the predictor space and at this point we can label or "color" this point according to the associated predictand. If this is done for each set of observations in a developmental sample we can visualize an array of red, blue, and green dots in the predictor space. If the relative frequency of red, blue, and green dots per unit volume of the predictor space is equal over the predictor space, the predictors contain no predictive information. However, if each of the three sets of colored dots forms a cluster in the predictor space and if each of the three clusters is well separated from the other two, the predictors then contain considerable predictive information.

Multiple discriminant analysis has several desirable characteristics. First in cases where certain non-linear predictor-predictand relationships exist, predictions made using a multiple discriminant analysis model will yield results that are superior to those of a linear regression model. For example, consider the case where above normal values of a predictor are associated with above normal values of a predictand but near normal values of the predictor are associated with below normal values of the predictand and below normal values of the predictor are associated with near normal values of the predictand. In this case discriminant analysis predictions will be decidedly more accurate than those of linear regression.

A second desirable property of a multiple discriminant analysis model is that it yields probability distributions which are functions of the current and near past synoptic patterns. This is in agreement with experience which indicates some synoptic situations present a difficult forecast problem while for other situations the subsequent weather is rather straightforward.

Sample size limitations, dictated by availablility of climatological records, make it necessary to use only a small number of predictors in a

given prediction model. Thus the problem of selecting a small set of predictors that contain most of the predictive information of a large set of possible predictors is a critical one in developing a statistical prediction model.

In both regression analysis and discriminant analysis the concept of screening has proved rather effective in selecting a good subset of possible predictors. The screening procedure for regression was suggested by Bryan [7] and developed and programmed for the IBM-704 by Miller [8]. From an array of possible predictors the predictor which has the highest linear correlation with the predictand in question is selected. Partial correlation coefficients between the predictand and each of the remaining predictors, holding the first predictor constant, are then examined and the predictor associated with the highest coefficient is the second predictor selected. Additional predictors are then chosen in a similar manner. This procedure is repeated until a selected predictor fails to explain a significant additional percentage of the remaining variance of the predictand.

The procedure for screening of predictors for multiple discriminant analysis, Miller [2], is analagous to screening for regression. In this case the selection criterion is to select that predictor with the maximum ratio of the overall dispersion of the predictor to the within predictand group (or category) dispersion of the predictor.

While screening does not guarantee the selection of the optimum subset of predictors experience has shown that it does select a good set. Thus the role of the meteorologist becomes one of incorporating all available professional knowledge in defining the set of possible predictors to be screened.

SUMMARY

Statistical prediction models have been developed where the effectiveness of possible predictors can be tested within a framework of linear and nonlinear predictor-predictand relationships.

It appears feasible at this point to test in a systematic fashion the numerous (and often conflicting) cyclogenesis forecasting rules by a series of statistical prediction experiments.

For example the series of case studies of Gulf of Mexico disturbances by Riehl [4] points up several quantitative measures of the low-level circulation patterns that are associated with the dissipation and intensification of Gulf disturbances. Riehl's studies further indicate several qualitative associations between upper tropospheric flow patterns and subsequent intensification.

Using these studies as a guide in defining possible predictors one could statistically relate the change of intensity of Gulf disturbances and the more important predictors, as determined by a screening procedure.

REFERENCES

1. E. N. Lorenz, "Prospects for Statistical Weather Forecasting," Final Report, Contract No. AF19 (604)-1566, Department of Meteorology, M.I.T., Cambridge, Mass. 1959, 185 pp.
2. R. G. Miller, "An Application of Multiple Discriminant Analysis to the Probabilistic Prediction of Meteorological Conditions Affecting Operational Conditions," Technical Memorandum No. 4, Travelers Research Center, 1961, 138 pp.
3. F. P. Ostby and K. W. Veigas, A Moving-Coordinate Prediction Model Applied to East Coast Cyclones, AFCRL-TN-60-675, The Travelers Weather Research Center, Scientific Report No. 1 on Contract AF19(604)-5207, 1960.
4. H. Riehl, Hurricane Formation in the Gulf of Mexico, Second Technical Report prepared for the American Petroleum Institute, 1960, 60 pp.
5. K. W. Veigas, R. G. Miller, and G. M. Howe, "Probabilistic Prediction of Hurricane Movements by Synoptic Climatology," Occasional Papers in Meteorology, No. 2, Travelers Weather Research Center, 1959, 54 pp.
6. K. W. Veigas, "Prediction of Twelve, Twenty-Four, and Thirty-Six Hour Displacement of Hurricanes by Statistical Methods," Final Report, Contract No. Cwb-9807, Travelers Research Center, 1961, 36 pp.
7. J. G. Bryan, "Special Techniques in Multiple Regression," 1944, (unpublished manuscript).
8. R. G. Miller, "A Statistical Procedure for Screening Predictors in Multiple Regression," Studies in Statistical Weather Prediction, AFCRC-TR-58-272, The Travelers Research Center, Final Report on Contract AF19(604)-1590, Dec. 1958, pp. 86-95.

CONCERNING THE MECHANICS AND THERMODYNAMICS OF THE INFLOW LAYER OF MATURE HURRICANES

Stanley L. Rosenthal
National Hurricane Research Project, Miami, Fla.

ABSTRACT*

The Malkus-Riehl model of the inflow layer is extended to include vertical variations of radial velocity and density. The tangential equation of motion is solved to obtain radial distributions of tangential velocity for various inflow angles. The radial velocity is obtained from the tangential velocity and the inflow angle. The pressure profile is obtained from the radial equation of motion. The vertical velocity is obtained from the equation of continuity. These solutions appear to be quite realistic.

The thermodynamic constraints implied by these velocity and pressure fields are examined in relation to the vertical shear of tangential velocity and the static stability. Convergences of eddy heat flux and various energy transformations needed to sustain the velocity and pressure fields are computed. The results appear to be quite reasonable.

Some remarks concerning the role of lateral mixing of momentum in sustaining the hurricane eye are made.

---

*The complete version of this paper is reproduced as NHRP Report No. 47.

RECENT RESULTS OF THEORETICAL STUDIES OF CONVECTION BY NUMERICAL METHODS

Douglas K. Lilly
U. S. Weather Bureau, Washington, D. C.

In the General Circulation Research Laboratory of the Weather Bureau we are interested in cloud-scale thermal convection for a number of reasons. First, as meteorologists we are aware of the role of thermal convection as a producer, over much of the earth's surface, of significant and often extreme local weather phenomena. From a larger-scale viewpoint observational studies of the general circulation have made abundantly clear the statistical importance of cloud convection as a heat and moisture transporting mechanism, especially, of course, in the tropical regions. It has not as yet been possible to include this mechanism satisfactorily in numerical general circulation experiments, and results in the tropical regions suffer thereby. In addition to the physical interest we find that the thermal convection process represents a relatively single field of application for the general numerical integration technique developed for simulation of larger-scale motions, and provides an opportunity independently to test some of these techniques.

The study of atmospheric convection by numerical simulation has been planned as a three-phase process, with the phases somewhat overlapping. First a computational model or models must be developed, suitable for studying a fairly broad range of convective phenomena. Secondly, the behavior of the model should be tested by performing experimental computations under conditions similar to and verifiable by adequate laboratory measurements or verified theory. Finally, upon satisfactory performance in such controlled experiments one may perform experiments with more realistic (and experimentally uncontrollable) atmospheric conditions. The work described herein is principally aimed at testing a model suitable for simulating dry turbulent gaseous cloud scale convection, while the laboratory experiments (those of Scorer, Woodward, and Richards) to be compared thereto were performed in an aquarium-sized water tank. The difference in medium and scale makes some comparisons difficult, although the laboratory experiment itself was originally designed to simulate certain convective processes of cloud scale.

At the suggestion of J. von Neumann a pioneering attempt at the numerical simulation of thermal convection was performed by a group at Los Alamos and published only recently in a widely available journal [1]. The computations simulated the overturning of an unstably stratified two-layer miscible fluid system, and the methods and results should still be of great interest to investigators considering use of such methods. Another significant advance resulted from the numerical experiments performed by J. S. Malkus and G. Witt [2], in which the early stages of a bubble-like atmospheric thermal were simulated. Several other recent studies deal with "meso" scale processes including Kasahara's [3] work on hurricanes, Sasaki's [4] on squall lines, and Estogue's [5] on sea breezes. The initial conditions of the computations to be described here are similar to those used in the Malkus-Witt study, though the computational model is considerably different.

The differential equations from which the numerical difference scheme was derived are the Eulerian equations of two-dimensional momentum, continuity, and potential temperature conservation, and the equation of state, all averaged over a significant spatial interval. The equations are written below in tensor notation, where indices may take the values 1 or 3 (for the present computations) and the usual summation convention holds:

$$\frac{\partial(\rho u_i)}{\partial t} + \frac{\partial}{\partial x_j}(\rho u_i u_j) + \frac{\partial p}{\partial x_i} + g\delta_{i3}\rho = \frac{\partial \tau_{ij}}{\partial x_j} \tag{1}$$

$$\frac{\partial \rho}{\partial t} + \frac{\partial}{\partial x_j}(\rho u_j) = 0 \tag{2}$$

$$\frac{\partial(\rho\theta)}{\partial t} + \frac{\partial}{\partial x_j}(\rho u_j \theta) = \frac{\partial H_j}{\partial x_j} \tag{3}$$

$$\left(\frac{p}{p_o}\right) = \left(\frac{R\rho\theta}{p_o}\right)^{c_p/c_r} \tag{4}$$

If the spatial averaging scale and a characteristic velocity of the system are sufficiently large we may assume motions are turbulent and the terms on the right of (1) and (3) are eddy flux divergences. We also assume that eddy fluxes are proportional to local mean gradients and write these terms as:

$$\tau_{ij} = \rho K_M \left(\frac{\partial u_i}{\partial x_j} + \frac{\partial u_j}{\partial x_i} - \frac{2\delta_{ij}}{\delta_{ii}} \frac{\partial u_j}{\partial x_j} \right) \tag{5}$$

$$H_j = \rho K_H \frac{\partial \theta}{\partial x_j} \tag{6}$$

where K_M and K_H are variable coefficients of eddy momentum and heat exchange. Smagorinsky has suggested a formulation for these coefficients based on an equilibrium theory of turbulence, which for the present case may be written:

$$K_M = \begin{cases} (k\Delta)^2 \left|Def\right| \sqrt{1 - \frac{K_H}{K_M} Ri}, & \text{if } Ri \leq \frac{K_M}{K_H} \\ \phi, & \text{if } Ri \geq \frac{K_M}{K_H} \end{cases} \tag{7}$$

$$Ri = - \frac{\frac{1}{\rho\theta} \frac{\partial p}{\partial x_1} \frac{\partial \theta}{\partial x_1}}{Def^2} \approx \frac{\frac{g}{\theta} \frac{\partial \theta}{\partial x_3}}{Def^2} \qquad (8)$$

Def^2 is the square of the finite difference deformation tensor, Δ is the spatial averaging interval, and k is an assumed universal constant similar to the Karman constant. The above expressions are similar to those applied to boundary layer turbulence by Kazansky and Monin [6], and by Ellison [7] with Δ here taking the place of the distance from the boundary in the latter. The ratio K_H / K_M is presumed to be a function of the generalized Richardson number Ri, but as in boundary layer flow the proper functional relationship is rather vague. For neutral stability (Ri=0) the formulation reduces to a form consistent with the Kolmogoroff similarity theory for turbulent flow.

The boundary equations for the present set of computations were chosen to correspond to solid, smooth, insulated surfaces. For the side boundaries these conditions presume reflective symmetry. For numerical computation the set of differential equations and boundary conditions was replaced by a set of centered difference equations on a space-time staggered grid, as outlined in a previous paper [8]. The auxiliary, or computational, boundary conditions required for closing the system were chosen in accordance with Smagorinsky's criteria [9] to eliminate truncation error from volume integrals of the difference equations.

The laboratory results which our computations most closely resemble are those of the experiments conducted at Imperial College by Scorer, Woodward, and most recently pertinently by J. Richards. In Richards' experiments a trough of saline solution, made visible with a tracer dye, was introduced into the top of a glass-walled tank. The resulting quasi-two-dimensional flow patterns are qualitatively similar to the axially symmetric thermals discussed by Scorer and Woodward, although the quantitative relations are somewhat different. Theoretical discussions by Batchelor, Scorer, and others have been based on the principle of self-preservation, or steady-shape, of the flow patterns. If L, W, and $\Delta \rho$ are the characteristic length, velocity, and density deviation of a thermal element, these are related to each other and to the time elapsed (from a virtual origin) as follows:

$$L \propto t^{2/3}$$

$$W \propto \frac{dL}{dt} \propto t^{-1/3}$$

$$L^2 \Delta \rho = \text{const.}$$

These and other related proportionalities seem to be fairly well verified by Richards' observations, and he has determined various proportionality constants and pattern shapes to the first approximation.

A series of over 30 numerical experiments was performed in order to test various computational features of the model. The majority of these were conducted on the "low resolution" grid of 16 x 16 points at 250 meter intervals. For all of these the same initial conditions were applied, and generally one computational parameter was varied for each subsequent case. The majority of these dealt with various methods of applying diffusive-type terms. When the viscosity coefficient was eliminated or made too small the system exhibited non-linear computational instability of the same general type as discussed by Phillips [10] and encountered by Malkus and Witt, Hinkelmann, and others. A constant viscosity-diffusion coefficient sufficiently large to maintain computational stability (250 m.^{2}/sec.) essentially eliminated most of the non-linear aspects of the system and resulted essentially in a Fickian diffusion computation. The turbulent viscosity formulation of equations (7) and (8) was applied with k = .25, .5, and 1.0 and $K_H = K_M$. The intermediate value of k at the time apparently yielded best results. The equality of K_H and K_M allows the coefficient to vanish for large positive static stabilities, and where this occurred there was a tendency for increasingly large truncation errors and slight instability, especially in the later high resolution experiments. When the Richardson number term was completely eliminated from equation (7) the flow patterns exhibited some irregularity in the statically unstable regions but were better behaved in the stable areas. Thus these results suggest that better computational behavior might be obtained by making $K_H / K_M \geq 1$ for Ri $< \emptyset$ and $K_H/K_M \leq 1$ for Ri > 0. These conclusions are not inconsistent with physical intuition and have been suggested as being valid for boundary layer flow by various authors, e.g., Ellison.

A few numerical experiments were performed to test various methods of differencing, especially in regard to the weight term in the vertical equation of motion. The discussion in the previous paper [8] although not entirely pertinent to this system, suggested that the choice of methods was of little importance. The tests conducted fully verified this suggestion and indicated that any computation which remained stable was sufficiently "smooth" so that spatial truncation errors were negligible. This perhaps implies that the smoothing effects of the viscous-type terms considerably reduce the effective resolving power of the grid.

A number of experiments have now been completed with a higher resolution grid - 32 points in the vertical and 48 in the horizontal, with 125-meter grid increments. The first two of these were initiated with conditions similar to one of the low resolution cases - that where k = .5 and all terms of equation (7) were used with $K_H/K_M = 1.0$. The disturbance was entered in the density field and made proportional to the cosine-squared in both directions, centered at the region. Figures 1a and 2a indicate the general arrangements. Development of the thermal may be divided into four stages as follows:

(1) Signal propagation. An initial small-amplitude sound wave passes through the area in about 15 seconds. After its passage the pressure-density fields are in quasi-static equilibrium and motions are largely non-divergent.

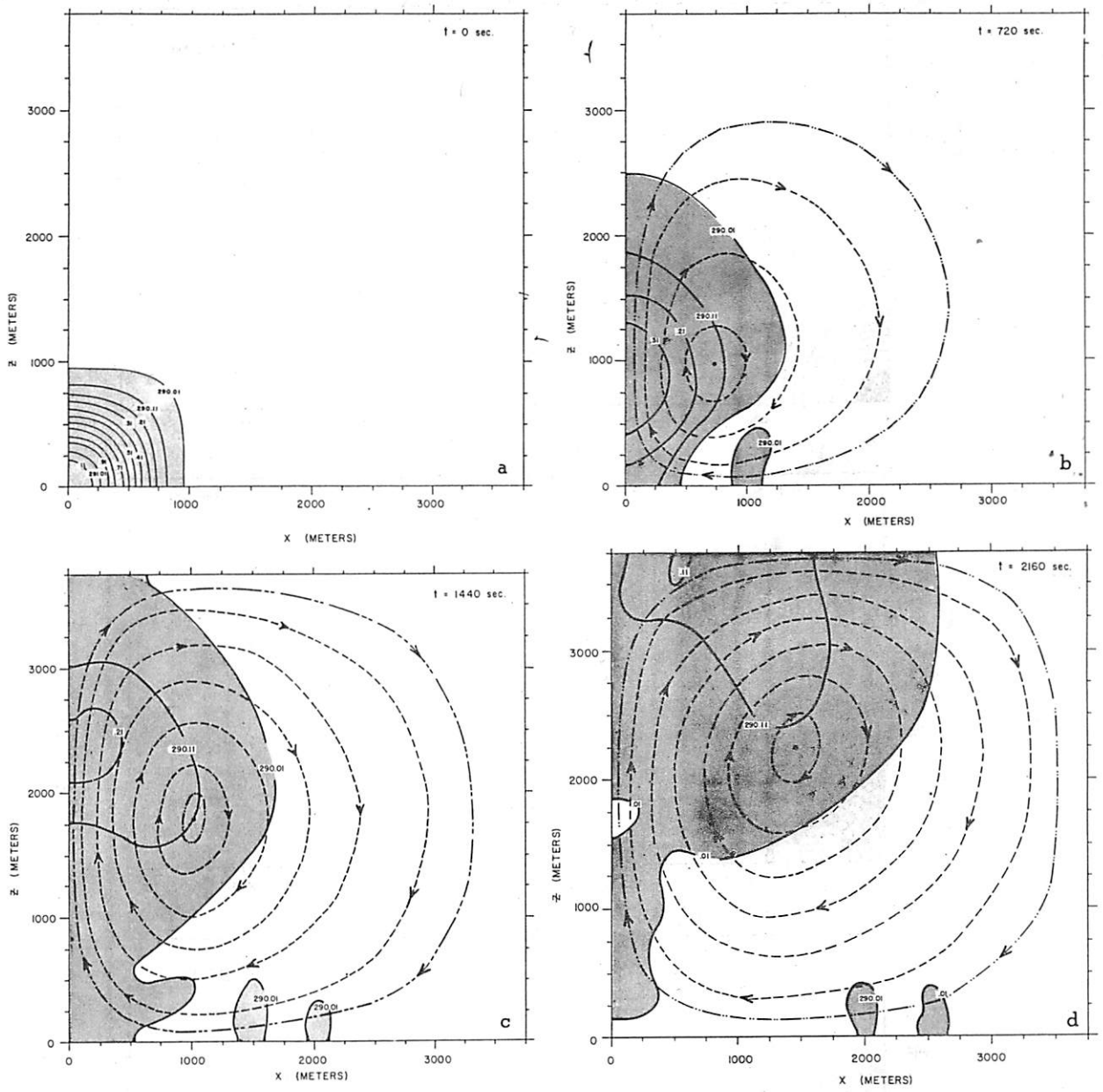

Figure 1. - Maps at 12 minute intervals of the potential temperature and stream fields for experiment No. 10. The shaded area includes potential temperatures greater than 290.01°.

(2) Acceleration. The thermal initially accelerates linearly and spreads vertically, because of the nearly constant (with time) exchange coefficient. The end of this stage is characterized by a lateral splitting of the bubble and formation of the typical "mushroom" shape. The experiments by Malkus and Witt beautifully illustrated the early part of this stage.

(3) Approach to the shape preservation stage. We will see that this is not accomplished uniformly by all observable parameters and is evidently not completed in any of the experiments to date.

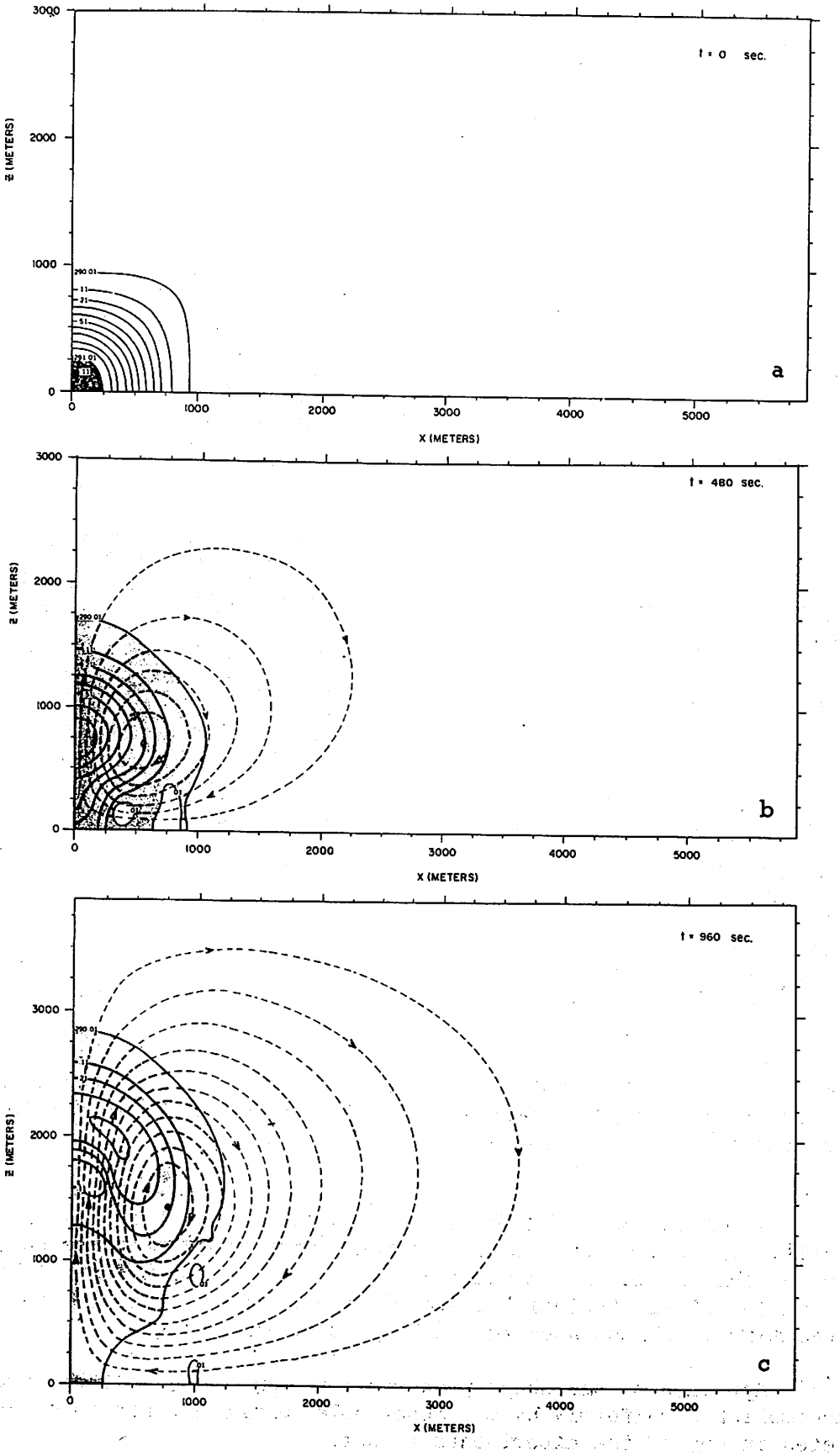

Figure 2. - Maps for experiment No. 101.

(4) Spreading out and dissipation. This occurs when the thermal runs into an upper boundary or strong stable layer. The end result is a stable gravity wave propagating outward.

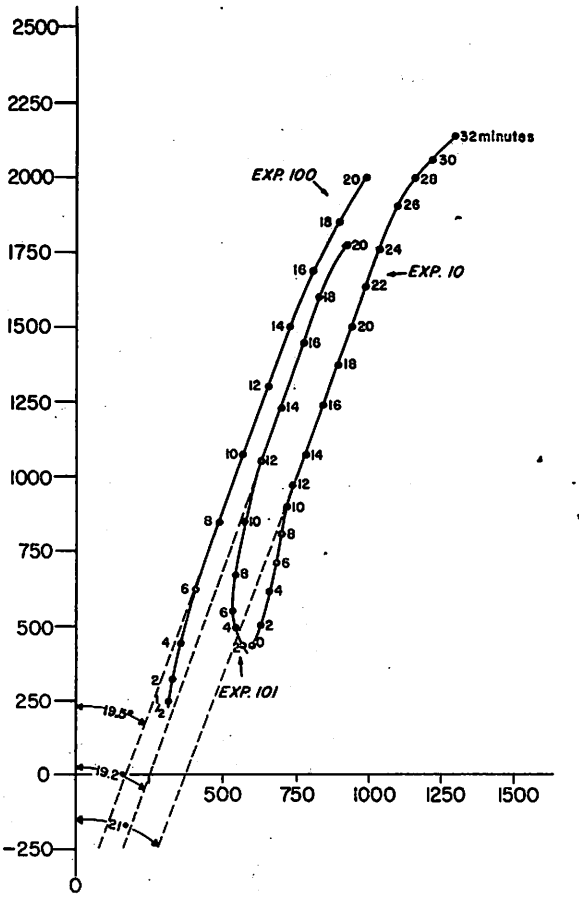

Figure 3. - Spatial trajectories of the vortex centers of experiments Nos. 10, 100, and 101.

We now compare some qualitative and quantitative results of the experiments illustrated in figures (1a -d) and (2a-c) denoted as No. 10 and No. 101 respectively. First one should note the generally increased rate of development of the higher resolution cases. This is essentially because in the early stages of the low resolution case the viscosity-diffusion terms are seriously interfering with the physics of the disturbance scale. Whether the high resolution cases are sufficiently free of such interference can probably only be determined by a further increase in resolution. Figure 3 illustrates the spatial trajectories of the vortex centers of the two experiments, plus another, No. 100, with somewhat different initial conditions. It can be seen that the angle from the vertical of these trajectories is nearly equal in all cases and remains nearly constant over a considerable period of time. This angle may be closely related to the entrainment rate. Other results indicate that it is essentially independent of k, given sufficient resolution. In figure 4 are sets of curves of various quantitative features of the three experiments plotted against time on a log-log scale. These quantities are comparable between experiments. They consist of the following:

(a) the distance of the vortex center from the center line;

(b) the maximum value of the (approximate) stream function;

(c) the total released potential energy;

(d) the total kinetic energy;

(e) the maximum value of vertical momentum;

(f) the rate of change of total kinetic energy;

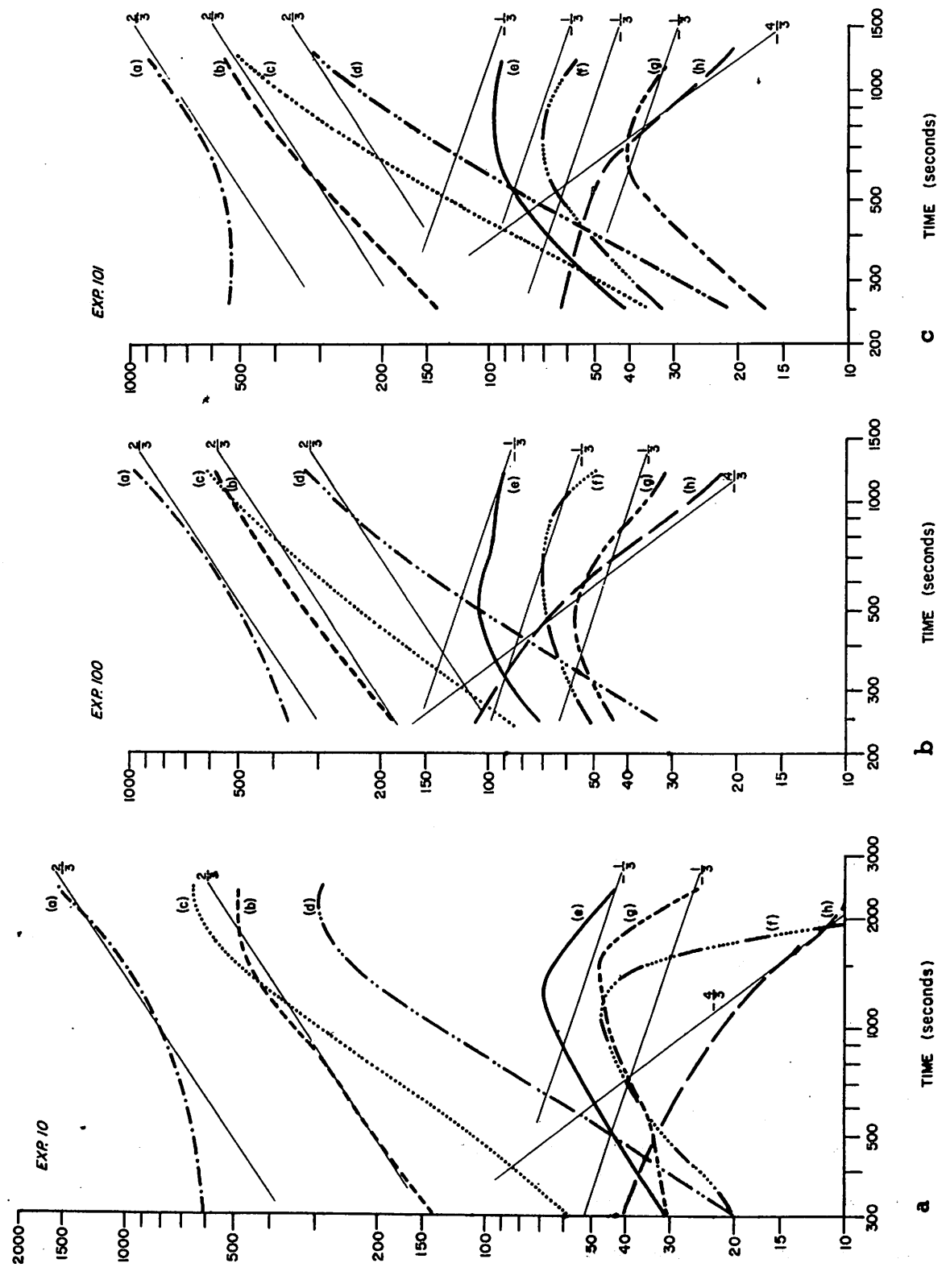

Figure 4. - Curves of various quantitative features of experiments Nos. 10, 100, and 101 as functions of time on a log-log-scale.

Table 1. - Comparison with Richards' experiments.

Quantity	Richards' Average	Expt No.100	Expt No.101
n	2.14	3.00	2.96
c	.52	.67	.64
$-\dot{E}_k/\dot{E}_p$	.37	.62	.64
$C/Z\dot{Z}$	1.09	1.47	1.44
$W_{max}/\dot{Z}$	1.46	1.90	1.95
$\dot{Z}/\sqrt{\frac{2}{R}\iint\frac{\Delta\rho}{\bar{\rho}}\,dxdz}$	.5	.72	.71

(g) the total energy dissipation rate:

(h) the maximum value of potential temperature.

The straight diagonal lines on figure 4 represent powers of time and are located adjacent to the curves to which they should correspond in the shape preservation theory. It is evident that different quantities approach desired rates non-uniformly, but that in all cases they approach closer for the high than the low resolution experiments.

In view of the reasonably close approach to the shape preservation exhibited by the high resolution experiments it is of interest to compare values of certain characteristic features and parameters with those obtained from Richards' experiments. Table 1 summarizes a few of the comparisons. The quantities compared are the following:

n = the ratio of Z, the height (from a virtual origin) of the thermal "front", to R its radius at the widest point.

c = the height of the widest part of the thermal divided by that of its front.

$-\dot{E}_k/\dot{E}_p$ = the rate of increase of total kinetic energy over that of loss of potential energy.

$C/Z\dot{Z}$ = the circulation over the product of the height and velocity of the thermal front.

$W_{max}/\dot{Z}$ = maximum vertical velocity over velocity of the thermal front.

$\dot{Z}/\sqrt{\frac{2}{R}\iint\frac{\Delta\rho}{\bar{\rho}}\,dxdz}$ = a quantity proportional to the ascent rate divided by the root mean released potential energy.

Evidently the numerically simulated thermal is too tall and narrow, the velocities are too large compared to the ascent rate, and the ascent rate itself is too large. It should be noted that, in spite of these indications of insufficient damping there is no evidence of computational instability. Thus we arrive at the important conclusion that computational dissipation sufficient to insure computational stability is less than that required to simulate observed motions.

Tentative results suggest that an increase in the value of the constant k would lead to some slight improvements in results. It is felt, however, that the general formulation of the eddy exchange terms requires some modifications to allow a closer approach to physical reality. One possibility would be to carry turbulent intensity as a forecast variable instead of assuming it to adjust instantaneously to the shear.

Recently some experiments have been performed with very large amplitude disturbances. The shape preservation solutions are not supposed to be valid when the density disturbance becomes of the same order as the mean density. Laboratory experiments have shown that entrainment and dilution become less for a rising low density bubble, and theory suggests that it might be greater for a falling high density bubble. Experiments run both ways with temperature amplitudes of about 200° showed somewhat unexpected though explainable behavior. The hot bubble did indeed rise with a slightly steeper vortex trajectory angle, but the cold bubble fell with an even smaller angle. The apparent reason for this discrepancy was the effect of the gas compressibility. Even with no entrainment (as in the case of a balloon) a bubble would expand while ascending and shrink in descent. The complicating factor must then be kept in mind when comparing liquid and gas results.

One rather interesting experiment was started with a hot bubble at the bottom and a cold bubble at the top directly overhead. Due to the mathematical symmetry of the system there was no possibility of the thermals by-passing each other. Figure 5 shows the development of this unusual experiment. The cold bubble evidently contained more available potential energy (this is not immediately apparent) and eventually overwhelmed the hot one, after both lost a great deal of their available energy through the diffusion of heat between them. The final pattern is not unlike a very large single cold thermal surrounded by a weak warm blanket. This illustrates the general tendency of small complex patterns to amalgamate into larger simpler ones. A more pertinent meteorological example of this would be the coagulation of two or more rising thermals into a larger one. It is planned to explore this in the near future.

Other future plans included development of a quasi-statically balanced model similar to that of Malkus and Witt but to allow the non-sonic effects of compressibility. This will allow greater resolution for a given amount of machine time and also make practicable the inclusion of moisture condensation effects.

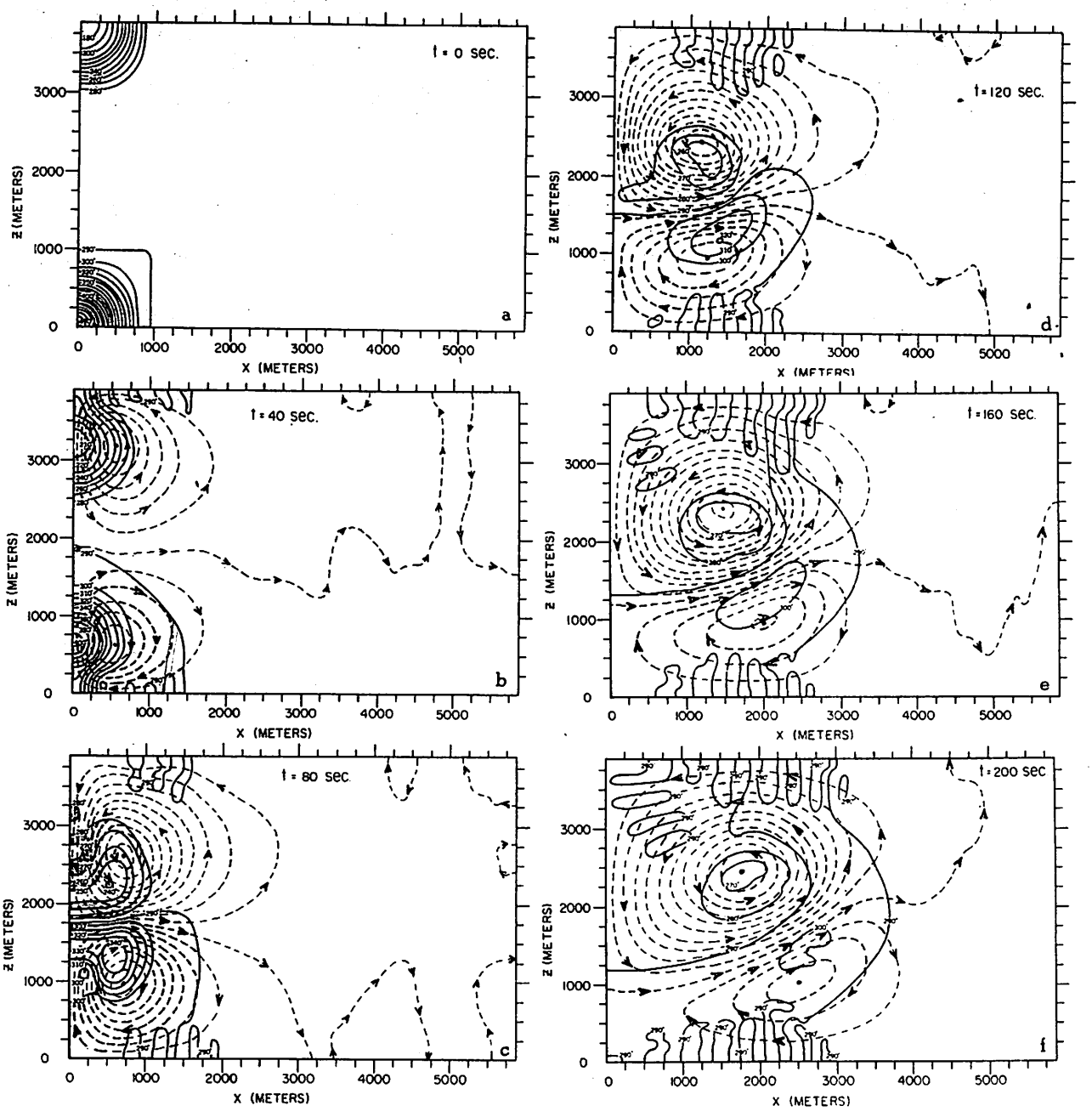

Figure 5. - Maps of the high-amplitude hot-over-cold thermal experiment at 40 second intervals.

REFERENCES

1. A. Blair, N. Metropolis, J. Von Neuman, A. H. Tabu, and M. Tsingou, "A Study of a Numerical Solution to a Two Dimensional Hydrodynamical Problem," Mathematical Tables and Other Aids to Computation, vol. 13, 1959, p.145.
2. J. S. Malkus and G. Witt, "The Evolution of a Convective Element: a Numerical Calculation," pp. 425-439 of The Atmosphere and the Sea in Motion, (the Rossby Memorial Volume), Rockefeller Institute Press, New York, 1959, 509 pp.
3. A. Kasahara, "A Numerical Experiment on the Development of a Tropical Cyclone," Department of Meteorology, University of Chicago, Technical Report No. 12 on Contract Cwb 9718, 1960, 85 pp.
4. Y. Sasaki, "Effects of Condensation, Evaporation, and Rainfall on the Development of Mesoscale Disturbances: a Numerical Experiment," Department of Meteorology and Oceanography, The A and M College of Texas, Technical Report No. 5, Project 208, Contract No. NSF-G7417, 1960.
5. M. A. Estoque, "A Theoretical Investigation of the Sea Breeze," Quarterly Journal of the Royal Meteorological Society, vol. 87, No. 372, Apr.1961, pp. 136-146.
6. A. B. Kazanskiĭ and A. S. Monin, "Turbulence in the Inversion Layer Near the Surface," [Turbulentnost' v prizemnykh inversiſakh] Izvestiſa, Akademiſa Nauk SSSR, Ser. Geofizicheskaiſa, pp. 79-86.
7. T. H. Ellison, "Turbulent Transport of Heat and Momentum from an Infinite Rough Plane," Journal of Fluid Mechanics, vol. 2, No. 5, July 1957, pp. 456-466.
8. D. K. Lilly, "A Proposed Staggered-Grid System for Numerical Integration of Dynamic Equations," Monthly Weather Review, vol. 89, No. 3, Mar. 1961, pp. 59-65.
9. J. Smagorinsky, "On the Numerical Integration of the Primitive Equations of Motion for Baroclinic Flow in a Closed Region," Monthly Weather Review, vol. 86, No. 12, Dec. 1958, pp. 457-466.
10. N. A. Phillips, "An Example of Non-Linear Computational Instability," pp. 501-504 of The Atmosphere and the Sea in Motion (The Rossby Memorial Volume), Rockefeller Institute Press, New York, 1959, 509 pp.

A MECHANISM FOR DEVELOPMENT OF TROPICAL CYCLONES

(A Condensed Version *)

Akira Kasahara
The University of Chicago

SUMMARY

There is no doubt that the primary source of energy of tropical cyclones is the latent heat of condensation released during the ascent of moist air in the storms. It is not clear, however, how the liberated latent heat becomes available for the development of warm-core vortical circulation in the storms. In order to throw light on this question, we have conducted a series of numerical experiments on development of tropical cyclones based upon a time integration of the basic equations which are the conservation equations of momentum, mass, water vapor, and heat in the hydrostatic system (Kasahara,[3,4]).

A comparison between two computations from the same initial conditions but with and without the supply of latent heat revealed an important effect of this energy source upon development of the warm-core circulation in a tropical atmosphere. However, the growth of cumulus-scale convections in the system became so intense that they eventually obscured the development of the large-scale motions.

Since the initial condition contains all scales of motion, the final form of circulation pattern must be dominated by the scale of motion which has the highest growth rate. It is pointed out that the horizontal scale of perturbation motion with the highest growth rate of a gravitational instability is in the order of 10 km. for ordinary magnitudes of eddy-exchange coefficients for momentum and heat in the atmosphere (Kasahara, [4] and Kuo,[6]). One may ask then: how does a large-scale convective system such as a hurricane form in the atmosphere with the released latent heat as the main energy source?

In order to obtain insight into this seemingly difficult question, stability properties of symmetric disturbances in a conditionally unstable atmosphere subject to destabilizing effects of horizontal temperature gradient and the released latent heat of water vapor are examined. A horizontal eddy diffusion process of Fickian type is postulated for dissipation of momentum and sensible heat. A similar study has been made by Kuo [5] in connection with a general-circulation experiment using a dishpan (e.g., Fultz et al., [2]). Earlier, Eliassen [1] developed an elegant theory of slow, thermally or frictionally controlled meridional circulation in an axially-symmetric vortex. In this paper, however, we shall investigate the growth rate of unstable perturbation motions and explore the physical processes involved in the growth.

---

*The complete paper will be published elsewhere.

The relevant basic equations (tangential and radial components of momentum, hydrostatic, mass continuity, and thermodynamic energy equations) expressed in cylindrical coordinates are linearized and the curvature terms, with the radial coordinate r undifferentiated in the denominator, are then omitted. The motions are regarded as perturbations superimposed on the steady tangential motion $\bar{u}$ which is a function of r and pressure p as the vertical coordinate. The vertical gradient of $\bar{u}$ is related to the radial gradient of $\bar{\alpha}$, specific volume, by the thermal wind relation,

$$\frac{\partial \bar{\alpha}}{\partial r} = - f \frac{\partial \bar{u}}{\partial p} \tag{1}$$

where f denotes the Coriolis parameter

By elimination of variables, the five perturbation equations are reduced to the following equation involving only a stream function ψ,

$$\frac{\partial}{\partial p}\left[\left\{\mathcal{L}^2 + f\left(f + \frac{\partial \bar{u}}{\partial r}\right)\right\}\frac{\partial \psi}{\partial p} + \frac{\partial \bar{\alpha}}{\partial r}\frac{\partial \psi}{\partial r}\right]$$

$$+ \frac{\partial}{\partial r}\left[\frac{\partial \bar{\alpha}}{\partial r}\frac{\partial \psi}{\partial p} + \sigma \frac{\partial \psi}{\partial r}\right] = \frac{\partial Q}{\partial r}, \tag{2}$$

where

$$\mathcal{L}\ (\ ) \equiv \frac{\partial}{\partial t} - \nu \frac{\partial^2}{\partial r^2}$$

with ν being kinematic eddy viscosity and diffusivity; and t time;

$$\sigma \equiv - \left(\frac{\partial \bar{\alpha}}{\partial p} + \frac{5}{7}\frac{\bar{\alpha}}{p}\right) \tag{3}$$

for static stability.

It is assumed that the atmosphere is saturated and the motion is moist adiabatic. Thus, the non-adiabatic heating term Q may be expressed by $- \mathbb{L} \omega$ where ω denotes the material derivative of pressure and $\mathbb{L}$ is a proportionality factor.

Equation (2) is solved with the boundary conditions that ω vanishes at the top and the bottom boundaries. The effects of lateral boundaries are ignored in the problem by assuming that the motion is harmonic in r. Thus, we may put $\psi \propto \exp\left(nt + i\frac{m}{a}r\right)$ in which n is growth rate, and m and a are respectively the radial modal number and a representative horizontal length of the system.

After some manipulations, we find the solution for the exponential growth rate N ($\equiv$ n f^{-1}) in the following nondimensional form

$$N = - A\, m^2 \pm \sqrt{\frac{S_p}{2}\left(\frac{m}{S\pi}\right)^2 - Z + \sqrt{\frac{S_p^2}{4}\left(\frac{m}{S\pi}\right)^4 + R_{OT}^2\left(\frac{m}{S\pi}\right)^2}}, \qquad (4)$$

where

$$A \equiv \nu\,(fa^2)^{-1},$$

$$S_p \equiv (\mathbb{L} - \sigma)\, d^2\,(fa)^{-2},$$

$$R_{OT} \equiv \frac{\partial \bar{\alpha}}{\partial r}\, d\,(f^2 a)^{-1},$$

$$Z \equiv 1 + \frac{\partial \bar{u}}{\partial r}\, f^{-1}. \qquad (5)$$

Here, d denotes the height of the system in terms of the difference in the pressures at the top and bottom. The quantity S indicates the vertical modality of the perturbation motion. For a given m, instability first sets in for the lowest mode S = 1. The motion is said to be unstable if one of the N's is positive and the corresponding motion grows exponentially with time. The four non-dimensional quantities defined in (5) are important parameters for the stability properties of geophysical fluids. The quantity A represents the ratio between frictional force and Coriolis force; S_p a measure of the ratio between buoyant instability due to the relased latent heat and rotational stability; R_{OT} is called a thermal Rossby number which expresses a combined effect of rotation and differential heating; and Z is the ratio between the absolute vorticity of the field and the Coriolis parameter.

The growth rate expressed by (4) is a function of the radial modal number m and the parameters A, Z, S_p and R_{OT}. We shall first examine separately the contribution of each parameter to the growth (or decay) rate.

(a) If one considers only A, equation (4) reduces to

$$N = -A\, m^2.$$

The corresponding disturbances ultimately decrease exponentially with time owing to the damping effect of Stokes-Reynolds type.

(b) If one considers only Z, equation (4) reduces to

$$N = \pm \sqrt{-Z}\,.$$

For $Z > 0$, disturbances manifest an inertial oscillation of V. Bjerknes type. For $Z < 0$, we have the case of well-known dynamic instability.

(c) If one considers only S_p, equation (4) reduces to

$$N = \pm \frac{m}{S\pi} \sqrt{S_p} .$$

For $S_p > 0$, it is the case of buoyant instability. The energy source of the instability in the present problem is the latent heat of condensation released during the ascent of moist air. If the effect of the latent heat is ignored ($\Gamma_A = 0$ in S_p), the motion becomes periodic with respect to time and is called a Brunt-Väisälä oscillation.

(d) If one considers only R_{OT}, equation (4) reduces to

$$N = \pm \sqrt{|R_{OT}| \frac{m}{S\pi}} .$$

The motion is said to be unstable so long as R_{OT} is different from zero. Note that the growth rate is proportional to $\sqrt{m}$ differing from those of dynamic instability (which is independent of m) and of buoyant instability (which is proportional to m). Margules [7], in his famous paper concerning the energy of storms, suggested the mechanism for this type of instability, namely, that horizontal temperature contrast sets up a meridional circulation to transport heat from warm source to cold source.

Now we shall investigate more general cases including the effects of diffusion and field rotation in the last two types of instability.

Gravitational instability

If one neglects only the horizontal temperature gradient in the steady state, equation (4) reduces to

$$N = - A m^2 \pm \sqrt{S_p \left(\frac{m}{S\pi} \right)^2 - Z} .$$

For $S_p \left(\frac{m}{S\pi}\right)^2 - Z > 0$, there are two real N's and motions are damped, neutral, or amplified according as $N \lessgtr 0$. We shall refer to this type of instability as gravitational instability.

Margulean instability

When the lapse rate of temperature in the steady state is moist adiabatic, S_p vanishes. In this case, equation (4) reduces to

$$N = - A m^2 \pm \sqrt{|R_{OT}| \left(\frac{m}{S\pi}\right) - Z} .$$

For $|R_{OT}| \left(\frac{m}{S\pi}\right) - Z > 0$, motions are amplified if $N > 0$. We shall refer to this type of instability as Margulean instability.

Details of the last two instabilities are discussed in this paper from the standpoint of the kinematic and thermal structures of the unstable motions and the energy transformations. The results are applied to infer the mechanism of development of tropical cyclones.

If gravitational instability alone is postulated as the driving mechanism for development of tropical cyclones, it seems to produce only cumulus-scale motions in the Tropics, unless a large value is assumed for the eddy-viscosity. It is found also that the growth rate of unstable motions is too large to account for storm intensification. However, this type of instability is very effective in forming a warm-core circulation by producing in the updraft areas a cyclonic convergent flow in the lower levels and anticyclonic divergent flow in the upper levels.

On the other hand, the horizontal scale of motion produced by Margulean instability is on the order of a hundred kilometers (assuming the same dissipation mechanism as in the case of gravitational instability). The growth rate is also reasonable, for it takes a few hours for the amplitude of unstable motions to be increased by a factor of e ($\doteq 2.7$). These are some of the attractive reasons why Margulean instability seems to provide an important driving mechanism for development of tropical cyclones. The main source of energy for the unstable motions is the "available" potential energy which may be stored in organized cloud areas in the storms. A large fraction of the converted energy goes to production of the tangential component of kinetic energy, contrary to the case of gravitational instability which converts the released latent heat mainly into the radial component of kinetic energy in the system.

The effect of dissipation for momentum and heat is to inhibit instability, and the horizontal scale of unstable motions depends strongly upon the magnitudes of lateral eddy-exchange coefficients. The field rotation expressed by the absolute vorticity Z has either an inhibitory effect or plays a cooperative role toward instability, depending upon whether this number is positive or negative. The cooperative role of a negative absolute vorticity, known as dynamic instability, has attracted many meteorologists as a possible explanation for the development of large-scale atmospheric disturbances. Sawyer [8] applied this reasoning to the intensification of tropical cyclones in order to explain the removal of air from the storm center. Perhaps one of the theoretical interests in the concept of dynamic instability is in the fact that the growth rate of the unstable motion is independent of the scale of motion. However, energy considerations reveal that the source of kinetic energy in this case is the kinetic energy of the basic flow. Therefore one must consider another mechanism for maintaining the required horizontal wind shear of the basic flow in order to apply the reasoning of dynamic instability alone as a continuous driving mechanism for development of tropical cyclones.

These speculations concerning the mechanism of storm development must be checked by means of numerical experiments based upon the relevant nonlinear equations and synoptic studies based upon abundant observations in tropical cyclones. The effects of sensible heat transfer from the sea surface as an

energy source and radiational cooling as an energy sink upon the storm development are not discussed in this paper, but will be considered in a forthcoming numerical experiment.

The details of this work, together with the illustrations, will be published elsewhere.

REFERENCES

1. A. Eliassen, "Slow Thermally or Frictionally Controlled Meridional Circulations in a Circular Vortex," Astrophysica Norvegica, vol. 5, No. 2, 1952, pp. 19-60.
2. D. Fultz, R. R. Long, G. V. Owens, W. Bohan, R. Kaylor, and J. S. Weil, "Studies of Thermal Convection in a Rotating Cylinder With Some Implications for Large-Scale Atmospheric Motions," Meteorological Monographs, American Meteorological Society, vol. 4, No. 21, 1959, 104 pp.
3. A. Kasahara, "A Numerical Experiment on the Development of a Tropical Cyclone," Journal of Meteorology, vol. 18,No.3, June 1961,pp. 259-282.
4. A. Kasahara, The Development of Forced Convection Caused by the Released Latent Heat of Condensation in a Hydrostatic Atmosphere, Department of Meteorology, The University of Chicago, 1960, 42 pp.
5. H. -L. Kuo, "Symmetrical Disturbances in a Thin Layer of Fluid Subject to a Horizontal Temperature Gradient and Rotation," Journal of Meteorology, vol. 11, No. 5, Oct. 1954, pp. 399-411.
6. H. -L.Kuo, "On initiation of tropical depressions and convection in a conditionally unstable atmosphere," National Hurricane Research Project Report, No. 40, 1960, 46 pp.
7. M. Margules, "On the Energy of Storms," published as Appendix to Yearbook of the Central Meteorological and Geodynamical Institute of Vienna, 1905. (Translated by C. Abbe, in The Mechanics of the Earth's Atmosphere, 3rd Coll., Washington, D. C., 1910.)
8. J. S. Sawyer, "Notes on the Theory of Tropical Cyclones," Quarterly Journal of the Royal Meteorological Society, vol. 73, 1947, pp. 101-126.

AN EXPERIMENTAL ANALOGY TO AND PROPOSED EXPLANATION OF HURRICANE SPIRAL BANDS *

Alan. J. Faller

Woods Hole Oceanographic Institution, Woods Hole, Mass.

INTRODUCTION

The origin of the spiral band structure observed in many hurricane cloud and precipitation patterns has eluded explanation although several hypotheses (usually of a vague and general nature) have been proposed. The thesis of this paper is that the spiral structure is a product of instability in the boundary layer of the hurricane; i.e., in the layer of surface inflow. The essential elements of the argument serving as an outline of this paper consist of:

(1) Established fact: A series of laboratory experiments which demonstrate the instability of a laminar Ekman boundary layer, the initial instability taking the form of spiral convective bands (fig. 1) whose spacing is proportional to the depth of the boundary layer; also, other experimental studies concerned with boundary layer instability.

(2) Analogy: Comparison of the form of the basic laboratory experiments with that of hurricanes; comparison of the characteristics of the instability with the banded structure of hurricanes, e. g., angles, spacings, etc.; and analogy between the laminar flow of experimental models and the turbulent structure of the atmospheric boundary layer.

(3) Conjecture: Discussion and rationalization of the differences between the experimental results and the hurricane phenomena.

THE LABORATORY EXPERIMENTS

Figure 2 contains a schematic diagram and an oblique photograph of the 4-meter diameter rotating tank at the Woods Hole Oceanographic Institution. As the tank rotates water is withdrawn from the center by a pump, is injected into a channel at the rim, and flows into the boundary layer at the bottom of the tank through a narrow slot beneath the rim. The pumping establishes a pressure difference between the center and the rim, and the steady-state flow which is established consists of a circular flow which satisfies the gradient wind balance and which is independent of depth except for the viscous boundary layer at the bottom where the radial transport of water toward the center occurs. The simple theory of this flow predicts that far from the side boundaries the relative circulation $C \equiv 2\pi rv$ should be constant independent of

*This work was supported by a contract with the Geophysics Research Directorate, AFCRC, ARDC and is Contribution No. 1210 from the Woods Hole Oceanographic Institution.

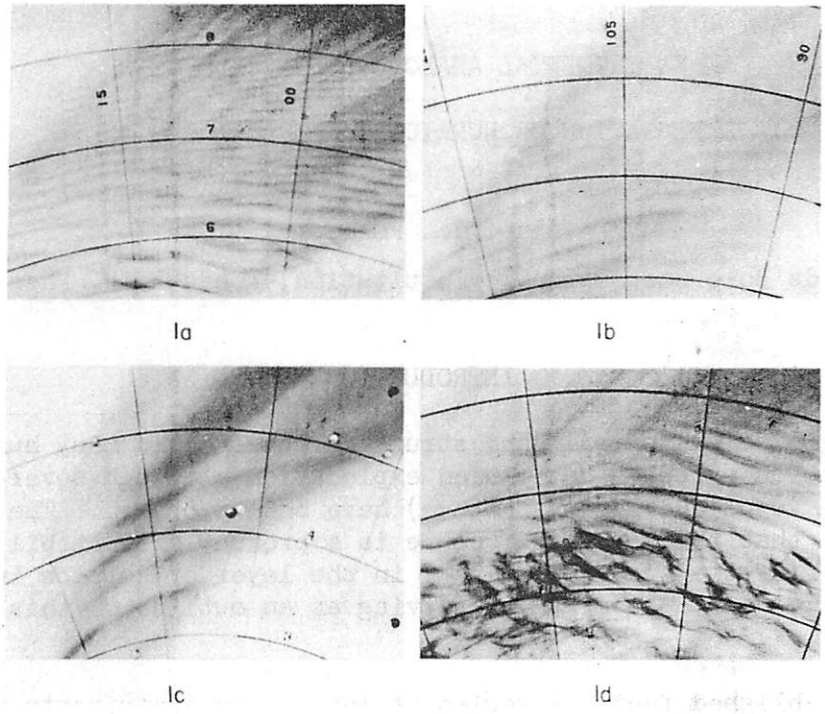

Figure 1. - Examples of the spiral band structure at the instability of the Ekman boundary layer

radius and that the boundary layer flow should be that described by the Ekman spiral (Ekman [1]). These predictions are well confirmed by observations.

In particular it should be noted that the zonal speed of flow, v, varies inversely as the radius, r, as do the speeds of flow in the boundary layer. Therefore it might be expected that at some radius approaching the center the flow should become sufficiently strong that the boundary layer flow should be unstable. This is found to be the case and the nature of the instability is illustrated in figure 1 where four cases of the form of the boundary layer instability are exhibited.

Streaks of dye from crystals of potassium permanganate introduced at the bottom near the rim show the pattern of circulation at the bottom of the boundary layer. The streaks are at first directed toward the center with the angle of 45° at the bottom of the Ekman boundary layer, and as they flow inward the plumes of dye merge into a sheet. At a particular radius (and speed of zonal flow) the dye is observed to form into a pattern of equiangular bands which suggest regions of convergence and divergence and, therefore, roll vortices. These vorticies are observed to occur at very nearly a constant value of a Reynolds number defined by $Re \equiv \frac{VD}{\nu} = \frac{v}{(\Omega\nu)^{1/2}}$ where ν is the molecular coefficient of kinematic viscosity, Ω is the angular rotation rate, and $D = \left(\frac{\nu}{\Omega}\right)^{1/2}$ is the characteristic depth of the Ekman boundary layer. The

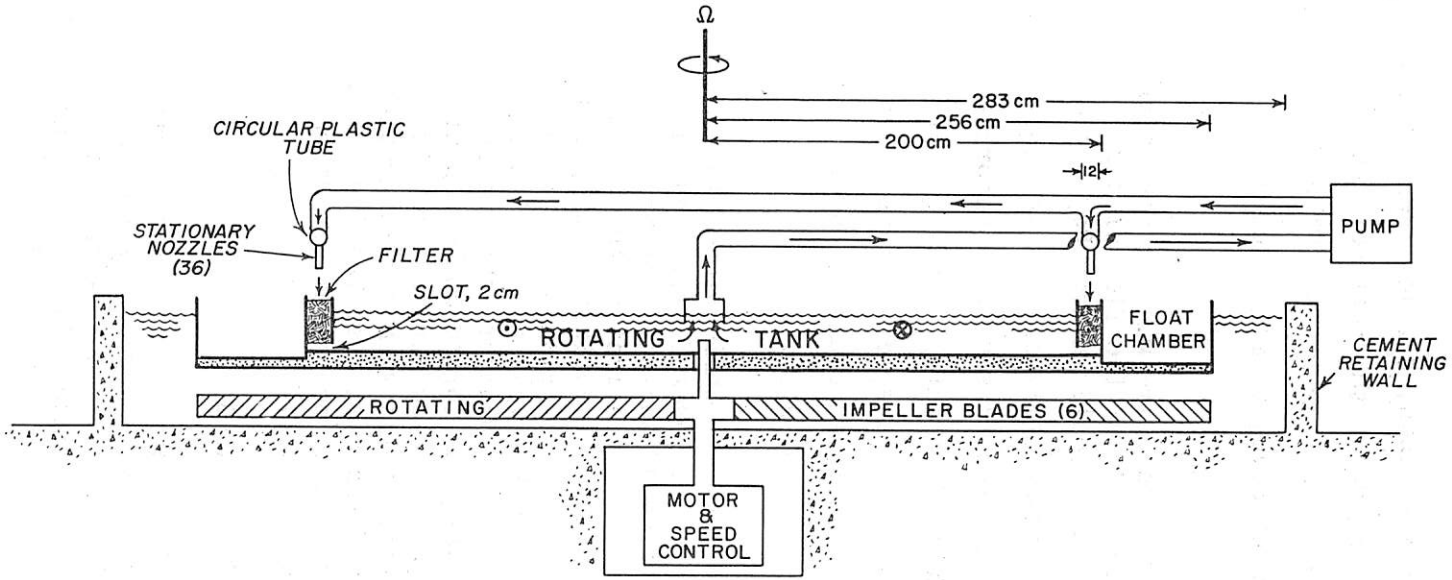

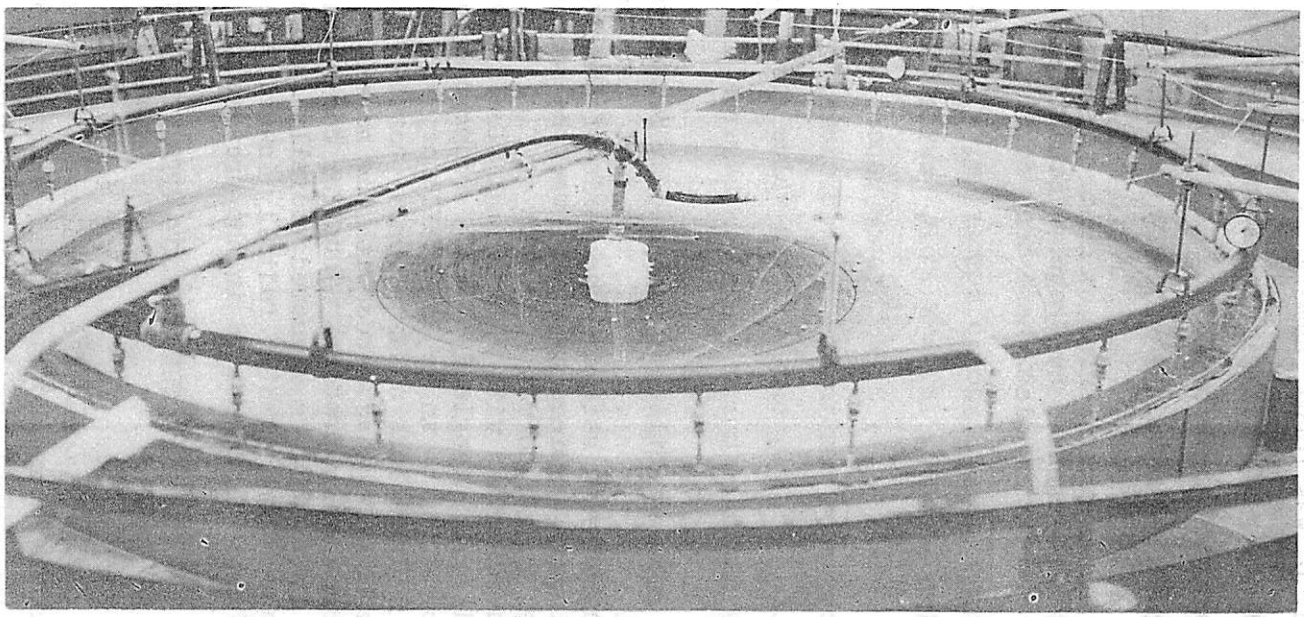

Figure 2. - (a) A schematic diagram of the 4-meter diameter rotating tank. (b) An oblique view of the rotating tank in operation.

average critical value of the Reynolds number for all experiments was Re_c = 145. Mention should also be made of the transition from well-ordered roll vortices to more irregular rolls and to fully developed turbulence. This began at the average transition Reynolds number Re_t = 177.

A constant relation between the spacing of the bands, ℓ_c, and the Ekman depth, D, was found, namely: ℓ_c = 10.9D. The angles of the roll vortices immediately after their formation were observed to be from 10° to 17° with the average angle of 14.7°, and the bands were observed to move slowly normal to their axes and radially inward.

Other experimental evidence of instability of the same general character has been presented by Gregory, Stuart, and Walker [2] for the flow of air over a rotating disc where they found the critical Reynolds number Re_c = 436, the transition Reynolds number Re_t = 533, the average angle of 14°, and the spacing of waves ℓ_c = 21.5 D, twice that of the present study. A theoretical analysis by Stuart (same paper) successfully "predicted" the angle of the observed stationary roll vortices, but the predicted spacing of the waves was ℓ_c = 5.5 D, one-half the value observed in the Ekman boundary layer study and one-fourth the value observed on the rotating disc.

The instability considered by Stuart was a form of "inflectional instability" associated with the fact that the boundary layer flow varied in direction with height. The basis of the prediction of the angle of the stationary vortices by Stuart was the selection of that direction for which a plot of the normal component of flow versus height had an inflection point which coincided with zero normal flow. For the boundary layer over a rotating disc this angle is 13-1/4° (compared to 14° as observed) and for the Ekman profile the angle for stationary vortices is 16°. However, the theory does not preclude non-stationary vortices, and vortices formed at some other angle should be advected with the normal component of flow derived from the basic velocity profile. Thus for the Ekman profile rolls with angles greater than 16° should be advected radially outward, and those with angles less than 16° should be advected radially inward, the latter case being the one which was frequently observed in the present experimental study.

THE ANALOGY WITH HURRICANE SPIRAL BANDS

I first wish to point out the similarity of the experimental arrangement with the structure of a hurricane. Although the energy sources are somewhat different we may consider each example as one in which fluid is withdrawn from the center and in which the radially inward flow takes place in a boundary layer, the total mass flux being essentially independent of radius up to the radius of strong convection.

Spiral bands in hurricanes are observed to have an average crossing angle of about 18° (Senn, Hiser, and Low [5]), and this angle is not far different

from those observed in the experimental studies with the rotating disc and with the Ekman boundary layer in the large rotating tank. This fact is the first suggestion that similar mechanisms may be responsible. For the further discussion it is convenient to assume that the vertical profile of radial inflow into a hurricane is that of an Ekman spiral given by

$$v_r = - ve^{-z/D} \sin z/D$$

$$v_\theta = v (1 - e^{-z/D} \cos z/D)$$

although it is fully realized that such a simple condition does not exist in the atmosphere. However this assumption enables one to speak of a constant eddy coefficient of viscosity and allows one to make certain simple computations.

Now we consider the spacings of the bands for which a spacing of 10 miles (16 km.) is perhaps typical (Wexler, [8]). From the experimentally determined relation cited above we then estimate the depth of the boundary layer to be D = 1.5 km., and the corresponding eddy coefficient of viscosity is, for latitude 30°, $\nu_e = .59 \times 10^6$ cm.^{2}/sec. These estimates are in good agreement with estimates of the conditions in the region of inflow in hurricanes. Furthermore, if one makes the assumption that the eddy coefficient of viscosity varies as the square of the tangential speed (tangential stress as the square of the speed) and if one uses the data of Malkus and Riehl [9] for a moderate model hurricane one obtains the Reynolds number Re = 750, so that upon the basis of the simple Ekman model the critical Reynolds number is exceeded at all radii.

The banded zones of vertical motion, which in the model experiment concentrate the dye in regions of convergence, would in the atmosphere give rise to the formation of condensation if the vertical motion ascended to a sufficiently high level. After the initial condensation, the convection may proceed or not proceed depending on the lapse rate and humidity conditions above the boundary layer, and the new source of energy, the latent heat of condensation, may eventually dominate over the initial source of energy, the instability. In particular the clouds may extend far above the boundary layer and may be advected out of the bands. This has been observed to be generally the case [7] and a similar feature was observed in the experiments when dye is convected upward into the main body of the fluid by the turbulence.

An objection to the arguments presented up to this point may be that the hurricane boundary layer flow is not that of an Ekman spiral. This is of course true, but some sort of a variation of wind with height must exist in the boundary layer as the wind varies from approximately 30° near the surface (Hubert [3]), to approximately 20° at 1000 ft. (Hughes [4]) and thence to circular flow at some higher level. With a different form of the profile one may well expect significantly different values of the critical Reynolds number for it has been stated by Gregory, Stuart, and Walker [2] and confirmed in the experiments, that higher critical Reynolds numbers are associated with less strong 3-dimensional flows; i.e., smaller angles of inflow. Therefore to the

extent that the surface inflow in a hurricane (30°) is less than for the Ekman spiral (45°) and less than for the rotating disc (40°) one might expect a higher critical Reynolds number in hurricanes than in the experiments.

From comparison with the experimental observations it would appear that the hurricane bands are sometimes in the region of well-formed rolls and sometimes in the region of irregular bands approaching fully developed turbulence. Therefore I wish to assume that Re = 750 as computed above corresponds to the transition Reynolds number, and, since for both the Ekman case and the rotating disc we find the same ratio $Re_t/Re_c = 1.22$, the critical value for the formation of rolls would be approximately $Re_c \approx 600$.

The fact that hurricane bands are observed to move outward normal to their axes (Senn and Hiser [6]) is an interesting difference for which two possible explanations consistent with the thesis of this paper are suggested: (1) that the average band angle is greater than that for the stationary roll vortices and that they are advected outward by the normal component of flow; (2) that the additional energy source from the release of latent heat may couple with the original source of convective motion in the bands so that the band shape is maintained but so that they tend to propagate outward.

Correlations of band crossing angle with other storm parameters [6] are in general agreement with the experimental findings. In particular the experiments show a decrease of the band crossing angle with radius; and the finding that the band crossing angle is dependent upon surface roughness is in agreement with the thesis that boundary layer instability is the source of the spiral structure.

CONCLUSIONS

The data and arguments presented above form a consistent picture of the mechanism for the formation of the hurricane spiral bands and one which is in agreement with the available observational data. Little more can be said to confirm or negate the theory until more detailed observations of the vertical profile of the radial and tangential components of flow are available. Such information is not only important for testing this theory but it is essential for the understanding of the hurricane mechanism as a whole.

The direct implication of the theory is simply that the organization and maintenance of the convection in a banded structure is due to the boundary layer processes. Whether or not the magnitude of the convection would be seriously altered in the absence of the mechanism discussed here is an important question since it then relates the mechanism of instability to the entire dynamics of the hurricane.

REFERENCES

1. V.W. Ekman, "On the Influence of the Earth's Rotation on Ocean Currents," Arkiv für Matematik, Astr. och Fysik, Stockholm, Bd. 2, No. 11, 1905, 53 pp.
2. N. Gregory, J. T. Stuart, and W. S. Walker, "On the Stability of Three Dimensional Boundary Layers with Application to the Flow Due to a Rotating Disc," Philosophical Transactions, of the Royal Society of London, Ser. A, vol. 248, 1955, pp. 155-199.
3. L. F. Hubert, "Distribution of Surface Friction in Hurricanes," Journal of Meteorology, vol. 16, No. 4, Aug. 1959, pp. 393-404.
4. L. A. Hughes, "On the Low Level Wind Structure in Tropical Storms," Journal of Meteorology, vol 9, No. 6, Dec. 1952, pp. 422-428.
5. H. V. Senn, H. W. Hiser, and E. F. Low, "Studies of Hurricane Spiral Bands as Observed on Radar," Final Report on Contract Cwb-8735, the Marine Laboratory and the Radar Research Laboratory, Univ. of Miami, No. 56-24, Oct. 1956.
6. H. V. Senn and H. W. Hiser, "Studies of the Evolution of Hurricane Spiral Bands and Their Relationship to Other Synoptic Storm Parameters," Final Report on Contract Cwb-9174, the Marine Laboratory and the Radar Research Laboratory, Univ. of Miami, Aug. 1958.
7. H. V. Senn, H. W. Hiser, and E. F. Low, "Studies of the Evolution and Motion of Hurricane Spiral Bands and the Radar Echoes Which Form Them," Final Report on Contract Cwb-9480, the Marine Laboratory and the Radar Research Laboratory, Univ. of Miami, Aug. 1959.
8. H. Wexler, "Structure of Hurricanes as Determined by Radar," Annals of the New York Academy of Sciences, vol. 48, 1947, pp. 821-845.
9. J. S. Malkus and H. Riehl, "On the Dynamics and Energy Transformation in Steady-State Hurricanes." Tellus, vol. 12, No. 1, Feb. 1960, pp. 1-20.

SURFACE PROCESSES IN HURRICANE DONNA

(Extended Abstract)

Herbert Riehl
Colorado State University

In previous studies of hurricane mechanisms (Palmén and Riehl [1], Malkus and Riehl [2], Riehl and Malkus [3]) interactions at the ocean boundary always had to be inferred. Many uncertain aspects of the actual physics of the interaction processes exist, such as surface drag and constraints relating surface pressure and heat sources.

Hurricane Donna offered an unusual opportunity for examining the low-level structure and mechanisms, since this storm passed in nearly steady state through a dense network of surface and upper-air stations while approaching Florida. Reports from these stations may be composited with respect to the moving center and thus offer insight into certain aspects of the low-level hurricane structure which of necessity is not available through research aircraft missions.

SURFACE DATA

Compositing proved easy for surface pressure, including asymmetries around the center. But the attempt to composite the windfield led to a very curious result, a very rapid drop of wind speed outward along the line $vr^{1.3} = \text{const.}$ This is much stronger than the drop obtained from low-level aircraft data or from records of well-exposed stations. A check was made by computing momentum balance holding the surface wind constant through a layer of 100-mb. thickness. The check failed as there was divergence of momentum flux through the bulk of the hurricane's area with nothing left for transfer to the ocean. The conclusion is that even the records of stations on small flat islands and along flat coasts are not representative of oceanic surface conditions.

UPPER-AIR DATA

Next, the rawin observations were composited, at first in 1,000-ft. steps to 4,000 ft. altitude. Then 2,000-ft. steps to 10,000 ft. and 5,000-ft. steps to 50,000 ft. were added, for the area up to the 6°-radius. The main inflow layer was below 4,000 ft., with weak inflow from there to 25,000 ft. except in the inner region where there was none. Outflow was concentrated near 45,000 ft. At 50,000 ft. a nearly symmetrical anticyclone, with small outflow only, was present. Perhaps for the first time in an individual case, precipitation computed from the inflow could be checked against that reported at rain gages. Excellent correspondence was obtained with use of these quite independent data sources.

At 1,000-ft. the mean tangential component follows the law $v_\theta r^{0.6} = \text{constant}$ from the 3° radius inward; this closely corresponds to the Malkus-Riehl model and earlier studies. Three sets of data - rawins, land-surface reports,

and lighthouse reports - all show 60 kt. at about the 1° radius, with very steep slope of the land-surface winds outward from there as already mentioned. This brings out the effect of increasing mechanical turbulence at high wind speeds in reducing the vertical shear.

MOMENTUM BALANCE

Balance of absolute angular momentum was computed for the layer 1000-100 mb. and outward to the 6° radius with two main questions to be answered:

(a) Is there a net stress at the level where the vertical profile of tangential velocity has a maximum or becomes quite flat ? - the median of all ascents gave this level as 4,000 ft.

(b) Is it necessary to make use of lateral small-scale mixing processes in order to obtain momentum balance?

The result is that total momentum flux across the 6° radius is equal to the momentum flux to the ocean as computed using the layer surface to 4,000 ft. alone, hence that there is no net stress at 4,000 ft. Lateral mixing need not be invoked provided that the computed surface drag coefficients are accepted as realistic. These coefficients, reduced to the altitude and wind speeds of the lighthouse stations (16-18 m.), are about 1.5×10^{-3} up to tangential speeds of about 50 kt., then rise inward to 5×10^{-3}. This result is very similar to all previous calculations, for instance, Riehl and Malkus [3], who then postulated lateral mixing on the hypothesis that 5×10^{-3} is too large in view of detailed wind observations made over the sea by other investigators. The low coefficient on the outside can be brought in agreement with previous measurements if it is assumed that the ocean water moves with a fraction of the air speed. This hypothesis is being investigated further.

DRAG COEFFICIENT FROM LIGHTHOUSE DATA

Observations from five lighthouse stations off the Florida coast were composited with respect to the center just like the upper-air data. It is considered that by this means a first approximation to air trajectories near the sea (16 m.) in hurricanes is furnished. Calculations were performed using one such trajectory which ended at pressure of 962 mb., wind 115 kt. Superposition of streamlines at 16 m. and 1,000 ft. showed no turning of wind with height and also, as brought out earlier, very little shear of wind speed at high speeds. Hence, following the method of Malkus and Riehl [2], the kinetic energy equation may be integrated following the surface trajectory over a layer 4,000 ft. thick. Since the stress is zero at the top of this layer, as demonstrated above, the bottom stress and drag coefficient are determinable. This calculation sustains the enhanced drag coefficients from the general momentum balance, where it must be noted, however, that the computation only samples conditions ahead of the center. If valid in all quadrants, small-scale lateral mixing may be omitted as an important hurricane mechanism.

SURFACE PROCESSES AT VERY HIGH SPEEDS

In the hurricane interior, air is known to move at constant temperature. Hence, the pressure of an air particle is controlled by the direct oceanic heat source. Malkus and Riehl [2] postulated uniform heat gain per given distance traveled, from the concept of a uniform exchange coefficient following a given mass. Thus, this mass must wind its way inward with ever decreasing inflow angle in order that the observed low pressures can be established. The Donna trajectory did not bear out this aspect of the model, though agreement in general was good. The pressure drop increased per distance travel with wind speed; thus, the turbulent heat flux also increased.

Drag coefficients can be computed along the high-velocity trajectory with isothermal expansion with two assumptions:

(a) The coefficients of heat and momentum flux are equal;

(b) The height to which the surface heat flux penetrates is known. This height is obtained by imposing the condition that at the wind speed at the outer limit of the trajectory the draf coefficient is the same as that determined from momentum and kinetic energy calculations.

The value of the computation lies in the fact that it yields the drag coefficient as a nearly continuous function along the trajectory, whereas from the kinetic energy computation only bulk values over distances of not less than 30 miles can be obtained in view of the difficulties inherent in determining the production of kinetic energy by pressure forces. This is not satisfactory in the core where wind speed changes very rapidly over 30 miles.

The computed depth of the layer through which the heat flow from the surface penetrates is 1,000 ft., a satisfactory value which agrees roughly with the cloud bases. As is well known, the temperature lapse rate becomes more stable at the cloud bases and the nature of turbulence, as experienced for instance in aircraft, changes from the "washboard type" of the subcloud layer to that typical of layers with convective clouds.

The drag coefficient rose by an order of magnitude from wind speed of 60 kt. to 115 kt., and a straight line is obtained in log-log representation of drag coefficient vs. kinetic energy. This relation suggests a new examination of the whole turbulence theory over sea at very high speeds, providing that the results in this single case are validated through examination of observations in other hurricane situations.

REFERENCES

1. E. Palmén and H. Riehl, "Budget of Angular Momentum and Energy in Tropical Cyclones," Journal of Meteorology, vol.14, No.2, Apr.1957, pp.150-159.
2. J.S.Malkus and H. Riehl, "On the Dynamics and Energy Transformation in Steady-State Hurricanes," Tellus, vol. 12, No.1, Feb. 1960, pp. 1-20.
3. H. Riehl and J.S. Malkus, "Some Aspects of Hurricane Daisy, 1958," National Hurricane Research Project Report, No. 46, 1961, 64 pp.

SCALE ANALYSIS OF THERMAL CONVECTION IN THE ATMOSPHERE AND THE BOUSSINESQ APPROXIMATIONS FOR A COMPRESSIBLE FLUID *

Yoshimitsu Ogura and Norman A. Phillips

Department of Meteorology, Massachusetts Institute of Technology

1. INTRODUCTION

In a recent paper on the behavior of convective phenomena in the atmosphere, Charney and Ogura [2] have used a certain simplified form of the hydrodynamic equations for a perfect gas. For convenience and for reasons to be developed later, we will refer to this simplified set of equations as the anelastic equations. They are identical with a set of equations derived by Batchelor [1] on what seems to be the simple assumption that the distributions of pressure and of density are always close to the distributions of pressure and density in an adiabatically stratified atmosphere. Charney and Ogura, on the other hand, used these equations because they were interested in the "elimination" of sound waves from the hydrodynamic equations. (Sound waves require that a very small time increment be used in a numerical finite-difference integration.) From this viewpoint, it is clear that an assumption about the time scale must be made in deriving the anelastic equations. In this paper we will present a more systematic scale analysis than was done by either Batchelor or by Charney and Ogura, and show that both assumptions are in fact necessary.

2. BASIC EQUATIONS AND ASSUMPTIONS

The equations of motion, the continuity equation, and the first law of thermodynamics may be written most conveniently for our purpose in the following way:

$$\frac{d\vec{v}}{dt} = - c_p \theta \nabla \pi, \tag{2.1}$$

$$\frac{dw}{dt} = - c_p \theta \frac{\partial \pi}{\partial z} - g, \tag{2.2}$$

$$\frac{d}{dt} \left[\ln \theta + \left(1 - \frac{1}{\varkappa}\right) \ln \pi \right] = \nabla \cdot \vec{v} + \frac{\partial w}{\partial z}, \tag{2.3}$$

$$\frac{d\theta}{dt} = \frac{Q}{c_p \pi}, \tag{2.4}$$

where $\vec{v}$ = horizontal velocity, ∇ = horizontal gradient operator, R = the gas constant for a perfect gas, $\varkappa = R/c_p = (c_p - c_v)/c_p$. π is the non-dimensional quantity

* The details of this work will be published elsewhere.

$$\pi = (p/P)^{\varkappa}, \tag{2.5}$$

where p is the pressure and P is a standard value of the pressure. θ is the potential temperature, and is a function of the specific entropy S for dry air:

$$\theta = T \pi^{-1} = \exp (S/c_p), \tag{2.6}$$

where T is the absolute temperature.

The basic assumption we will make is that the potential temperature within the region of interest is almost uniform. This can be expressed in the following way:

$$\theta = \textcircled{H} + (\Delta \textcircled{H}) \theta' = \textcircled{H} (1 + \varepsilon \theta'),$$
$$\varepsilon = \frac{\Delta \textcircled{H}}{\textcircled{H}} . \tag{2.7}$$

$\textcircled{H}$ is a constant and represents some appropriate average value of θ. $\Delta \textcircled{H}$ represents the difference between the maximum and minimum values of θ in the region. We assume that this is much smaller than $\textcircled{H}$, so that ε is a small non-dimensional number. The variable θ' is non-dimensional and of order unity.

Assuming that the region of interest is limited by fixed level surfaces at the bottom ($z = 0$) and top ($z = d$), we will use this depth as the length unit to derive non-dimensional equations.

Since we are interested only in motions whose time scale is larger than that of acoustic waves, we shall choose the reciprocal of the Brunt-Väisälä frequency N as the time scale:

$$N^2 = \frac{g}{T} (\frac{g}{c_p} + \frac{dT}{dz}) = g \frac{d \ln \theta}{dZ} . \tag{2.8}$$

That is, our time scale, τ, is given by

$$\tau = \sqrt{\frac{d \textcircled{H}}{g \Delta \textcircled{H}}} \sim \frac{1}{N} . \tag{2.9}$$

By using d and τ to scale the space and time coordinates and the velocities, and by scaling θ according to (2.7), the non-dimensional forms of (2.1) - (2.4) are

$$\varepsilon\beta \frac{d}{dt'} (\vec{v}') = - (1 + \varepsilon \theta') \nabla' \pi, \tag{2.10}$$

$$\varepsilon\beta \frac{d}{dt'}(w') = -(1 + \varepsilon\theta')\frac{\partial \pi}{\partial z'} - \rho \tag{2.11}$$

$$\frac{d}{dt'}\left[\ln(1 + \varepsilon\theta') + (1 - \frac{1}{\varkappa})\ln\pi\right] = \nabla' \cdot \vec{v}' + \frac{\partial w'}{\partial z'} \tag{2.12}$$

$$\varepsilon \frac{d}{dt'}(\theta') = \varepsilon \frac{Q'}{\pi} \left(= \frac{\tau Q}{c_p \pi (H)} \right) \tag{2.13}$$

A prime superscript indicates a non-dimensional variable. β is defined as

$$\beta = \frac{d}{H}, \tag{2.14}$$

where $H = c_p (H)/ g$. For typical values of (H) in the low atmosphere, H is about 30 km. The equations we derive will be valid only for the case $\beta \leq 1$.

In deriving (2.13), $c_p \Delta(H)/\tau$ is used to scale the non-adiabatic heating, Q.

3. THE ANELASTIC EQUATIONS

The basic approximation we apply is that ε is a small quantity, while all other variables, parameters, and differentiations are of order unity or smaller. We expand all dependent variables ($\vec{v}$, w', π, θ' and Q') as a power series in ε:

$$\vec{v}' = \vec{v}'_o + \varepsilon \vec{v}'_1 + \ldots, \text{ etc.} \tag{3.1}$$

Substituting these expressions into (2.10)~(2.13) and equating terms of zero order in ε, we get

$$\nabla' \pi_o = 0, \tag{3.2}$$

$$\frac{\partial \pi_o}{\partial z'} = -\beta, \tag{3.3}$$

$$(\frac{1}{\varkappa} - 1)\left(\frac{\partial}{\partial t'} + w'_o \frac{\partial}{\partial z'}\right) \ln \pi_o + \nabla' \cdot \vec{v}'_o + \frac{\partial w'_o}{\partial z'} = 0. \tag{3.4}$$

Equations (3.2) and (3.3) show that the π_o obtained this way corresponds to the π_o field in a hydrostatic atmosphere with a uniform θ equal to (H).

By assuming that the horizontally averaged value of the pressure at z=d is independent of time, we can eliminate the time derivative of $\ln \pi_o$ in the left hand side of (3.4). Then the continuity equation takes the form

$$\nabla' \cdot \rho_o \vec{v}'_o + \frac{\partial}{\partial z'} (\rho_o w'_o) = 0. \tag{3.5}$$

Next, we equate terms of 1st order in ε:

$$\beta \left(\frac{d'}{dt'} \right)_o (\vec{v}'_o) = - \nabla' \pi_1 , \tag{3.6}$$

$$\beta \left(\frac{d'}{dt'} \right)_o (w'_o) = - \frac{\partial \pi_1}{\partial z'} + \beta \theta'_o \tag{3.7}$$

$$\left(\frac{d}{dt} \right)_o (\theta'_o) = \frac{Q'_o}{\pi_o} , \tag{3.8}$$

with

$$\left(\frac{d'}{dt'} \right)_o = \frac{\partial}{\partial t'} + \vec{v}'_o \cdot \nabla + w'_o \frac{\partial}{\partial z'} . \tag{3.9}$$

These equations, together with the continuity equation (3.5), give four equations for the four unknowns $\vec{v}'_o$, w'_o, π_1, and θ'_o.

Equations (3.5) - (3.8) satisfy the following energy conservation equation:

$$\frac{\partial}{\partial t'} \int \rho_o \left[\frac{1}{2} \left(u'^2_o + v'^2_o + w'^2_o \right) - z' \theta'_o \right] d V' = - \int \frac{\rho_o z' Q'_o}{\pi_o} d V'. \tag{3.10}$$

If dimensional variables are introduced into (3.10), the term $-z'\theta'_o$ is multiplied by g, showing that this term represents a form of potential energy. For small perturbations, using the original equations (2.1)~(2.4), it can be shown that the total energy of the perturbations consists not only of kinetic and potential ("thermobaric") energy, but contains a term proportional to the square of the pressure perturbation (Eckart [3]). This latter form of energy is called"elastic" energy, and is missing from (3.10). For this reason it seems appropriate to give the name anelastic equations to (3.5)~(3.8).

Several additional remarks may be of interest. First, by assuming wave-type solutions for the linearized version of (3.5)~(3.8), it is easy to demonstrate that the anelastic equations do not contain frequencies larger than N.

Secondly, when β is also a small quantity, we can expand all dependent variables in the anelastic equations as a power series in β, substitute them into the anelastic equations, and equate terms of zero and 1st order in β respectively. The resulting form of the continuity equation (3.5) turns out to be identical with that for an incompressible fluid, and the remaining equations become identical with the well known Boussinesq equations of motion.

4. THE RELEASE OF LATENT HEAT

Defining a mixing ratio w *:

$$w^* = \frac{\rho_\ell + \rho_v}{\rho_o}, \tag{4.1}$$

(ρ_ℓ : mass of liquid water per unit volume, ρ_v : mass of water vapor per unit volume,) we postulate the following law for w*:

$$\frac{dw^*}{dt} = 0. \tag{4.2}$$

The total specific entropy for moist air may be expressed approximately by

$$\bar{\Phi} = c_p \varepsilon \theta'_o + \left(\frac{\rho_v}{\rho_o} \right) \frac{L}{\bar{T}} \tag{4.3}$$

where $\bar{T}$ is a suitable mean temperature and L is the latent heat. For a reversible process, $\bar{\Phi}$ is conserved

$$\frac{d\bar{\Phi}}{dt} = 0 \tag{4.4}$$

For unsaturated air, $\rho_\ell = 0$ and $w^* = \rho_v / \rho_o$. (4.3) becomes

$$\bar{\Phi}_{unsat} = c_p \varepsilon \theta'_o + \frac{L}{\bar{T}} w^* . \tag{4.5}$$

For saturated air we have

$$\frac{\rho_v}{\rho_o} = \frac{\rho_{vs}}{\rho_o} \leq w^*, \tag{4.6}$$

where ρ_{vs} is the saturation value of ρ_v:

$$\rho_{vs} = \frac{e_s(T)}{R_v T}, \tag{4.7}$$

R_v is the gas constant for water vapor, while e_s is the saturation vapor pressure. Setting T equal to $T_o + \varepsilon T_1$, we find

$$\rho_{vs} \simeq \frac{e_s(T_o)}{R_v T_o} \left[1 + \frac{\varepsilon T_1}{T_o} \left(\frac{L}{R_v \bar{T}} \right) \right]. \tag{4.8}$$

Since the ratio $L/ R_v \bar{T}$ is large (~ 20) for water vapor at atmospheric temperature, the ε term in the bracket in (4.8) cannot be neglected. Intro-

ducing the relation $T_1 \sim T_o\ (\theta_o' + \varkappa \pi_1 / \pi_o)$ which can be obtained from (2.6), (2.7), and (3.1), we have

$$\frac{\rho_{vs}}{\rho_o} = 0.622\ \frac{e_s(T_o)}{\rho_o}\ [\ 1 + \frac{\xi L}{R_v \bar{T}}\ (\theta_o' + \varkappa \frac{\pi_1}{\pi_o}\ )]. \tag{4.9}$$

This equation demonstrates that we cannot evaluate ρ_{vs}/ρ_o without a knowledge of both θ_o' and π_1/π_o. However, π_1 must be determined from the solution of an elliptic equation, since w_o' and $\vec{v}_o'$ must always satisfy (3.5). This equation is of the form

$$\nabla' \cdot \nabla' (\rho_o \pi_1) + \frac{\partial}{\partial z'}\ (\ \rho_o\ \frac{\partial \pi_1}{\partial z'}\ ) = g\ (\ x', y', z'), \tag{4.10}$$

where $g(x',y',z')$ is a non-linear function of not only $\vec{v}_o'$, w_o', and their derivatives, but also of the vertical derivative of θ_o'. θ_o' is determined by Φ, but the relation between θ_o' and Φ depends on the saturation criterion (4.6). Therefore, to evaluate θ_o' and π_1 (and eventually to determine the occurrence of saturation), a suitable numerical iteration process would seem to be necessary.

REFERENCES

1. G. K. Batchelor, "The Conditions for Dynamical Similarity of Motions of a Frictionless Perfect-Gas Atmosphere," Quarterly Journal of the Royal Meteorological Society, vol. 79, No. 340, Apr. 1953, pp. 224-235.
2. J. Charney and Y. Ogura, Paper presented at International Symposium on Numerical Weather Prediction, Tokyo, Nov. 1960.
3. C. Eckart, Hydrodynamics of Oceans and Atmospheres, Pergamon Press, New York, 1960, 290 pp.

ON THE ROLE OF CONVECTION IN HURRICANES

N. E. La Seur
Florida State University, Tallahassee, Florida

Since 1955, participation in research aircraft reconnaissance of hurricanes, and in the analysis of data thereby collected, have left one impression which stands out above all others. This is the importance of convection in these storms. Of course, the idea that convection is a significant characteristic of hurricanes is neither new nor original. Historically, it can certainly be traced back as far as Espy more than a century ago, and in recent years the utilization of radar has revealed increasing evidence of its significance. Thus, it was not surprising to encounter convection in these storms, rather it has been the degree of its importance - the dominance of its role - which has been so impressive. This is especially true of the annular ring of convection which surrounds the eye; indeed, this characteristic is perhaps the best criterion for distinguishing the relatively rare hurricane from the much more numerous tropical disturbances.

Although I speak now only of my own concept of a hurricane prior to the first-hand encounters provided by reconnaissance experience of the past five years, I believe it was shared by many others. This concept was that although convection occurred in hurricanes, and in a highly organized fashion such as spiral bands, its role in the storm was secondary to that of synoptic-scale processes, and that probably it was primarily a manifestation of the fact that the tropical air was convectively unstable. Certainly one of the major advances in our knowledge of hurricanes has been the establishment that they have a synoptic life-cycle, and form only in pre-existing, recognizable synoptic-scale disturbances. The experiences mentioned above, however, have altered my own beliefs to the point of view that, beyond a certain stage, it is convective - rather than synoptic - scale motions which play the primary role in determining the structure and formation of hurricanes, and probably play a significant role in their motion. The purpose of this discussion is to present such evidence as I could gather in support of this idea.

First, let us consider some data which I believe illustrate rather explicitly the important role of convection in determining hurricane structure. The first four figures were prepared from a flight at 500 mb. into hurricane Ione of 1955. It was this flight and the subsequent analysis of these data which first prompted an upward revision in my own estimate of the importance of convection in hurricanes. The essential points illustrated are:

(1) Despite the large size of Ione at 500 mb. (diameter 600 n. mi.) it is only in an extremely small fraction of this area (about 60-100 miles in diameter) that the various meteorological parameters assume values characteristic of a hurricane.

(2) This inner 1 to 3 percent of the area is dominated by the annular ring of convection which encloses the eye.

(3) Hydrostatically, the pressure field in the mid-troposphere must be associated with relatively warm air in the upper troposphere, and the evidence

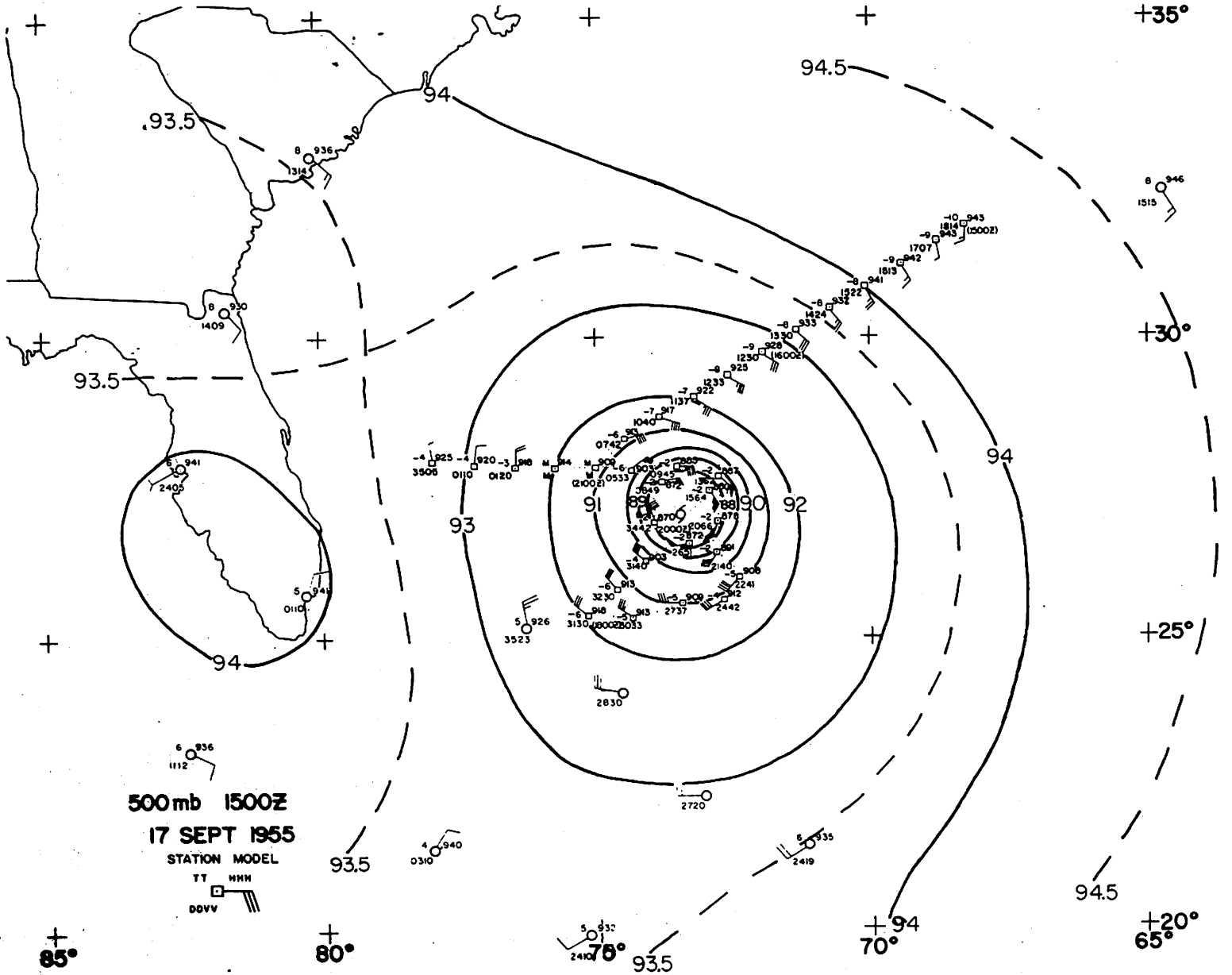

Figure 1. - Synoptic scale view of Ione on Sept. 17, 1955. Analysis based on available upper-air reports and aircraft reports at 10 minute intervals.

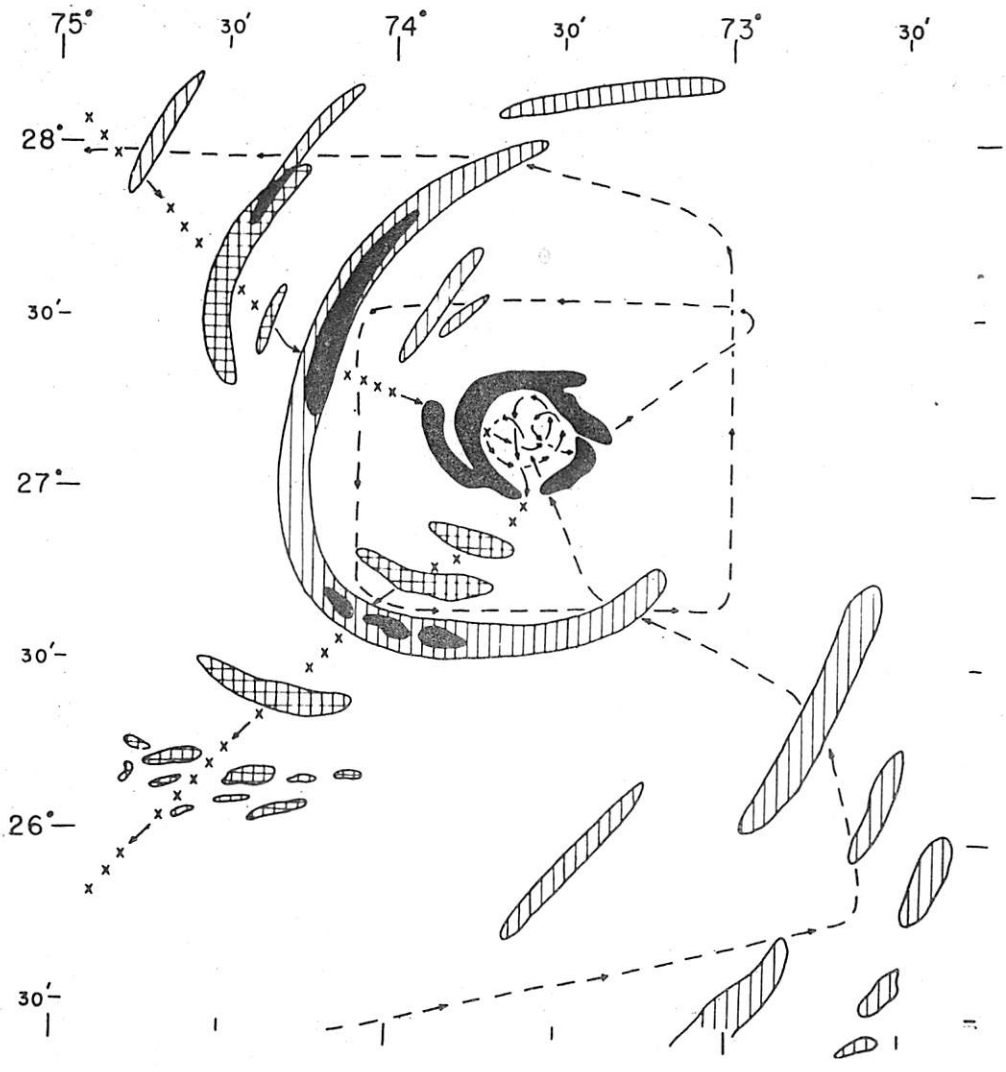

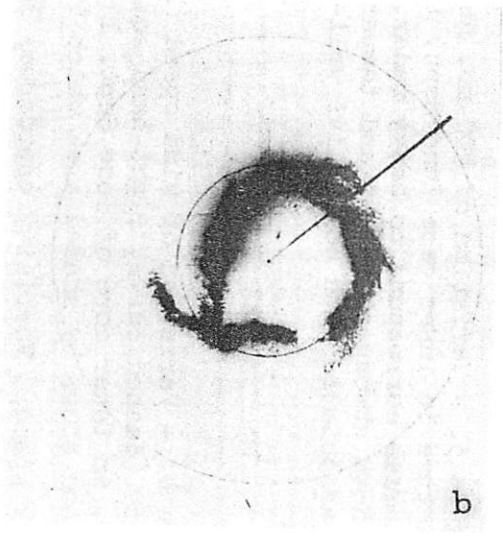

Figure 2. - Illustration of "strong" radar echoes in Ione, Sept. 15, 1955. (a) All such echoes observed within about 100 n.mi. of center as plane flew along track indicated. (b) Actual PPI scope photograph of annular echo around eye. Range marks are 20 n.mi., north is at top , and plane is located at center dot within eye heading as indicated by straight line. Visual wall cloud with which radar echo is associated rose almost vertically to an estimated 50,000 ft.

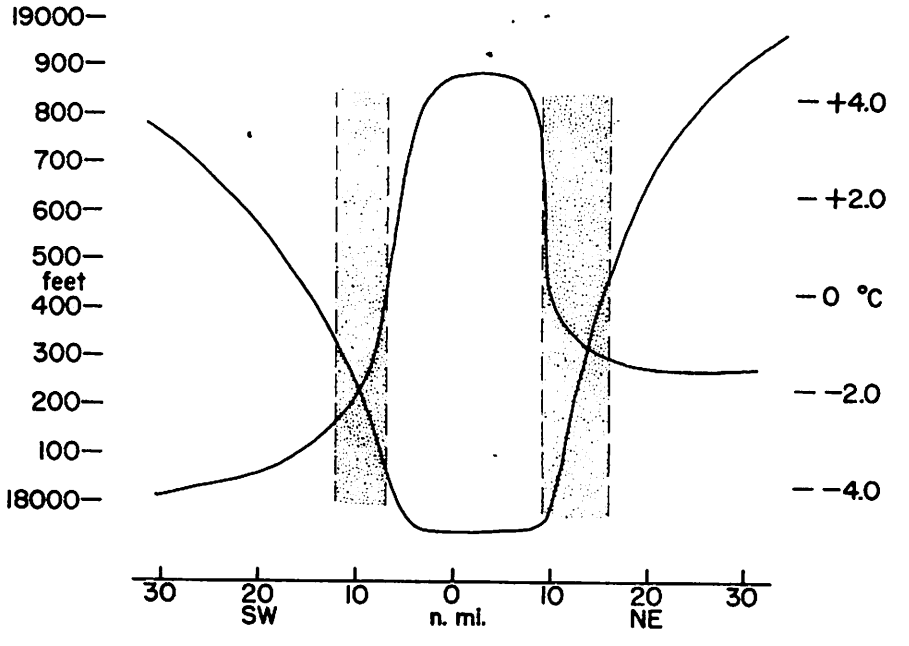

Figure 3. - Variation of 500-mb. height and temperature in inner case Ione Sept. 17, 1955. Shaded areas correspond to heavy radar echo of figure 2b. Note strongest height and temperature gradients associated with convective wall-cloud.

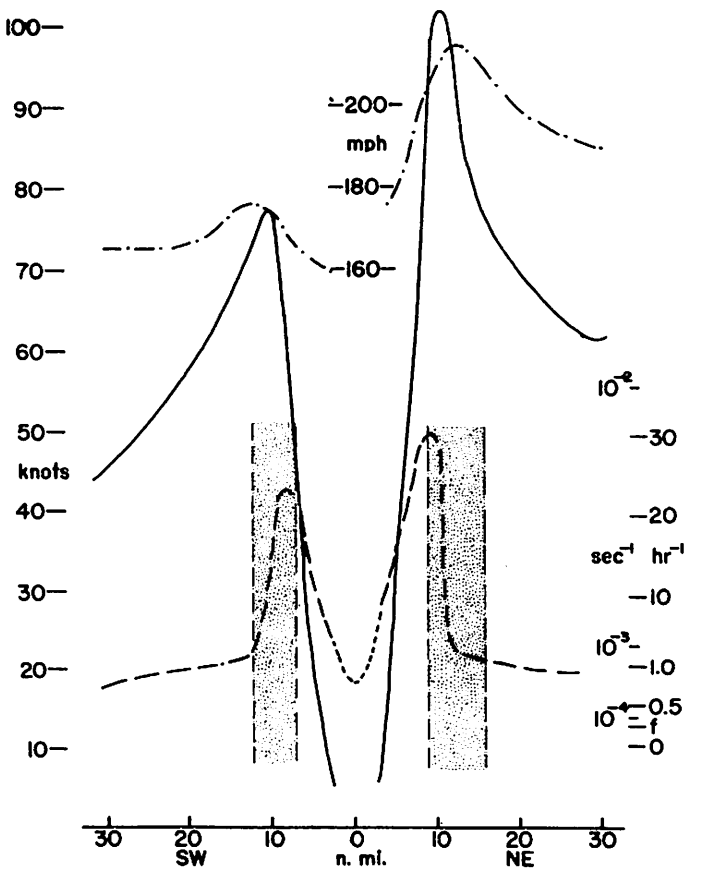

Figure 4. - Variation of wind speed (solid curve, left-hand scale), vertical component of absolute vorticity (dashed curve, right-hand scale), and indicated air speed (dash-dot curve, center scale), at 500 mb. in inner core of Ione Sept. 17, 1955. Note hurricane force winds are confined to region of wall cloud shown by shaded area which is also region of strong updraft as shown by increases in indicated air speed. Vorticity approaches 10^{-2} sec.$^{-1}$ at inner edge of eye characteristic of convective rather than synoptic-scale motion.

at this level suggests that it is convective rather than synoptic-scale motions which are producing the warm air aloft.

Supplementary comments can be found in the figure captions.

Obviously data from only one level are incomplete and inconclusive. The first opportunity to analyze nearly synoptic information from several levels was provided by the successful three-level reconnaissance of hurricane Cleo of 1958 by NHRP aircraft. A small portion of these analyses which is pertinent to the present discussion is given in figures 5-8. The important additional points illustrated by these figures are:

(4) The pattern of temperature anomalies from mean tropical conditions suggests strongly that convection in the eye-wall is the dominant mechanism in their production and distribution even on a synoptic scale;

(5) That, in turn, these convectively produced temperature anomalies account hydrostatically for the pressure field also on a synoptic scale.

Again supplementary remarks are included in the individual figure captions and a more complete discussion will be available shortly in the NHRP Preprint Series.

If we now grant that the convective eye wall cloud is an essential structural characteristic of a hurricane, it is then logical to conclude that convective-scale processes, perhaps of a particular organized type, play a significant role in its development and, therefore, in hurricane formation. Furthermore, since strong convective bands are typically found 100-200 miles distant from the center of the synoptic-scale disturbances in which hurricanes form, we should expect that eye formation usually occurs some distance away from the center of the synoptic-scale system. Conclusive evidence that these hypotheses are valid is not easy to obtain. Some available sequences of radar observations strongly suggest that eye formation is associated with strong convective bands, but they alone do not show the separation in distance from the synoptic center. Figures 9-13 show data for the case which is the best illustration of these hypotheses that I have been able to locate. Reconnaissance data, ship reports, and radar observations are shown without analysis to avoid bias in their interpretation.

I believe it is reasonable to interpret these data from the formative stages of Judith (1959) as follows:

(6) The center of the synoptic-scale disturbance remains distinct from the location of the incipient (but never quite successful) eye formation which occurs in association with bands of convection some 150 n. mi. away.

(7) It is of a size and structure which suggests strongly that convective scale processes play a significant causal role in its formation.

Additional comments are again included in the individual figure captions.

Finally, I would like to show you some measurements obtained on a low-level traverse through a strong convective band in hurricane Edith in 1955.

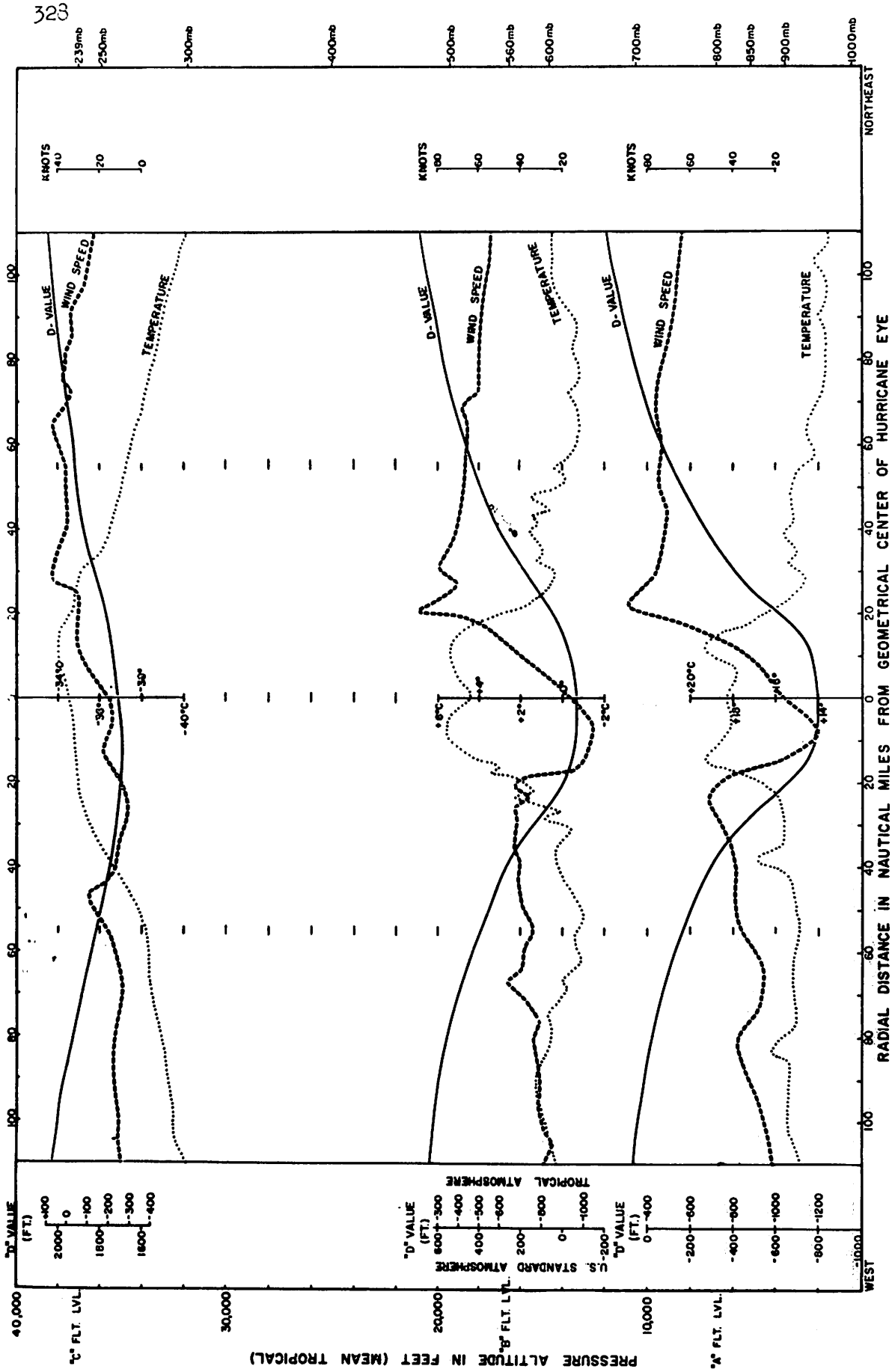

Figure 5. - Variation of wind speed (scales on right), "D" value (left scales), and temperature (center scales) at three flight levels in inner core of Cleo Aug. 18, 1958. Strongest gradients and extreme values again associated with convective eye region.

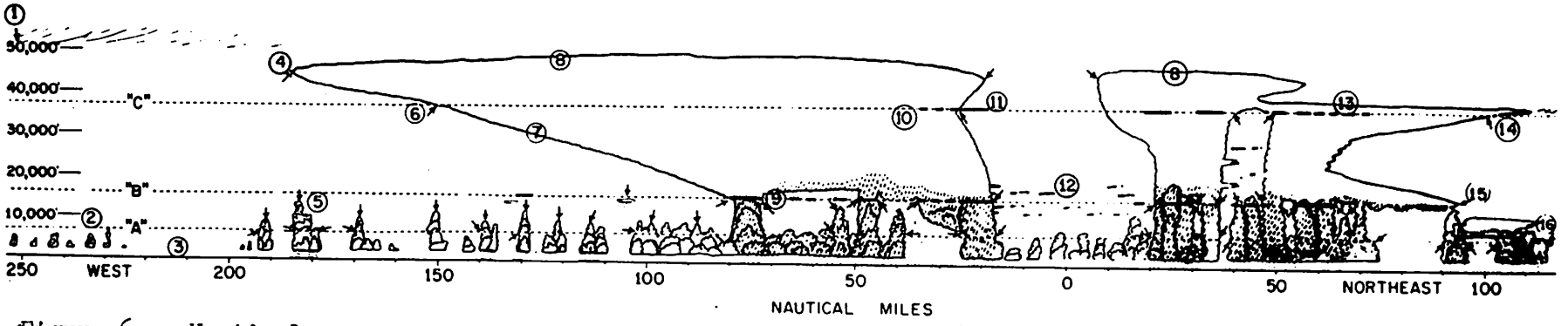

Figure 6. - Vertical cross section through Cleo Aug. 18, 1958 showing cloud structure and heavier radar echoes. Note that convection is concentrated in inner portion of storm, especially in wall cloud around eye.

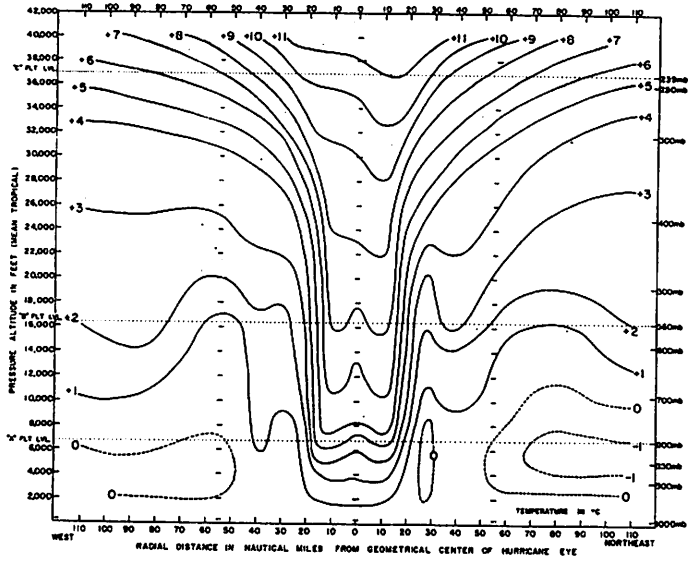

Figure 7. - Vertical cross section of temperature anomaly from mean tropical conditions in Cleo Aug.18, 1958. Pattern suggests these anomalies produced by latent heat released in convective ascent in eye wall spreading out and mixing with environment in upper outflow layer.

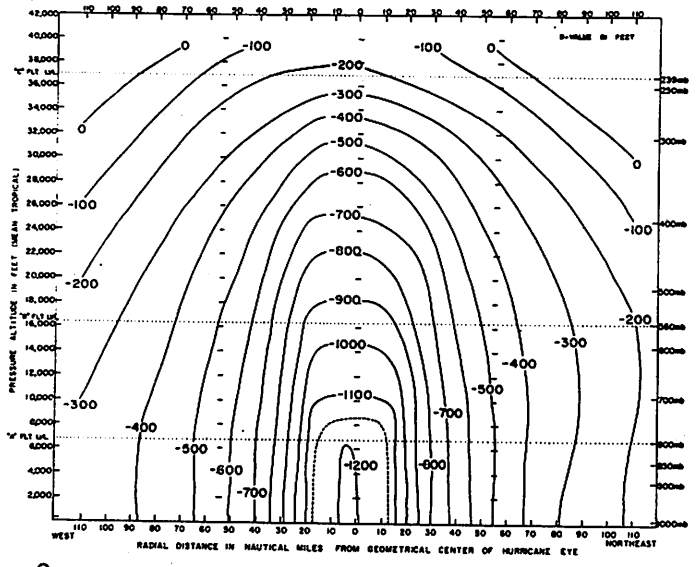

Figure 8. - Vertical cross section of height anomaly ("D" value) from mean tropical conditions in Cleo Aug. 18, 1958. Comparison with figure 7 reveals large negative "D" values in lower levels are due hydrostatically to large positive temperature anomalies in upper troposphere.

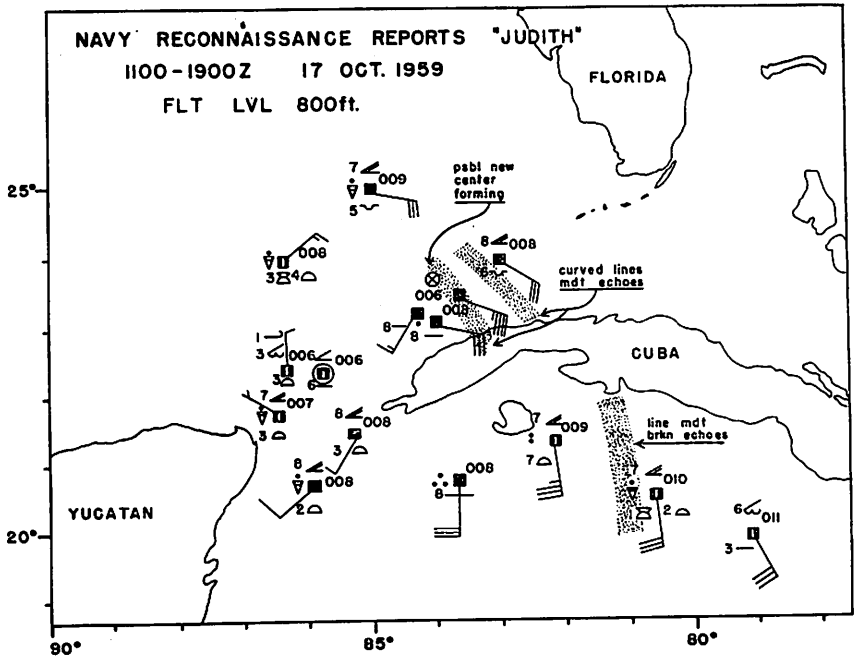

Figure 9. - Low-level reconnaissance reports from Navy flight into Judith in early formative stage. Note tropical storm structure with major convective bands 100-200 n. mi. from center. Last report from aircraft leaving storm reports possible new center forming near radar band 150 mi. NE synoptic center.

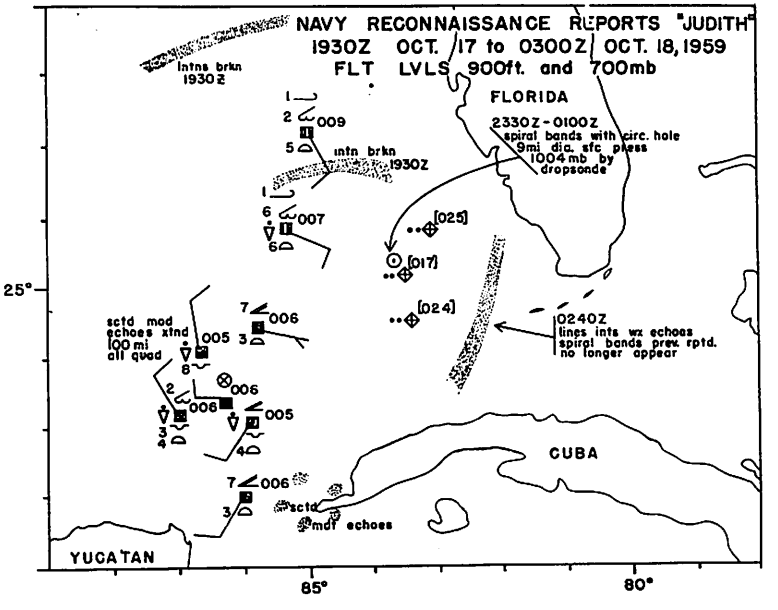

Figure 10. - Reconnaissance reports from Navy flight into Judith at low levels and at 700 mb. Note synoptic center fixed by low-level winds and pressures and report of short-lived spiral bands (orientation unspecified) and circular hole in echo pattern 175 n. mi. from synoptic center.

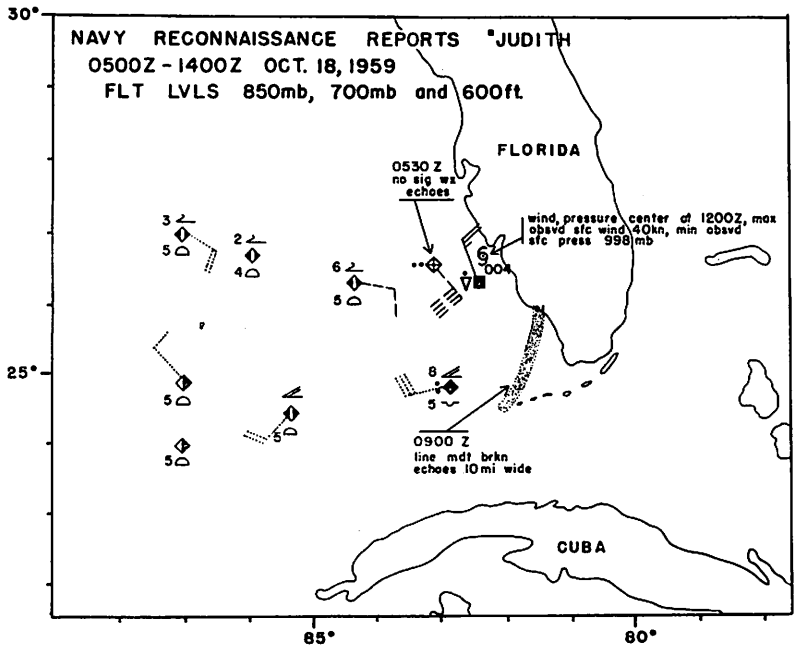

Figure 11. - Reports from third Navy reconnaissance of Judith. Note center of synoptic scale cyclone at 700 mb. near NW portion of flight far from eye centered just off Florida coast.

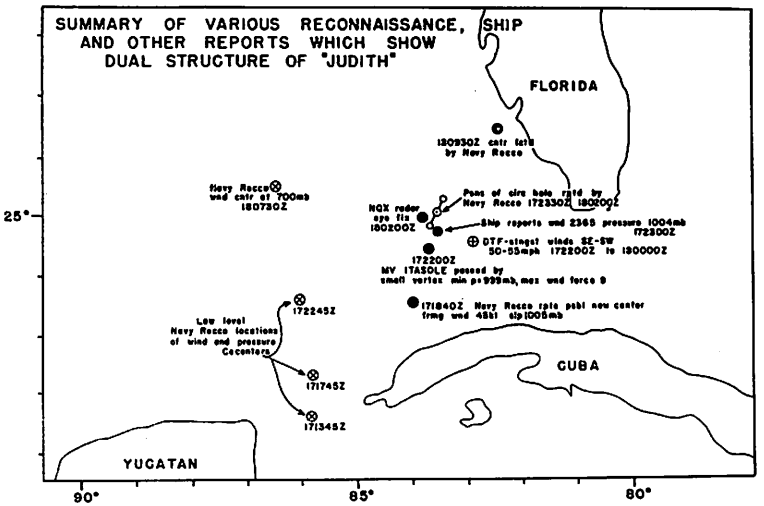

Figure 12. - Summary of various reports which show separation of synoptic and convective centers in Judith. Following complete report from MV ITALSOLE: "24.5N 83.7W at 172200Z, brisk fall of barometer from 1008.5 to 999.3 mb. Sudden wind up to force nine from ESE veering gradually to SW in about half an hour. Actually at 2220Z barometer raised to 1003.7 mb. and still rising," illustrates small size of convective center 150 mi. from synoptic center located at 172245 GMT by low level Navy reconnaissance.

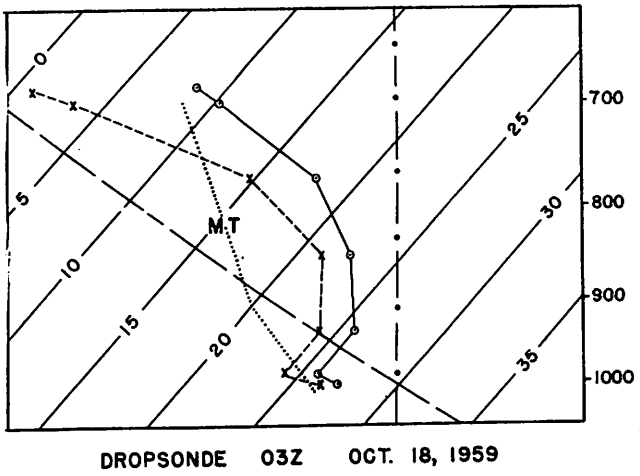

Figure 13. - Portion of Skew T - log diagram showing temperature (solid curve) and dew point (dashed curve) obtained by dropsonde in or very near circular hole in radar echo reported on second Navy flight (see fig. 10). Note large positive anomaly of temperature from mean tropical conditions (dotted curve) which, in view of high dew points, were probably produced by convective ascent.

At this stage in her development Edith did not have a true eye; but outside a region some 100 n.mi. in diameter with cyclonic winds less than 30 kt. and broken clouds below 10,000 ft., there occurred at least four convective band segments in which winds exceeded hurricane force with heavy rain.

Data in figure 14 clearly show the large variations in horizontal wind superimposed on the synoptic scale flow by the convective band. These are accompanied by an increase of an order of magnitude in the divergence and vertical motion plus, of course, increased rainfall intensity and turbulence. I would like to conclude this portion of the discussion by stating my conviction that such convective-scale processes are a necessary factor in the formation and maintenance of the hurricane eye structure. I would add that this view is not inconsistent with what is known about the converse phenomenon of dissipation. Factors which have been proposed as contributing to dissipation, such as, invasion by cooler, drier air, elimination of oceanic heat source after movement over land, and large vertical shear of the horizontal wind, are all factors which inhibit convection. A further implication of this view is that formation (or dissipation) may occur more rapidly than would be expected if only synoptic influences were operative. Judith, Debra and Ethel of the past two seasons, which all underwent very rapid changes of intensity, may be cited as examples. The fact that these storms all occurred close to coastal areas points to the value of radar surveillance to the warning service.

Although I have no observational evidence to present in support of the contention, it is also logical to conclude that convection should play a significant role in hurricane motion. Just as it has been a step forward to view the motion of extratropical cyclones as the differential result of synoptic-scale factors which create the cyclone on one side and destroy it on another, we should view hurricane motion in the same way rather than as an object "carried" along by the surrounding flow. Since hurricane motion is essentially the movement of the eye which has been shown to be a convective-scale structure, it seems inevitable that convective processes should be important. However, their role is likely to be more subtle and indirect insofar as motion is concerned, and to involve rather complex interactions with their synoptic-scale environment. For example: the height reached by convective ascent in the eye wall before it spreads out and mixes with the environ-

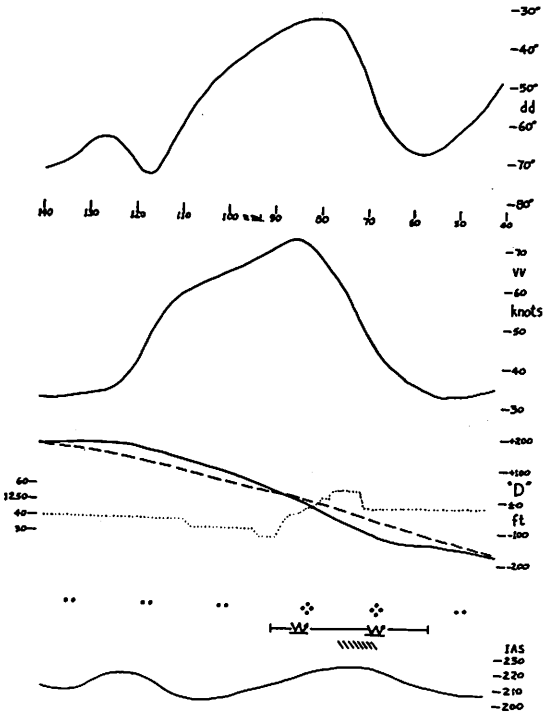

Figure 14. - Variation of wind direction, wind speed, "D" value, pressure altitude, and indicated air speed on N-S traverse under strong E-W oriented band of convection in Edith Aug. 27, 1955. Note strong difluence just N of band and strong confluence (50×10^{-5} sec.$^{-1}$) in band. Vertical motion downward in difluent region and upward in confluence as shown by variation in indicated air speed and pressure altitude. "D" value curve suggests slight trough under band and slight ridge to north.

ment may vary considerably and, since upper tropospheric flow patterns in the vicinity of hurricanes change rapidly with height, the resulting influence on storm motion could be significantly different. I suspect that any direct influences of convection on hurricane motion are associated with the short-period oscillations about a smooth track which are sometimes observed.

In closing I would like to express the hope that more of you are now better convinced that convection is not just a passive manifestation of the convective instability of the tropical air in hurricanes. Rather that, under appropriate circumstances and with the proper degree of organization, it plays an active and necessary role in hurricane structure, formation, and motion. Belief in the latter point of view suggests several recommendations for future research:

1. Further multi-level investigation of the eye and its wall-cloud to determine more completely the role of convective processes in hurricane structure and motion. Two levels at which data are now meager, the inflow layer

(say 1000 ft.) and the upper outflow (near the tropopause), deserve special effort. Preferably data should include calibrated radar (both PPI and RHI) photographs which can be interpreted in terms of liquid water content, and, if feasible, direct measurement of vertical velocity and liquid and solid water content.

2. Research reconnaissance of developing storms for both synoptic-scale information and detailed data from convective bands embedded within the disturbance. Several such flights in cases where eye development occurs, and in cases where it does not, may reveal those factors which organize convection into bands and the degree and type of organization necessary before convective-scale processes can play a role in eye formation.

3. Theoretical studies of the synoptic scale factors which may initiate and organize convective scale motions into bands, and of the dynamics and kinematics of such bands which may result in eye formation.

ON THE BALANCE OF FORCES AND RADIAL ACCELERATIONS IN HURRICANES

(A Condensed Version*)

William M. Gray
The University of Chicago

When the National Hurricane Research Project of the U. S. Weather Bureau began flying through hurricanes during the 1956-57 seasons, it was noticed by some of the meteorologists aboard, particularly by Prof. Herbert Riehl, that the winds and pressure gradients along many of the radial leg penetrations did not always vary in a similar fashion. At certain times the wind speed would change appreciably yet the pressure gradients would remain nearly constant and vice versa. Certain radial force imbalances must be occurring.

The NHRP flights that were made during the 1957-58 seasons are especially well suited for an investigation of this feature to determine the amount and character of these apparent imbalances which were occurring above the surface friction layer.

Flights at 10 pressure levels on 8 separate days in 4 different storms are available in which 6 or more radial legs into or out of the storm eyes were flown, except for 1 level which has 5 radial legs (table 1). All these levels were between 6,000 and 15,000 ft., at heights where it has usually been supposed that gradient or near gradient wind flow should prevail. Figure 1 is typical of the kind of radial leg flown.

In this study cylindrical coordinates are used throughout, and the assumption that the storms remained essentially in a steady state for the duration of the flights is made. The first step taken was to plot the "D" values and the tangential wind components along the constant pressure radial legs flown (fig. 2 and 3).

The radial cylindrical equation of motion on a constant pressure surface with respect to an instantaneously fixed coordinate system with origin corresponding to the storm center is

$$\frac{dv_r}{dt} = - g \frac{\partial D}{\partial r} + f v_\theta + \frac{v_\theta^2}{r} + F_r \qquad (1)$$

where v_r and v_θ are the radial and tangential wind components
r is distance along the radial leg - positive outward
D stands for height deviations from the standard atmosphere
f is the Coriolis parameter
t is time
F_r is the radial component of friction.

*The full text of this paper is reproduced as Atmospheric Sciences Report, No. 1, Colorado State University, Fort Collins, Colorado, Feb. 1961.

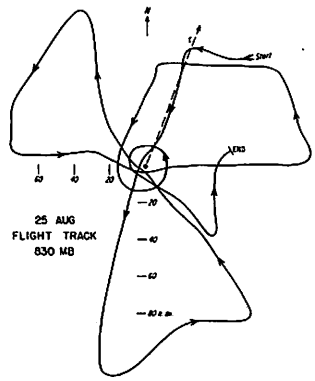

Figure 1. - Typical radial leg path.

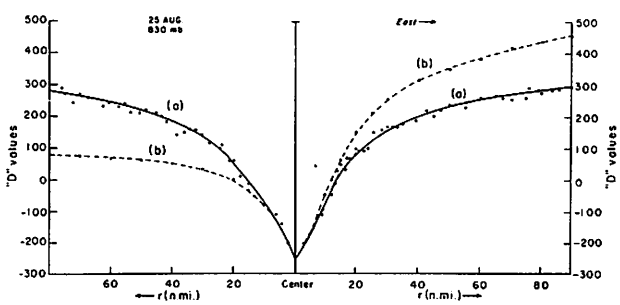

Figure 2. - Example of "D" value plot.

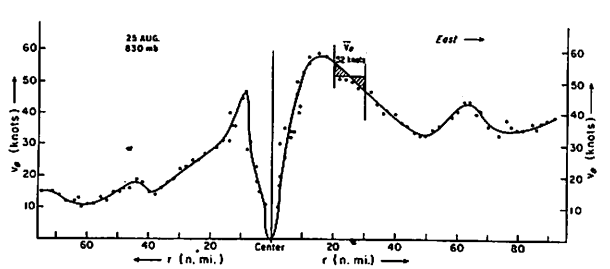

Figure 3. - Example of tangential wind plot.

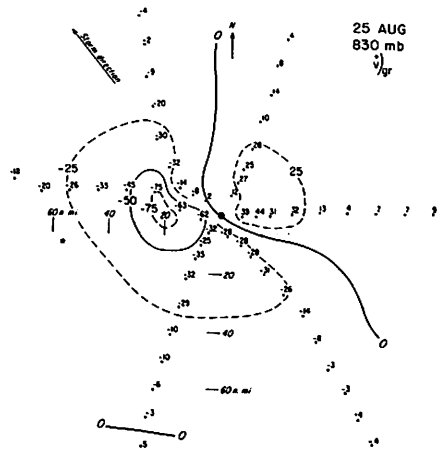

Figure 4. - Radial Wind component.

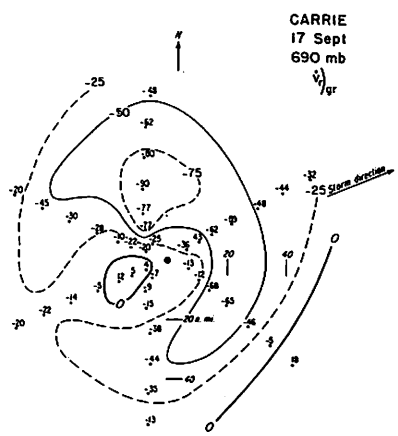

Figure 5. - Radial wind component.

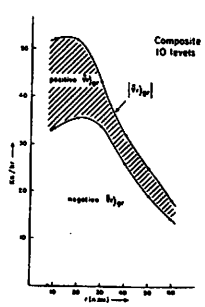

Figure 6. - Showing predominance of pressure gradient over centrifugal and Coriolis forces.

Table 1.

Storm, Date and Level	Max. Wind Right Quad. (knots)	Max. Wind Left Quad. (knots)	Difference Right-Left Quad.(kt.)	Speed of Storm X Two (kt.)	Column 4 / Column 5 (kt.)
1. Daisy 25 Aug 830 mb.	65	35	30	14	≈2
2. Daisy 25 Aug 570 mb.	60	45	15	14	≈1
3. Daisy 27 Aug 630 mb.	120	85	35	16	≈2
4. Daisy 28 Aug 620 mb.	105	55	50	36	≈1-1/2
5. Cleo 18 Aug 820 mb.	90	50	40	28	≈1-1/2
6. Cleo 18 Aug 570 mb.	85	45	40	28	≈1-1/2
7. Carrie 15 Aug 965 mb.	85	50	35	24	≈1-1/2
8. Carrie 17 Aug 970 mb.	95	65	30	26	≈1-1/4
9. Helene 24 Sept 635 mb.	60	55	5	20	≈ 1/4
10. Helene 25 Sept 810 mb.	80	55	25	12	≈2

If we define $\dot{v}_r)_{gr} = \frac{dv_r}{dt} - F_r$, then the radial imbalance is given by

$$\dot{v}_r)_{gr} = - g \frac{\partial D}{\partial r} + f v_\theta + \frac{v_\theta^2}{r} \qquad (2)$$

The three terms on the right were integrated along the radial legs over 10 n.mi. intervals as

$$\int_{r_1}^{r_2} g \frac{\partial D}{\partial r} \, dr = g(D_2 - D_1)$$

$$\int_{r_1}^{r_2} \frac{v_\theta^2}{r} \, dr = \overline{v_\theta^2} \ln \frac{r_2}{r_1}$$

$$\int_{r_1}^{r_2} f \, v_\theta \, dr = f \, \overline{v_\theta} \, (r_2 - r_1)$$

where the bar signifies a radial mean.

The resulting mean radial leg imbalances in finite difference form are then given by

$$\overline{\dot{v}_r}\Big)_{gr} = -\,g\,(D_2 - D_1) + \overline{v_\theta^2}\,\ln\frac{r_2}{r_1} + f\,\overline{v_\theta}\,(r_2 - r_1) \qquad (3)$$

Values of these radial accelerations with respect to the instantaneously fixed center were computed along all of the radial legs. On nearly all the 61 radial legs there was a substantial lack of radial balance. In a few cases the imbalances were even larger than the combined centrifugal and Coriolis forces. Figures 4 and 5 show typical values for the individual levels. Negative values of $\overline{\dot{v}_r}\Big)_{gr}$ were much more prevalent than positive values. The winds were thus weaker than that required for gradient wind balance. Figure 6 illustrates this predominance of pressure gradient over centrifugal and Coriolis forces.

From equation (1) it can be seen that this imbalance may be accounted for by the local and advective changes of the substantial derivative, dv_r/dt, by internal radial friction F_r, or by a combination of the two. As all flights were above the surface friction layer, it was originally thought that the substantial derivative would account for this radial imbalance. This was not the case however. The local and advective changes of the substantial derivative are given by

$$\frac{dv_r}{dt} = \frac{\partial v_r}{\partial t} + v_\theta\,\frac{\partial v_r}{r\partial\theta} + v_r\,\frac{\partial v_r}{\partial r} + w\,\frac{\partial v_r}{\partial z}$$

This term was computed and compared with the radial imbalances. It accounted on the average for approximately half of the radial imbalance. The other half of the imbalance must then be made up by internal radial friction (F_r) due to eddies. The frictional acceleration is gotten by subtracting equation (2) from equation (1); i.e. $F_r = \frac{dv_r}{dt} - \dot{v}_r\Big)_{gr}$.

Figure 7 shows a composite without respect to sign of all 10 levels of the pressure gradient force, centrifugal and Coriolis forces, $\overline{\dot{v}_r}\Big)_{gr}$, and F_r plotted against radius.

The above calculations have shown the radial accelerations with respect to an instantaneously fixed coordinate center. It might be thought that a calculation of the acceleration with respect to the moving storm center might substantially reduce these imbalances. These calculations were made under the assumption that the storms move at constant speed and direction (which they all closely approximated). The imbalances can then be calculated by subtracting the component of the storm motion from each wind and performing the same calculations as with the imbalances with respect to the fixed storm center. These accelerations are denoted $\overline{\dot{v}_{rr}}\Big)_{gr}$.

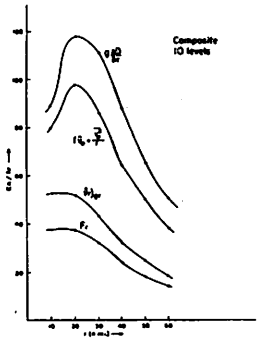

Figure 7. - Radial imbalance.

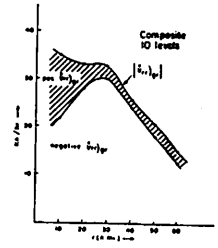

Figure 8. - Same as figure 6 but for moving storm center.

The resulting radial imbalances with respect to the moving storm center differed noticeably but not significantly from those of the $\overline{\dot{v}_r}\Big)_{gr}$ values as follows - -

(1) The values with respect to the moving center were generally 60 to 80 percent of those with respect to the instantaneously fixed center.

(2) The positions of many of the $\overline{\dot{v}_{rr}}\Big)_{gr}$ centers were shifted from those of the $\overline{\dot{v}_r}\Big)_{gr}$ centers.

(3) There was greater predominance of negative $\overline{\dot{v}_{rr}}\Big)_{gr}$ than $\overline{\dot{v}_r}\Big)_{gr}$ (fig.8).

The conclusion seems unavoidable that large amounts of internal radial friction are present in the hurricane. It follows immediately from this that the gradient wind equation in both cyclindrical and natural coordinates does not closely approximate the balance of forces in hurricanes.

An order of magnitude estimate of radial friction using the cylindrical Navier-Stokes radial friction term

$$\nu\left[\frac{\partial^2 v_r}{\partial r^2} + \frac{\partial}{\partial r}\left(\frac{v_r}{r}\right) + \frac{\partial^2 v_r}{\partial z^2}\right]$$

and taking ν (coefficient of eddy viscosity) to be 10^4 cm.^{2}/ sec. does not give the required frictional magnitudes. Calculations fall 2 to 3 orders of magnitude below the value required for F_r by the above calculations.

One should probably look at the friction from the Reynolds stress point of view where space means and deviations are used. In cyclindrical coordinates F_r then has four terms

$$\frac{\partial \widetilde{v'_\theta v'_r}}{r\partial\theta}, \quad \frac{\partial \widetilde{rv'^2_r}}{r\partial r}, \quad \frac{\partial \widetilde{v'_r w'}}{\partial z}, \quad \frac{\widetilde{v'^2_\theta}}{r}$$

where the wavy bar denotes an area average and the prime represents deviations from the area mean.

In this form the term $\frac{\partial \widetilde{v_r' w'}}{\partial z}$ would be the vertical gradient of the horizontal integrated product of the radial and vertical wind eddies.

Evaluation of v_r' and v_θ' values and their tangential and horizontal gradient was made on a number of mid-tropospheric levels here studied from continuous recordings from pitot tubes which the University of Chicago Cloud Physics Section had mounted on the aircraft during the 1957-58 seasons. These pitots measure changes in atmospheric pressure as the aircraft travel along the radial and tangential legs. These minute pressure changes are converted into their equivalent eddy wind variations. From such information the Reynolds stresses can be computed.

From the preliminary computations $\frac{\partial \overline{v_\theta' v_r'}}{r\partial\theta}$, $\frac{\partial \overline{rv_r'^2}}{r\partial r}$ and $\frac{\overline{v_\theta'^2}}{r}$ turn out to be quite small and cannot account for F_r. An order of magnitude estimate of the $\frac{\partial \overline{v_r' w'}}{\partial z}$ term, using determined values of v_r' from the pitot tubes and assuming Malkus' and Riehl's calculations of vertical velocities in hurricane Cb's, indicates that this term may have the required magnitude.

Vertical gradients of $\overline{v_r' w'}$ were determined with a two-layer model; i.e., estimates were made for the mid-tropospheric levels and zero values were assumed for the surface and the tropopause. This is a crude approximation, but it encourages one to seek further experimental data. With improved sampling and measuring techniques a reliable estimate of the importance of the $\frac{\partial \overline{v_r' w'}}{\partial z}$ term can be achieved. New instrumentation and special flight planning with NHRP aircraft are being contemplated for the 1961 and 1962 seasons with this purpose in mind.

CHANGES IN THE EYE PROPERTIES DURING THE LIFE CYCLE OF TROPICAL HURRICANES

José A. Colón
National Hurricane Research Project, Miami, Fla.

1. INTRODUCTION

Studies on the dynamics and thermodynamics of hurricanes have made it increasingly clear that the air motions in the eye are of considerable importance in the development and maintenance of the hurricane circulation. Significant contributions to this subject have been made recently by Riehl [20], Palmén [17], Malkus [15], Miller [16], Riehl and Malkus [22], Kuo [11], and by C. L. Jordan in a series of well-known papers [6, 7, 8, 9, 10]. The importance of the eye was emphasized by Riehl and Malkus [22], who showed, by means of hydrostatic computations, that central pressures below about 960 mb. require the type of temperature distribution that can only be produced by subsidence in the interior of the eye. This of course, does not limit the importance of subsidence to cases in which the central pressure is that low.

In view of the importance that has been ascribed to the eye, it was considered of interest to examine the time variations in the thermal and moisture properties of the eye during the evolution of intense hurricanes and to try to develop a clear understanding of the manner in which these variations are produced. Adequate observations, by dropsondes released within the eye by military reconnaissance aircraft, and flight level data obtained by the NHRP research planes, are available for hurricanes Daisy and Helene of 1958, both of which attained central pressures below 950 mb. A total of 14 dropsondes were made in the eye of hurricane Daisy and 24 in the eye of Helene; most of them were released in the vicinity of the 700-mb. level. Some remarks on the general accuracy of the data are included in a later section.

The changes in the eye properties during the intensification and dissipation stages of these two hurricanes were studied in a coordinate system moving with the eye center. The results are presented below. A qualitative discussion is then presented of the mechanisms which produce the observed variations in the eye and their relation to the deepening and dissipation processes. This discussion emphasizes the importance of the vertical circulations in the eye core in the evolution of tropical storms.

2. CHANGES IN THE PROPERTIES OF THE DAISY EYE

The variations in intensity of hurricane Daisy are shown in figure 1, where we notice that the central pressure dropped steadily from about 1002 mb. at 2300 GMT on August 24 to a minimum of 948 mb. late on August 27, then increased to a value of about 985 mb. on August 29. In the following discussion the period during which the central pressure was decreasing will be referred to as the deepening or intensification stage; the interval when the pressure was filling is called dissipation stage. Figure 2 contains the track of Daisy superimposed on an analysis of the normal water temperatures as obtained from

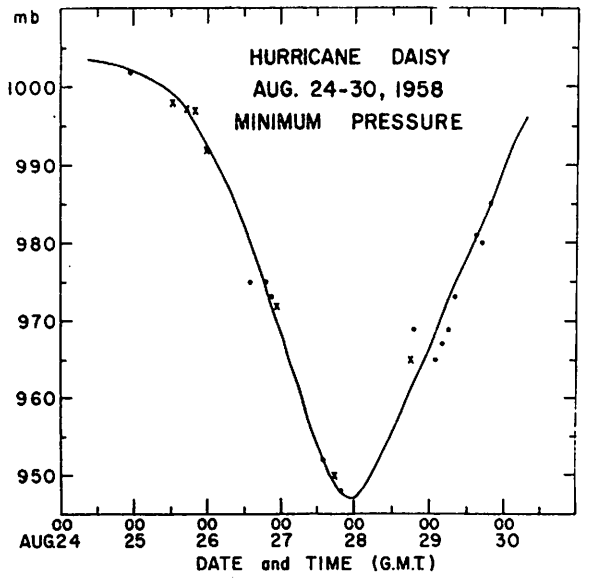

Figure 1. - Time changes in the central pressure of hurricane Daisy. The x's indicate values estimated from NHRP data; the dots show values obtained from dropsonde soundings by the military reconnaissance aircraft.

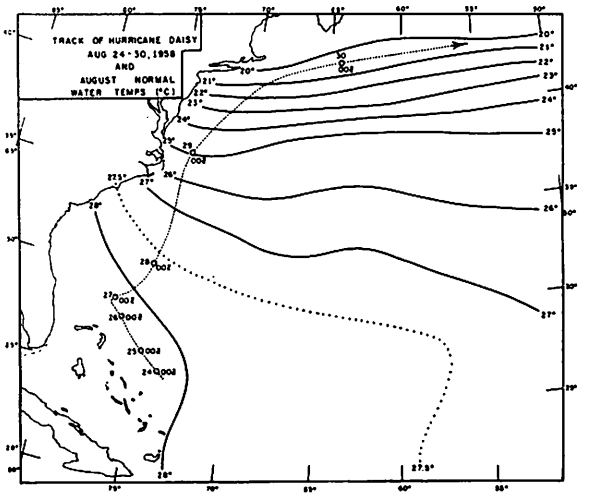

Figure 2. - Track of hurricane Daisy, August 24-30, 1958, with normal water-temperature distribution for August.

the Climatic Charts of the Ocean [26]. A cursory investigation of the water temperatures in the period August 23 to 25, 1958, showed values warmer than normal in the area to the northeast of the Bahamas. For the purpose of this discussion it is assumed that the distribution shown in figure 2 is representative of the one that existed at the time of Daisy. It is noticed that during the period of intensification, hurricane Daisy was moving over warm waters in a track essentially parallel to the 28°C. isotherm and the dissipation started close to the point of recurvature when the center began to move rapidly northward toward cooler water temperatures.

The changes in temperature and mixing ratio in the eye at prescribed pressure levels during the period August 25 to 29, 1958, appear in figures 3 and 4. The data for August 25 were obtained from an eye sounding (see fig. 5) approximated from NHRP observations at selected levels [3]. Our interest here is mainly in the over-all trend of the variations during the deepening and dissipation stages and not in the changes over smaller intervals of time shown by some of the individual soundings. There was a warming of about 3°C. at the surface and of 4° to 6°C. in the layers from 900 to 700 mb. during the intensification stage, and a corresponding cooling during the dissipation stage. There is some uncertainty in the values at the surface on August 25, but the variations at the other levels are better substantiated. The variations at the 700-mb. level during the dissipation are more irregular than at the lower levels. The moisture curve (fig. 4) shows a trend similar to that of the temperature at all levels, but individual values fluctuate more. The values of relative humidity (not illustrated), in the levels from the surface to 800 mb. were quite high throughout the entire period from August 25 to 29 with no definite difference in trend between the deepening and dissipation

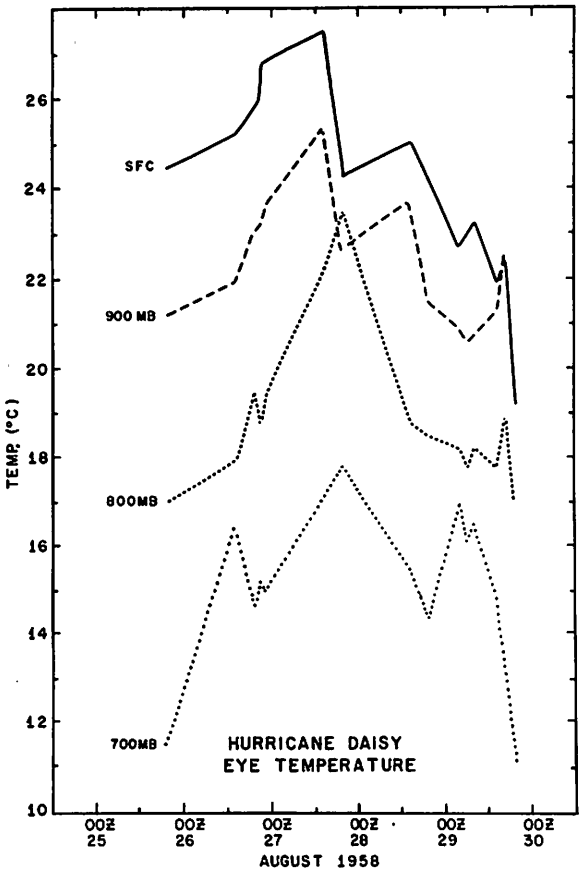

Figure 3. - Time variations of temperature in the eye of hurricane Daisy measured along specified pressure levels.

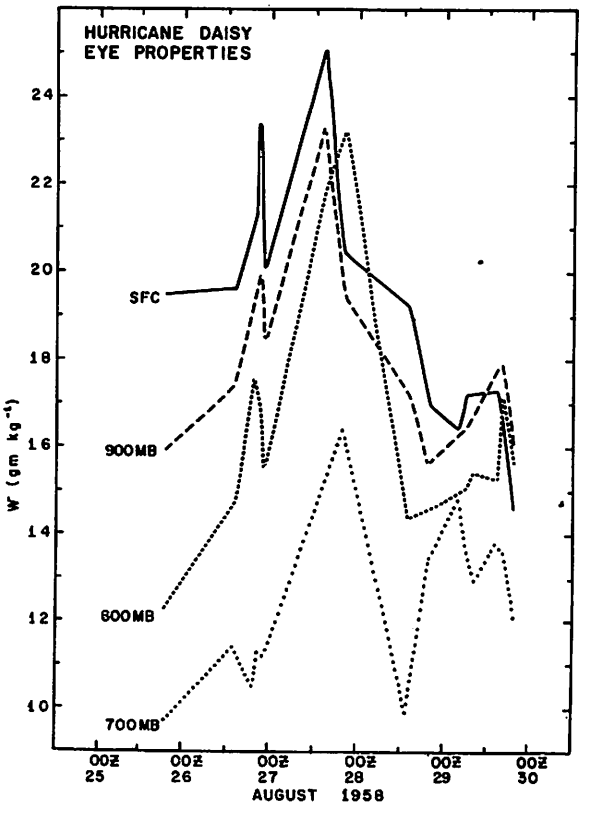

Figure 4. - Time variations in mixing ratio in the eye of hurricane Daisy measured along specified pressure levels.

stages, but at the 700-mb. surface there was a tendency for lower relative humidities in the period of maximum intensity.

A complete picture of the time changes at the levels above 700 mb. was not available. An idea of the variations during the intensification stage in the levels up to 250 mb. was obtained by use of NHRP data for August 25 and August 27. Figure 5 shows a plot of selected eye soundings; the one for August 25 was approximated from the NHRP observations. The one for August 27 is composed of a dropsonde for the levels below 500 mb. and NHRP data for the levels above 600 mb. A comparison between NHRP and dropsonde observations is possible at the 620-mb. level on August 27. The two values are within 1° C. of each other; the difference between the time of observation was only about 2 hours. These two soundings show a net warming of 5°-6° C. at all levels above 700 mb. One can see that if these soundings were continued upward with the same trend in lapse rate, the level of zero temperature anomaly for August 25 would be located near the 150-mb. surface, while on August 27 it would be located just below 100 mb.

The variations in moisture between the 700-mb. and 500-mb. levels from August 25 to August 27 (fig. 6) show a tendency for larger values in the more

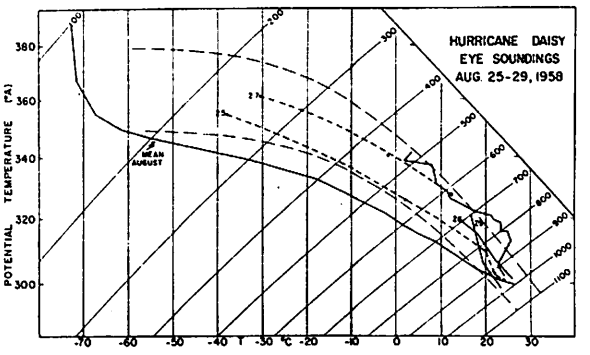

Figure 5. - Temperature soundings in eye of Daisy, August 25 - 29, 1958. The sounding for August 25 was reconstructed from observations (dots) made by NHRP aircraft; the ones for August 26 and 29 are dropsondes by Air Force aircraft. The curve for August 27 is a combination of a Navy dropsonde at low levels (solid) made at 1945 GMT, and a reconstructed curve from NHRP observations (dots) for the upper levels. Curves in long thin dashes are moist adiabats.

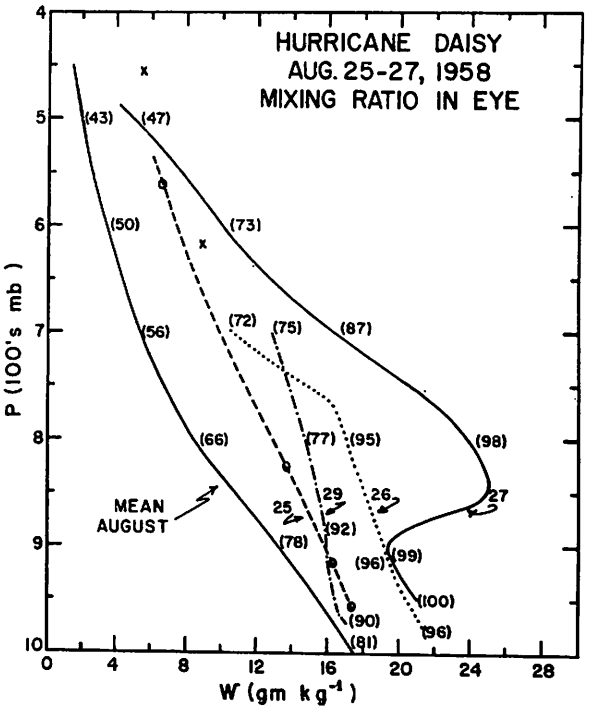

Figure 6. - Mixing ratio soundings in the eye of hurricane Daisy, August 25 to 29, 1958; data corresponds to temperature soundings shown in fig. 5. The circles show the observations by NHRP aircraft for August 25; and the two x's are the observations for August 27. The numbers in parenthesis represent the relative humidity at the indicated levels; no relative humidities are shown for August 25.

intense day up to the 560-mb. level. Near 500 mb. the data are incomplete, but the difference in moisture content between the two days appears to be quite small. The agreement between the dropsonde and NHRP humidity values is satisfactory also, although not as good as in the case of temperatures. Comparison between NHRP and dropsonde data on Daisy was also possible on August 27 and August 28; in all cases the magnitudes were quite close to each other.

3. CHANGES IN THE EYE PROPERTIES OF HURRICANE HELENE

Figures 7 to 11 illustrate the same type of information for hurricane Helene that was presented above for Daisy. There was a rather close parallel between these two hurricanes in regard to the variations in central pressure along the track of the center. The central pressure in Helene (fig. 7) decreased gradually from about 1012 mb. on September 22 to around 1000 mb. on September 24, then more rapidly to a minimum central pressure of 935 mb. observed around 0600 GMT on September 27. During the deepening period the center was moving northwestward (fig. 8) in a direction parallel to the isotherms and with mean monthly water temperatures of 27° to 28° C. The point of

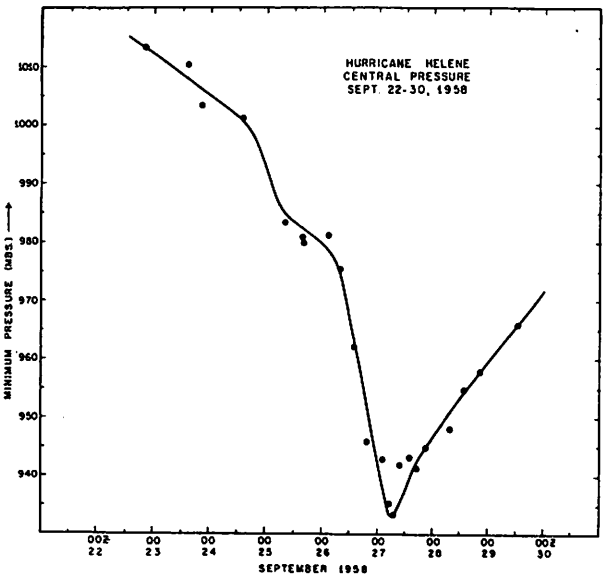

Figure 7. - Time changes in central pressure of hurricane Helene, September 22-29, 1958.

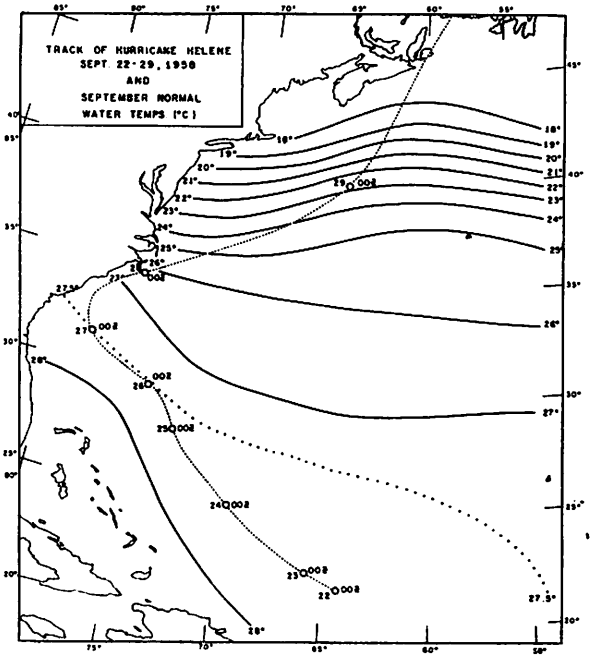

Figure 8. - Track of hurricane Helene, September 22-29, 1958, with normal water-temperature distribution for September.

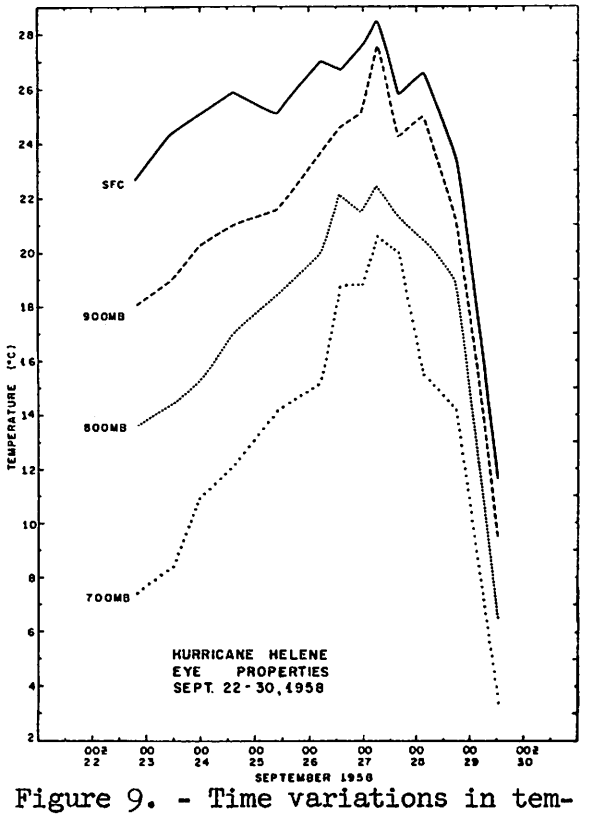

Figure 9. - Time variations in temperature in the eye of hurricane Helene measured along specified pressure levels.

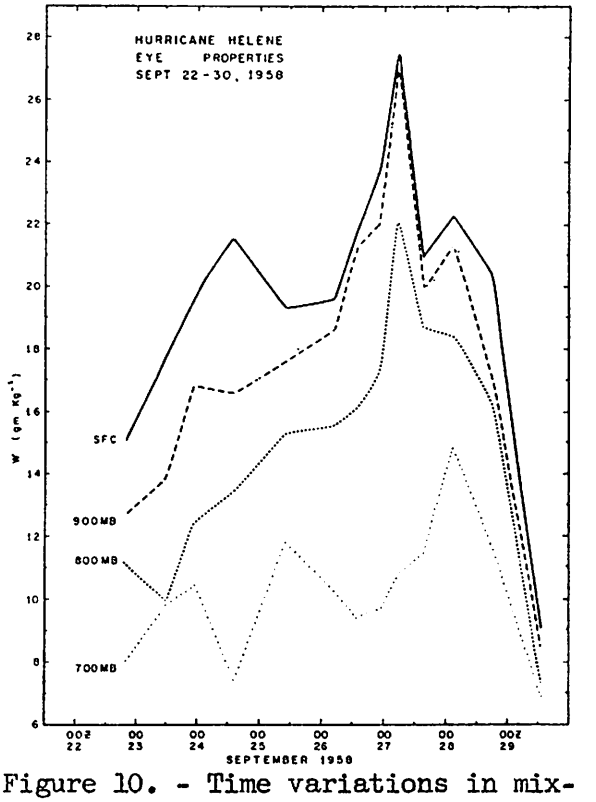

Figure 10. - Time variations in mixing ratio in the eye of hurricane Helene measured along specified levels.

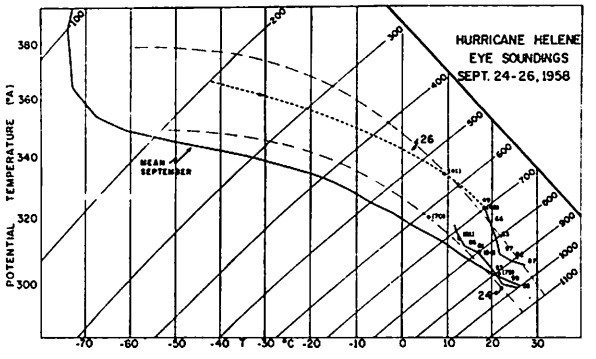

Figure 11. - Temperature soundings in the eye of hurricane Helene, Sept. 24 and 26, 1958. The sounding for Sept. 24 consists of a dropsondes (solid curve) taken at 1423 GMT; observations made by NHRP aircraft are shown by heavy dots. The sounding for Sept. 26 is a combination of a dropsonde taken at 1956 GMT (solid curve) and a reconstructed curve based on NHRP data (heavy dots) for the upper levels. Numbers indicate relative humidity, corresponding to the NHRP observations in parenthesis, and to the dropsonde without parenthesis. Curves in long thin dashes are moist adiabats.

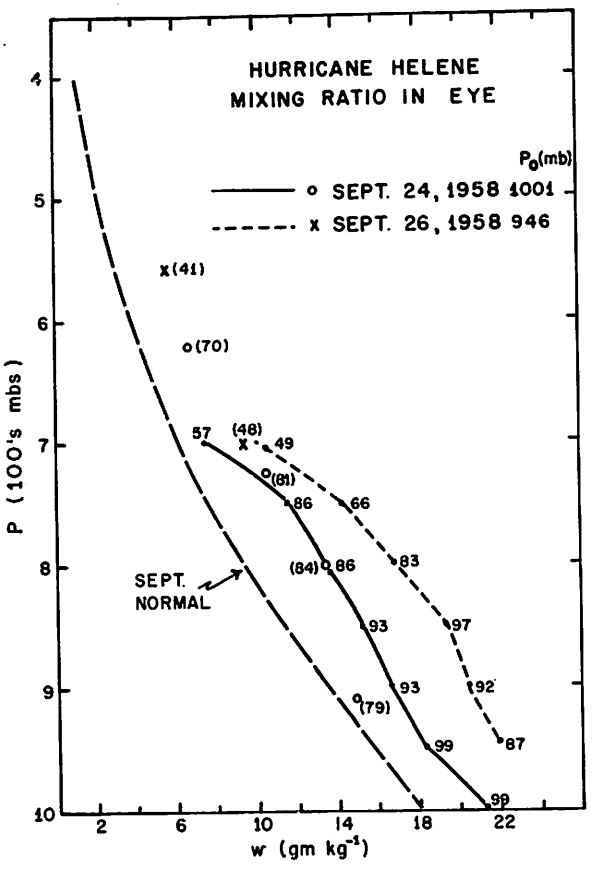

Figure 12. - Mixing ratio soundings in the eye of hurricane Helene, Sept. 24 and 26, 1958; data corresponds to the soundings shown in fig. 11. Observations made by NHRP aircraft on Sept. 24 are shown by circles, for Sept. 26 by x's. Numbers indicate relative humidities.

minimum pressure occurred at the point of recurvature. As the eye moved northward toward colder waters the central pressure increased steadily and reached a value of 966 mb. on September 29 at the time the center was near latitude 46°N. It is not intended to imply here that the field of water temperatures was the only factor influencing the changes in intensity, but as suggested by figures 2 and 8 and as will be discussed later, it undoubtedly played a significant role.

The variations in temperature (fig. 9) show warming of about 6°C. at the surface increasing to about 13°C. at 700 mb. during the deepening stage, and an even more pronounced cooling during the dissipation stage. The increase in pressure from September 27 to September 29 was not large, which suggests that the cooling at the high levels in the eye must not have been as pronounced as in the low levels. The changes in moisture (fig. 10) are similar to those in temperature; there was a very pronounced increase in mixing ratio during the deepening and decrease during the dissipation. Again, as was the case in the Daisy data, the changes at the 700-mb. level show a more diffuse and indistinct pattern. The values of relative humidity (not illustrated) revealed a trend

for drier conditions around the period of maximum intensity at the 700-mb. level, and generally large values with no definite change in trend at the levels below.

The variations at upper levels are more incomplete than in the case of hurricane Daisy. Two approximate soundings which combine dropsonde with NHRP data are shown in figure 11, but the initial one for September 24 extends only to 600 mb. At the time of the sounding for September 24 the central pressure was around 1000 mb. There was a dropsonde from the 700-mb. level made at 1423 GMT and NHRP observations (indicated by heavy dots in fig. 11) at the 910-mb., 800-mb., and 725-mb. levels, taken close to 1700 GMT; and at the 620-mb. level, taken close to 1900 GMT. The sounding for September 26 combines a dropsonde (central pressure of 946 mb.) made at 1956 GMT, with NHRP observations at 700 mb. taken near 2000 GMT, at 557 mb. taken near 2100 GMT, and at the 248-mb. level, taken near 1800 GMT.[1] There were two dropsondes with central pressure of 935 mb. made in the early hours of September 27, but it is felt that the one illustrated in figure 11 was closer in time to the NHRP data and is satisfactory for the purpose of this discussion.

On September 24 (fig. 11) the temperature near the surface was cooler than normal; positive anomalies were observed above 900 mb. At the 620-mb. level there was a positive anomaly of about 3°C. On September 26 the anomalies were about 4°C. in the layer up to 850 mb., about 10°C. near 700 mb., and about 13°C. at the 250-mb. level. The warming between the two days was from 3° to 5°C. in the layer up to 800 mb. and about 7°C. in the layer from 700 to 600 mb. If the sounding for September 26 were extended upward to meet the normal curve the level of zero temperature anomaly would be located near the 100-mb. level, about the same as in the case of Daisy on August 27. The changes in moisture content at the levels above 700 mb. during the deepening stage are illustrated in figure 12. The main interest in this figure is the observations made by the NHRP aircraft near the 700-mb. level and above. The observations recorded at the 725-mb. and 620-mb. levels on September 24, and the ones at 700-mb. and 557-mb. levels on September 26 reveal no significant changes in the moisture content during the intensification. The moisture is higher than normal, but all four points can be joined in a single curve that reveal only the normal gradient with elevation. However, on account of the increase in temperature, the relative humidity shows a significant decrease with intensification, evident in figure 12 at all the levels above 800 mb.

The agreement between the NHRP aircraft and the dropsonde data is remarkable, both in temperature and in humidity. The only discrepancy noted was in the humidity value at the 910-mb. level on September 24. Other comparisons between NHRP and dropsonde data, with equally satisfactory results, were made also during September 25.

---

[1] The NHRP observations are average values of all the readings taken by the research aircraft within 2 miles of the geometric center of the radar eye.

4. SOME REMARKS ON THE ACCURACY OF THE OBSERVATIONS

There are two major factors that usually lead to serious uncertainties in the representativeness of the temperatures as measured by dropsondes; one is lag in the sensing probes, and the other is the possibility of the instrument drifting outside the eye as it falls. The Air Force and Navy reconnaissance are usually careful in releasing the instruments in the center of the eye; furthermore, the balloon takes about 10-12 minutes to descend from the vicinity of the 700-mb. level to the surface and quite strong outflow would be required to force the balloon into the wall cloud. Therefore, the possibility of the instrument drifting outside the eye can be generally ruled out. There is nothing much that can be said in regard to possible lag in the probes, except that this effect, if real, should be fairly consistent from one observation to the next. The major argument that leads us to believe that the observations are generally accurate is the remarkable agreement between the measurements by the dropsondes and those by the NHRP aircraft in the cases in which a comparison was possible. However, these comparisons were made at levels from 900 to 600 mb., and some question may be raised about the measurements at the surface. There is one feature of the surface temperatures that appears to be unreasonable and that is the coolness of the air in the initial days of Helene. There is no question that these temperatures look cold and that a possible lag in the instrument may be responsible for them. A further check on this point can be made by comparing the data with ships observations in the vicinity; this was done but the results were rather unsatisfactory due to the lack of observations. However, for the purpose of the present discussion in which we are essentially interested in the general trend during the intensification and dissipation stages, the inaccuracies that may exist in the surface temperatures are not serious. Finally, the major feature that points to the representativeness and general accuracy of the observations is the fact that they follow a systematic and unmistakable trend that agrees with what one would normally expect on the basis of the accepted ideas.

5. DISCUSSION OF THE OBSERVATIONS

The main points illustrated in the diagrams can be summarized as follows: In the levels from the surface to 800 mb. there was an increase in temperatures and in moisture content with little or no increase in relative humidity during the deepening and a decrease in temperature and moisture content and little change in relative humidity during the dissipation. At the 700-mb. level and above there was a large increase in temperature, little or no increase in moisture, and therefore a decrease in relative humidity during the deepening, and inverse changes during the dissipation. The variations above 700 mb. are entirely consistent with the model of a subsiding current in the eye, but the changes in moisture content near the surface are not.

The fact that the lower levels of the eye have a relatively high moisture content was noticed in the early eye observations (Riehl [18], Jordan [6]). Malkus [15] presented numerical calculations in which, with a steady state model of a subsiding current that starts at the upper levels of the eye and entrains air from the wall cloud as it descends, she was able to obtain realistic values of temperature and humidity all the way to the surface for a

hurricane of central pressure of about 970 mb. It might be mentioned that the temperatures and humidities of her numerical model sounding do not differ materially from the properties of the Daisy and Helene eyes at the time they had a central pressure equal to that of the model. However, if the properties in the surface layer were determined wholly by the subsiding circulation, one would expect little change in moisture content and a decrease in relative humidity with intensification, the same as in the layers above 700 mb. The data presented above show a significant increase in both temperature and humidity in the layer up to 800 mb., which suggests a large influence of the underlying surface in determining the air properties in the lower levels.

The magnitude of the temperature increase at the surface was larger than expected and, perhaps, also larger than seems reasonable. This is due primarily to the relatively low temperatures measured in the initial days. As mentioned previously, there is a possibility of inaccuracies in these observations because of a possible lag in the dropsonde temperature probe. However, one could advance some arguments which indicate that this pronounced warming may not be totally unrealistic. There is one particular observation, that for the Helene eye on September 22, 2000 GMT (fig. 9), that looks too cold and may perhaps be erroneous or unrepresentative. However, the readings of 24°-26°C. (76°-79°F.) observed in the eye of Helene from September 23-25 and in the eye of Daisy from August 24-26 may be accurate. Initially, the perturbation must have been essentially cold-core, as are all minor synoptic perturbations in the Tropics. In the early stages of development there is no definite eye, but only a given volume of air that has been already subjected to the cooling influence of the conditions in the pre-existing disturbance; gradually this volume becomes organized into an eye as the hurricane circulation develops and the air is then subjected to the warming effect of the underlying surface and of the descending motion of the growing eye circulation. A check of observations of ship reports in the vicinity of the observation points of the dropsonde data revealed occasional readings of temperatures between 75° and 78° C., but usually the ship data are uncertain or inadequate to corroborate the dropsonde data presented above.

The amount of warming observed in the layers around 700 mb. in proportion to that observed at the upper levels was also larger than expected. As a result the remark that has been made to the effect that the warming during intensification is concentrated in the upper troposphere was not true in the cases presented here. Hydrostatic computations were made with the soundings for hurricane Daisy on August 25 and August 27 and for hurricane Helene on September 24 and September 26 to determine the distribution of the deepening with elevation. A relatively large contribution due to density changes in the lower half of the troposphere was obtained. By expressing the deepening as millibar-drop along fixed-height levels, it was found that the 50-mb. drop in the surface pressure in the eye of Daisy between August 25 and 27 was reduced by 50 percent at the 4.5 km. level. The same result was obtained for the 55-mb. drop in central pressure in the eye of Helene between September 24 and 26. However, if the deepening is expressed as height depression of isobaric levels, then the height depression of the 500-mb. level in the eye of Daisy from August 25 to 27, for example, is about 75 percent of that observed near the surface. This difference is due to the larger conversion factor from millibar to height-depression at the upper levels because of the lower densities. The distribution in terms of the pressure units is more directly

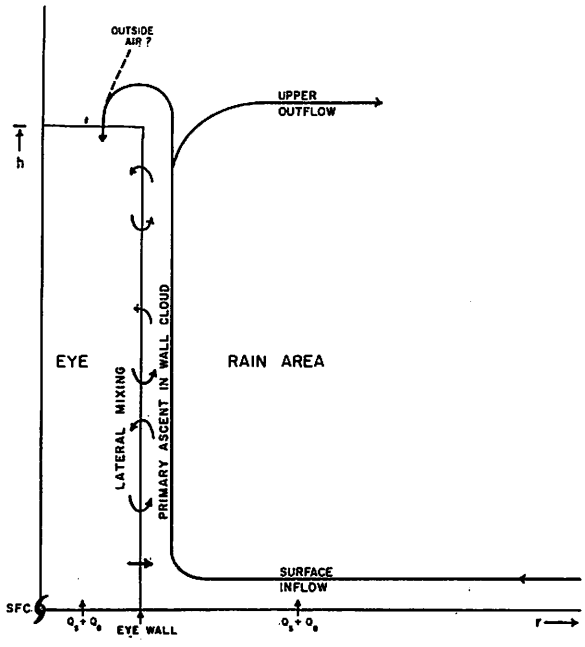

Figure 13. - Schematic representation of the mean vertical circulations in the eye core of a hurricane.

related to mass changes in the vertical column and one must conclude that mass changes in the lower levels of the eye made a significant contribution to the surface-pressure fall. In fact, it can be reasoned that extreme reduction in the central pressure would not take place unless the heating extended to the denser air in the lower troposphere (Haurwitz [5] pp. 26-29).

The above computations give the distribution of changes with height once hydrostatic balance has been achieved in the initial and final days. No conclusions based on these results can be made in regard to the levels at which the heating is initially introduced in the eye column. Some discussion of the processes by which the observed temperature and moisture changes in the eye are probably brought about is offered in the next section.

6. ENERGY CHANGES IN THE EYE AND THE DEEPENING OF TROPICAL STORMS

One of the main purposes of this study, at the outset, was to carry out a quantitative analysis, to the extent possible, of the energy transformations in the eye and of the air motions in the boundary necessary to produce them. This phase of the work has not been completed, but it is possible to discuss qualitatively the factors that should operate during the deepening and dissipation stages in order to produce the observed variations.

The time variations in eye properties in Daisy and Helene can be transformed to energy units and they bring out the fact that the heat content of the eye increased during the deepening and decreased during the dissipation stage. We can think in terms of a heat balance for the eye volume and see how local time changes in the energy content can be brought about. Consider a simplified schematic diagram of the mean circulations in the hurricane core, as shown in figure 13.

Local energy changes in the eye come about as the net result of the sources and sinks inside the volume and the flux through the boundaries. The usual sources and sinks inside include the radiation, which is a cooling factor, and the precipitation heating, which should be nil. Therefore, increase in heat content must come through the air motions at the boundaries and other cooling effects in the eye must be overcome before a reduction in the surface pressure is produced. The motion through the eye boundaries must undoubtedly be very complex and encompass different scales of motion. For example, we may consider fluxes by small-scale diffusion and by larger-scale motions in which an air current may enter in one section of the eye and go out in another, as

envisioned by Riehl [21]. Also, some evidence has been presented by Simpson [23] and LaSeur [13] which suggest that the subsidence may be concentrated in a ring around the outer edge of the eye. For the purpose of the present discussion we refer to the net residual motions as sketched in figure 13.

A study of the thermodynamic effects of the air motions in the boundaries immediately leads to the conclusion that heating in the eye can come only through the top and bottom boundaries; i.e., by vertical motions. Horizontal mixing through the eye wall, regardless of the scale of motion, should lead to cooling in the eye and is to be considered as a dissipating factor. Two things can be mentioned in this regard; one, that the air coming from the wall cloud is colder; and second, that the cloud matter evaporates in the eye and introduces a cooling effect (Malkus [15]).

The importance of the underlying surface is paramount. It affects the properties of the eye in two ways: one, directly, by contact through the lower boundary; and second, indirectly, by its effect on the properties of the inflow current in the rain area, which in turn affects the properties of the ascending convective current in the wall cloud, and this in turn affects the eye by the horizontal mixing process in the eye-wall and by its effect on the initial conditions of the descending current. In the light of this the variations in central pressure in hurricanes Daisy and Helene with respect to the mean field of water temperatures, as suggested by figures 2 and 8, become quite meaningful.

The other important factor is the properties of the current descending through the upper boundary. If we consider an eye volume extending from the surface to some upper boundary not reaching the top of the eye (for example, the layer from the surface to 500 mb.), then the air coming in at the upper boundary is a mixture of air that has entered at the top of the eye and air that has mixed in from the wall cloud. Clearly, the higher the temperature at which the initial current starts at the top and the less the mixing that takes place with the wall cloud the greater the increase in heating at the volume below and the larger the reduction in surface pressure. With respect to the entire eye-volume from the surface to the top of the eye (assuming that such a top can be defined), one can raise the question as to where the initial current comes from. Circulation diagrams presented by Riehl [19], Simpson [23], and Kuo [11], have all suggested that it is composed essentially of normal tropical air. Malkus [15] also used normal tropical air as the starting point for her numerical computation. However, it can be easily visualized that a significant portion of this current may be air that had originally ascended in the wall-cloud and that a circulation as suggested in figure 13 is realistic. A vertical cross-section of the wall-cloud in hurricane Daisy, as seen by radar on August 27, 1958 (Jordan et al. [9]) suggests a more vertical orientation of the convective ascent in the wall cloud than has been considered in the past. Therefore, a spilling-over of the air ascending in the wall cloud into the descending flow in the eye, in the manner suggested in figure 13, may take place. Convincing evidence of the existence of this type of motion can be observed in the photographs from the top of a typhoon presented by Bundgaard [2] and Fletcher et al. [4].

From the point of view of the thermodynamics in the cycle discussed above, one can see that energy changes inside the eye depend very much on the strength

and thermal properties of the convective updraft in the wall-cloud. The relationship between this ascending current and the intensification process is quite interesting; through the vertical motions it assists in the deepening process, through the horizontal motions in the eye-wall it introduces a dissipating factor. However, the most important relationship probably comes from dynamic considerations, since it is quite evident that organized descent in the eye would not exist unless there was first a well-developed and organized ascent in the wall-cloud. Why and under what conditions this organization takes place continues to be one of the most difficult problems in hurricane research (Kuo [12], Alaka [1]).

One important point to realize is that only air motions in the boundary can affect the energy transformations in the eye, and, therefore, lead to changes in the central pressure. Everything else in the rain area has at most an indirect effect, as can be deduced from the thermodynamic processes discussed above. Any cooling or dissipating agency, as well as a deepening one, would have to enter the eye core in order to be effective. This was very clearly demonstrated by Snellman [24].

On the basis of the above discussion, we can summarize the conditions or factors that lead to a reduction in the central pressure.

1. An adequate heat source in the underlying water surface,
2. Development and organization of the ascent in the eye-wall in such a way that the subsiding current in the eye is also organized and concentrated in a small area. Once this is accomplished, then there should be
3. A minimal amount of cloud matter entering the eye, and
4. No transport of cooler air from the outside into the eye core.
5. As a fifth factor one can mention what may be referred to as verticality of the thermal core in the eye. That is, the vertical distribution of flow should be such that the net heating in the eye is distributed as much as possible in a vertical column, so that it is more effective in causing a surface pressure fall.

For filling of the central pressure, i.e., dissipation, the above arguments should be reversed.

The first two conditions above are most important and one can argue that no real warm-core type of intensification can occur unless both are present. An adequate heat source from the ocean is present in most of the oceanic areas south of latitude 30° to 35° N., therefore, the organization of the eye-core circulation is undoubtedly the most important and most difficult to realize. From the practical and operational point of view one might be able to detect the onset of the organization of the eye-core circulation by means of radar. One example of this was offered by LaSeur [14] for the case of hurricane Judith of 1959. It appears also that a certain amount of reduction in the central pressure can take place in spite of the presence of unfavorable conditions.

An evaluation of the intensification and weakening of hurricanes Daisy and Helene in the light of the factors listed above revealed the following. In the case of hurricane Daisy the eye-core circulation was organized quite

early in the development stage [3] and intensification proceeded apparently as long as the heat from the ocean was maintained. In the case of Helene the development up to September 24 was quite slow. A weak circulation with surface winds up to 35 and 40 m.p.h. in squalls existed from September 21 [25]. The disturbance was moving over warm waters; but evidently something was lacking and it is believed that it was the development of the eye-core circulation. Hurricane Helene was investigated by NHRP aircraft on September 24 and by that time a definite eye formation was evident in the radar scope. Afterward, deepening proceeded rapidly until the center started to recurve and move into cooler waters. No evaluation has been made of the synoptic factors that affected Helene and Daisy in the period during and after recurvature, but the hurricanes were then located in a geographical region in which the fourth factor listed above, namely, cool air from the outside entering the eye-core, also may have been present. In regard to the verticality of the thermal core, there is some evidence to indicate that in the case of hurricane Daisy during the early part of the dissipation stage on August 28, the warmest air at middle levels in the eye was not located vertically over the surface pressure center, but apparently had a significant tilt [3].

REFERENCES

1. M. A. Alaka, "On the Occurrence of Dynamic Instability in Incipient and Developing Hurricanes," "Proceedings, Second Technical Conference on Hurricanes, June 27-30, 1961," NHRP Report No. 50, pp. 51-56.
2. R. C. Bundgaard, "Meteorological Dynamics of Tropical Cyclones from Superior Photographic Reconnaissance," Paper presented at the Second Technical Conference on Hurricanes, held at Miami Beach, Fla., June 27-30, 1961. (Abstract in, Bulletin of AMS, vol. 42, No. 5, May 1961, p. 363.)
3. J. A. Colón and Staff NHRP, "On the Structure of Hurricane Daisy (1958)," NHRP Report No. 48, 1961.
4. R. D. Fletcher, J. R. Smith, and R. C. Bundgaard, "Superior Photographic Reconnaissance of Tropical Cyclones," Weatherwise, vol. 14, No. 3, June 1961, pp. 102-109.
5. B. Haurwitz, Dynamic Meteorology , McGraw-Hill Book Co., Inc., New York, 1941, 365 pp.
6. C. L. Jordan, "On the Low-Level Structure of the Typhoon Eye," Journal of Meteorology, vol. 9, No. 4, Aug. 1952, pp. 285-290.
7. C. L. Jordan, "Mean Soundings for the Hurricane Eye," NHRP Report No. 13, 1957, 10 pp.
8. C. L. Jordan, "The Thermal Structure of the Core of Tropical Cyclones," Geophysica, vol. 6, No. 3/4, (Palmén 60th Birthday Volume) 1958, pp. 281-297.
9. C. L. Jordan, D. A. Hurt, Jr., and C. A. Lowrey, "On the Structure of Hurricane Daisy on August 27, 1958," Journal of Meteorology, vol. 17, No. 3, June 1960, pp. 337-348.
10. C. L. Jordan, "Marked Changes in the Characteristics of the Eye of Intense Typhoons Between the Deepening and Filling Stages," NHRP Report No. 44, 1961, 20 pp.
11. H.-L. Kuo, "Dynamics of Convective Vortices and Eye Formation," pp. 413-424 of The Atmosphere and the Sea in Motion (Rossby Memorial Volume), The Rockefeller Institute Press, New York, 1959.

12. H.-L. Kuo, "Survey of Theoretical Studies of Cyclogenesis in the Tropics and Initial Value Approach," "Proceedings Second Technical Conference on Hurricanes, June 27-30, 1961," NHRP Report No. 50, pp. 277-283.
13. N. E. LaSeur, "An Analysis of Some Detailed Data Obtained by Aircraft Reconnaissance of a Hurricane," Scientific Report No. 5, Contract No. AF19 (604)-753, Dept. of Meteorology, Florida State University, 1957, 27 pp.
14. N. E. LaSeur, "The Role of Convection in Hurricanes," "Proceedings, Second Technical Conference on Hurricanes, June 27-30, 1961," NHRP Report No. 50, pp. 323-334.
15. J. S. Malkus, "On the Structure and Maintenance of the Mature Hurricane Eye," Journal of Meteorology, vol. 15, No. 4, Aug. 1958, pp. 337-349.
16. B.I. Miller, "On the Maximum Intensity of Hurricanes," Journal of Meteorology, vol. 15, No. 2, Apr. 1958, pp. 184-195.
17. E. Palmén, "Formation and Development of Tropical Cyclones," Proceedings of the Tropical Cyclone Symposium, Brisbane, Australia, Dec. 1956, pp. 213-231.
18. H. Riehl, "A Radiosonde Observation in the Eye of a Hurricane," Quarterly Journal of the Royal Meteorological Society, 74, 1948, pp. 194-196.
19. H. Riehl, Tropical Meteorology, McGraw-Hill Book Co., Inc., New York, 1954, 392 pp.
20. H. Riehl, "Formation of Hurricanes," Proceedings of WMO Symposium on Hurricanes, Ciudad Trujillo, 1956.
21. H. Riehl, On the Maintenance of the Eye of Tropical Cyclones, unpublished mimeographed notes, 1957.
22. H. Riehl and J. S. Malkus, "On the Dynamics and Energy Transformations in Steady State Hurricanes," Tellus, vol. 12, No. 1, Feb. 1961, pp. 1-20.
23. R. H. Simpson, "On the Structure of Tropical Cyclones as Studied by Aircraft Reconnaissance," Proceedings of the UNESCO Symposium on Typhoons, Tokyo, Japan, November 9-12, 1954, 1955, pp. 129-150.
24. L. Snellman, "On the Relationship Between Intensity and Speed of Hurricanes after Recurvature," "Proceedings, Second Technical Conference on Hurricanes, June 27-30, 1961," NHRP Report No. 50, pp. 27-33.
25. Staff, Weather Bureau Office, Miami, Fla., "The Hurricane Season of 1958," Monthly Weather Review, vol. 86, No. 12, Dec. 1958, pp. 477-485.
26. U. S. Weather Bureau, Atlas of Climatic Charts of the Oceans, Washington, D. C. 1938.

ON THE VERTICAL VELOCITY FIELD IN HURRICANES

T. N. Krishnamurti
University of California, Los Angeles, California

ABSTRACT

Steady Symmetric Hurricanes: It is shown how a system of equations (motion, mass continuity, and the first law of thermodynamics) can be integrated for a steady symmetric vortex with a prescribed tangential motion. The method of characteristics is used to obtain a solution for the vertical velocity field. For the normally observed characteristic lines in a hurricane no vertical velocity is possible for a frictionless atmosphere, and therefore numerical experiments are carried out with different magnitudes of the momentum exchange coefficients. It is also shown that as long as the ratio of the lateral and the vertical exchange coefficient is kept fixed, one calculation of the vertical velocity field permits an examination of a wide range of variation of the individual coefficients. A consistent structure of an Atlantic hurricane is constructed from the National Hurricane Research Project data.

Asymmetric Hurricanes: An extension of the method is made to include asymmetries. The vertical velocity field is again examined under different conditions. The results show that it is possible to obtain spiral bands in the vertical velocity without any of the friction terms; an eye wall is obtained only when radial momentum exchange by internal friction is included.

1. INTRODUCTION

A method for obtaining the vertical motion field for a steady symmetric hurricane with a prescribed tangential motion will be presented, and it will be shown how one can extend the analysis to obtain the vertical velocity field in an asymmetric hurricane with a prescribed tangential motion.

The National Hurricane Research Project at Miami, Fla., has provided a considerable amount of aircraft flight data in recent years, and this has enabled us to understand the structure of the hurricane much better than before.

The recent work of Berkofsky [1] and Kasahara [2] includes perhaps the very few approaches in which hurricane development is treated as an initial value problem. It is the aim of all research workers to see the complete development of a hurricane in a model where one integrates the non-linear equations of motion and brings about many of the observed features. The present calculation of vertical motion is obtained from a complete system of equations.

Table 1

Symbol	Meaning of Symbol
t	Time.
r	Radius increasing outward.
θ	Angle increasing in the counter clockwise sense.
p	Pressure used as a vertical coordinate.
u	Tangential wind velocity positive along increasing θ.
v	Radial wind velocity positive along r.
ω	Vertical velocity in isobaric coordinates.
z	Height of constant pressure surface above sea level.
T	Temperature.
H	Rate of nonadiabatic heating per unit mass of air.
c_p	Specific heat of air at constant pressure.
R	Gas constant of air.
ν	Coefficient of lateral momentum exchange.
K	Coefficient of vertical momentum exchange.
g	Acceleration of gravity.
f	Coriolis parameter.

2. THE STEADY SYMMETRIC HURRICANE

Cylindrical isobaric coordinates will be used with the radius vector r pointing outward, θ the angle increasing in the cyclonic sense. Table 1 lists the symbols used in this paper.

The equations of motion may be written in the form:

$$v\left(\frac{\partial u}{\partial r}+\frac{u}{r}+f\right)+\omega\frac{\partial u}{\partial p}=\frac{\partial}{\partial r}\left[\nu\left(\frac{\partial u}{\partial r}+\frac{u}{r}\right)\right]+\frac{\partial}{\partial p}\left(K\frac{\partial u}{\partial p}\right) \tag{1}$$

$$v\frac{\partial v}{\partial r}-u\left(\frac{u}{r}+f\right)+\omega\frac{\partial v}{\partial p}=-g\frac{\partial z}{\partial r}+\frac{\partial}{\partial r}\left[\nu\left(\frac{\partial v}{\partial r}+\frac{v}{r}\right)\right]+\frac{\partial}{\partial p}\left(K\frac{\partial v}{\partial p}\right) \tag{2}$$

$$0=-g\frac{\partial z}{\partial p}-\frac{RT}{p} \tag{3}$$

The equation of continuity,

$$0=\frac{1}{r}\frac{\partial vr}{\partial r}+\frac{\partial \omega}{\partial p} \tag{4}$$

and the thermodynamic energy equation

$$H = c_p \left[v \frac{\partial T}{\partial r} + \omega \frac{\partial T}{\partial p} \right] - \frac{RT}{p} \omega \qquad (5)$$

It u, the tangential velocity, is prescribed at each point, then in principle, we can solve for v, ω, z, T, and H, provided we have knowledge about the distribution of ν and κ.

Instead of immediately assigning certain reasonable values for ν and κ, equations (1) to (5) were non-dimensionalized through choice of a fundamental length unit L_o, a time unit t_o, and a pressure unit p_o. The non-dimensional equations were solved by the following procedure:

Since u is prescribed, equations (1) and (4) can be treated as two equations for the unknowns v and ω. Equation (1) can be rewritten as

$$v = b + a\,\omega \qquad (6)$$

where

$$b = \frac{\frac{\partial}{\partial r}\left[\nu \left(\frac{\partial u}{\partial r} + \frac{u}{r} \right) + \frac{\partial}{\partial p} \left(\kappa \frac{\partial u}{\partial p} \right)\right]}{\frac{\partial u}{\partial r} + \frac{u}{r} + \frac{2f}{f_o}} \qquad (7)$$

and

$$a = - \frac{\frac{\partial u}{\partial p}}{\frac{\partial u}{\partial r} + \frac{u}{r} + \frac{2f}{f_o}} \qquad (8)$$

Eliminating v from (4) and (6) the following equation in ω may be obtained:

$$\frac{\partial \omega}{\partial p} + a \frac{\partial \omega}{\partial r} + \frac{\omega}{r} \frac{\partial ar}{\partial r} + \frac{1}{r} \frac{\partial br}{\partial r} = 0 \qquad (9)$$

The two newly introduced quantities a and b possess certain interesting properties. a is the slope of the characteristic lines of equation (9) and determines the slope of the vortex lines in the vertical plane. b is a term representing the role of the lateral and vertical friction in the determination of the vertical velocity field.

Equation (9) may be written in the form:

$$\frac{\delta \omega}{\delta p} + \frac{\omega}{r} \frac{\partial ar}{\partial r} + \frac{1}{r} \frac{\partial br}{\partial r} = 0 \qquad (10)$$

where $\delta\omega$ will denote a change in ω along the characteristic line of slope a.

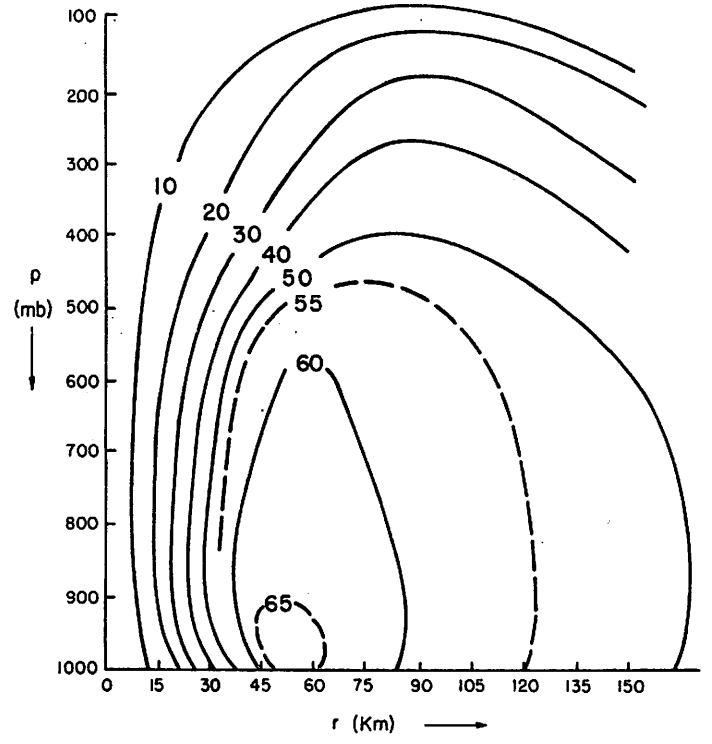

Figure 1. - Mean cross-section of the tangential wind velocity field in hurricane Cleo. Units: knots.

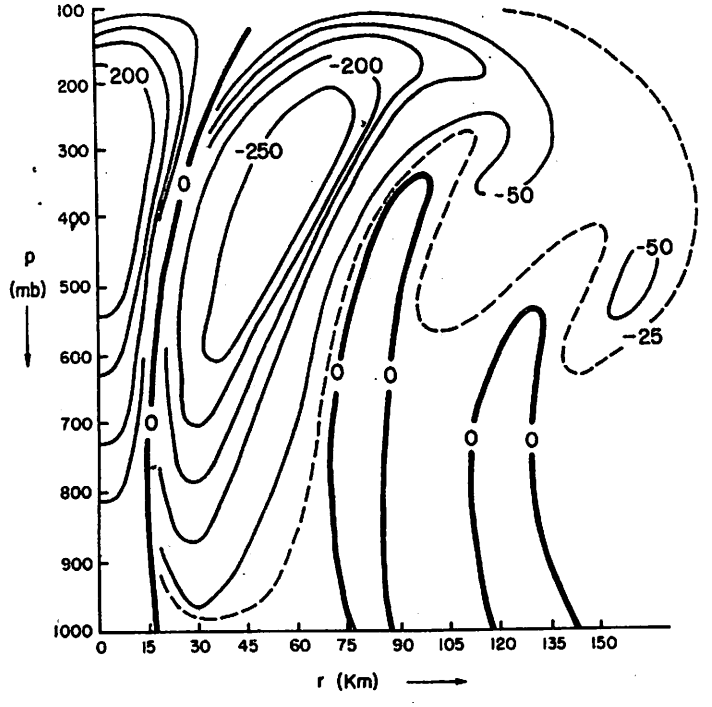

Figure 2. - Cross-section of the vertical-velocity field (mb./hr.) in hurricane Cleo, August 18, 1958.

Further, let

$$\left.\begin{aligned} \frac{1}{r}\frac{\partial ar}{\partial r} &= X \\ -\frac{1}{r}\frac{\partial br}{\partial r} &= Y \end{aligned}\right\} \tag{11}$$

An explicit solution of equation (10) can be written in the form:

$$\omega(p) = \omega(p_o) + e^{-\int X dp} \int_{p_o}^{p} e^{\int X dp}\, dp \tag{12}$$

If $\omega(p_o) = 0$ then for $Y = 0$, $\omega(p) = 0$ and we get the important result that, in a steady symmetric frictionless system no vertical motion is possible if the vertical velocity is zero at any point of a characteristic line.

In examining the characteristic lines in various atmospheric systems, the author found that these lines are usually vertical, i.e., $a \simeq 0$, and they intersect the 1000 mb. surface usually vertically. A boundary condition of the type $\omega = 0$ at $p = 1000$ mb. therefore would lead to no vertical motion for a steady, symmetric, frictionless system. In such a system therefore one must have friction to have any vertical motion.

We next let $\frac{\nu}{\kappa} = N$ and $\nu = M$

A machine program can be easily set up to investigate the field of vertical velocity for different values of ν and κ. A study of the structure of steady symmetric vortices for N = 1 and M taking different values was made.

Once $\omega(p)$ is determined for any value of M, equation (6) may be used to obtain a corresponding field of v.

If $z(L_o,p)$ is prescribed at $r = L_o$ then $z(r,p)$ can be obtained from equation (2) since

$$\frac{\partial z}{\partial r} = -\frac{1}{g}\left[v\frac{\partial v}{\partial r} - u\left(\frac{u}{r} + \frac{2f}{f_o}\right) + \omega\frac{\partial v}{\partial p} - \frac{\partial}{\partial r}\left\{\nu\left(\frac{\partial v}{\partial r} + \frac{v}{r}\right)\right\} - \frac{\partial}{\partial p}\left(\kappa\frac{\partial v}{\partial p}\right)\right] \tag{13}$$

Further, $T(r,p)$ can be obtained from the hydrostatic equation (3) for the calculated $z(r,p)$ field, and the right hand side of equation (5) can be computed to give a distribution of $H(r,p)$, the non-adiabatic heating.

Data from hurricane Cleo of 1958 were used to carry out the analysis. Figure 1 shows the mean tangential wind field in the storm. It was then assumed that this storm was a steady symmetric disturbance. Solutions for v,ω, z,T,and H were obtained by the proposed method. It was found that even for simple non-dimensional values of ν and κ (=0.1 for instance), rather interesting solutions for v,ω,z,T,and H showed up. The vertical motion field, figure 2 had an eye with sinking motion, very large vertical motion at the eye wall and much weaker upward vertical motion at large distances from the center. The dimension and magnitude of v,ω,z,T,and H appeared reasonable when compared with certain observed magnitudes. Much still needed to be said about the magnitudes of ν and κ. It was found that the final pattern of ω was largely determined by the lateral eddy exchange of momentum. The role of vertical eddy exchange of

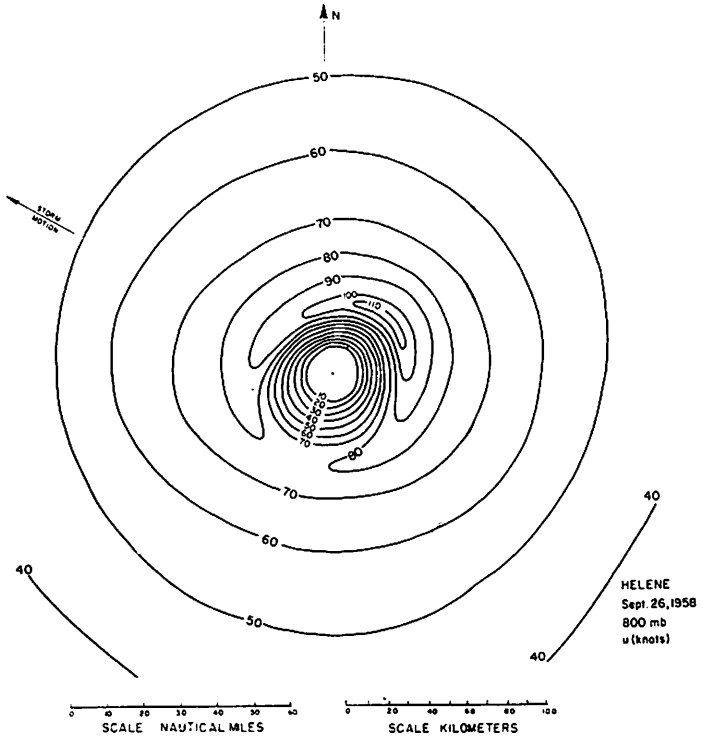

Figure 3. - The tangential wind velocity field (kt.) in hurricane Helene at 800 mb., September 26, 1958.

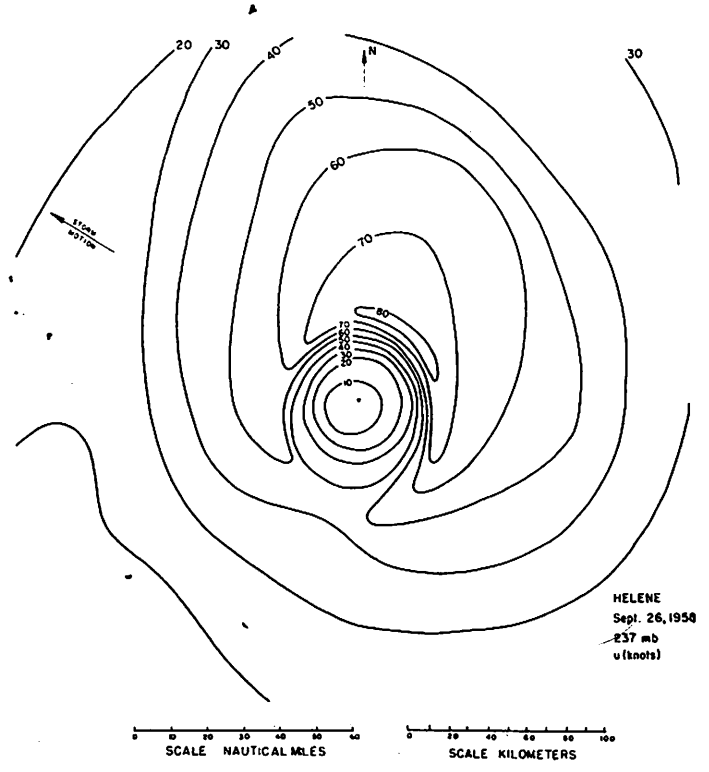

Figure 4. - The tangential wind velocity field (kt.) in hurricane Helene at 237 mb. September 26, 1958.

momentum, though small in the determination of the vertical motion field, appeared significant for exchanges of momentum with the ground.

3. THE ASYMMETRIC SYSTEM OF EQUATIONS

The following assumptions will be made:

(i) Steady state, i.e., $\frac{\partial u}{\partial t} = \frac{\partial v}{\partial t} = \frac{\partial T}{\partial t} = 0$

(ii) As a first approximation $-g \frac{\partial z}{r \partial \theta}$ is much smaller than other terms in the tangential equation of motion.

(iii) As a first approximation, the friction term $\frac{2}{r^2} \frac{\partial (v \nu)}{\partial \theta}$ is smaller than other friction terms in the tangential equation of motion.

The system of equations is written as:

$$u \frac{\partial u}{r \partial \theta} + v \left(\frac{\partial u}{\partial r} + \frac{u}{r} + f\right) + \omega \frac{\partial u}{\partial p} = \frac{\partial}{\partial r} \left[\nu \left(\frac{\partial u}{\partial r} + \frac{u}{r}\right)\right] + \frac{\partial}{r \partial \theta} \left[\nu \left(\frac{\partial u}{r \partial \theta}\right)\right] + \frac{\partial}{\partial p} \left[\kappa \left(\frac{\partial u}{\partial p}\right)\right] \tag{14}$$

$$u \frac{\partial v}{r \partial \theta} + v \frac{\partial v}{\partial r} - u\left(\frac{u}{r} + f\right) + \omega \frac{\partial v}{\partial p} = -g \frac{\partial z}{\partial r} + \frac{\partial}{\partial r} \left[\nu \left(\frac{\partial v}{\partial r} + \frac{v}{r}\right)\right] + \frac{\partial}{r \partial \theta} \left[\nu \left(\frac{\partial v}{r \partial \theta}\right)\right]$$

$$+ \frac{\partial}{\partial p} \left[\kappa \left(\frac{\partial v}{\partial p}\right)\right] - \frac{2}{r^2} \frac{\partial (u \nu)}{\partial \theta} \tag{15}$$

$$0 = -g \frac{\partial z}{\partial p} - \frac{RT}{p} \tag{16}$$

$$\frac{\partial u}{r \partial \theta} + \frac{\partial v}{\partial r} + \frac{v}{r} + \frac{\partial \omega}{\partial p} = 0 \tag{17}$$

$$H = \left(u \frac{\partial T}{r \partial \theta} + v \frac{\partial T}{\partial r} + \omega \frac{\partial T}{\partial p}\right) - \frac{RT}{p} \omega \tag{18}$$

These equations may be treated as five equations for the five unknowns v, ω, z, T, and H if the distribution of u is known. Our interest here lies in seeing what sort of a system can be obtained by imposing the familiar crescent-shaped geometry of the tangential wind in a mature hurricane.

It was possible to extend the analysis to this asymmetric system and carry out numerical integrations. We present here some results for hurricane Helene of September 1958.

The storm Helene was over the Atlantic and the National Hurricane Research Project flew two complete flights at the 800- and 250-mb. surfaces. There was a very good coverage of data and it was easy to obtain a reasonable analysis of the tangential wind field. Figures 3 and 4 show these fields. The two important features, namely the crescent-shaped geometry and the small vertical variation of the wind are apparent.

Figures 5, 6, and 7 show some calculations of the vertical motion field at the 700-mb. surface. Respectively they signify the contribution by (i) pure asymmetry of the wind field without any of the friction terms, (ii) contribution by radial stresses of the tangential wind, (iii) contribution by the complete friction terms. Figure 8 shows a radar composite chart for the same storm.

In figure 5 one notices spiral bands with up and down motion due to the presence of asymmetries $\frac{\partial u}{r\partial\theta}$ and $u\frac{\partial u}{r\partial\theta}$ in the input wind field $u(r,\theta,p)$. One may notice that no closed eye wall shows up in this calculation. In figure 6 we have included the friction term due to the radial stress of the tangential wind The most interesting feature is the presence of an eye with sinking motion. The following additional features may be noted: The largest upward vertical motions are found around the eye. The magnitude of the upward motion falls off rapidly as r increases. The order of magnitude of the vertical motion at r = 150 km. (100 n. mi.) is one to two orders of magnitude smaller than that near the eye. To obtain the magnitude of vertical motion in units of millibars per hour, the non-dimensional numbers should be multiplied by $p_o f_o/2$ 131.0 mb./hr. The magnitudes compare very closely with those the author found for the steady symmetric storm. Figure 7 shows the contribution by the complete system including all of the friction terms. We notice that figures 6 and 7 appear rather similar, indicating that the contribution by the friction term due to tangential and vertical shear of u is small.

In the radar composite chart for the storm Helene one sees dark and light echoes. A comparison of figures 7 and 8 shows very close similarity. The position of the bands of rising motion compares very well with the positions of the echoes. In regions of downward motion there is an absence of echoes. The eye, though a little elongated in shape in the numerical calculations, appears to agree very well with the radar eye.

4. CONCLUDING COMMENTS

The results presented here form an outline of a method the author has presented elsewhere in greater detail [3,4]. The reader is referred to these papers for various aspects of the problem not included here.

This method of estimating vertical motion in the atmosphere is found to be of great potential in several cases investigated. Further work on similar lines is being carried out.

ACKNOWLEDGMENT

The author wishes to thank Mr. Harry F. Hawkins of the National Hurricane Research Project for providing the data presented here.

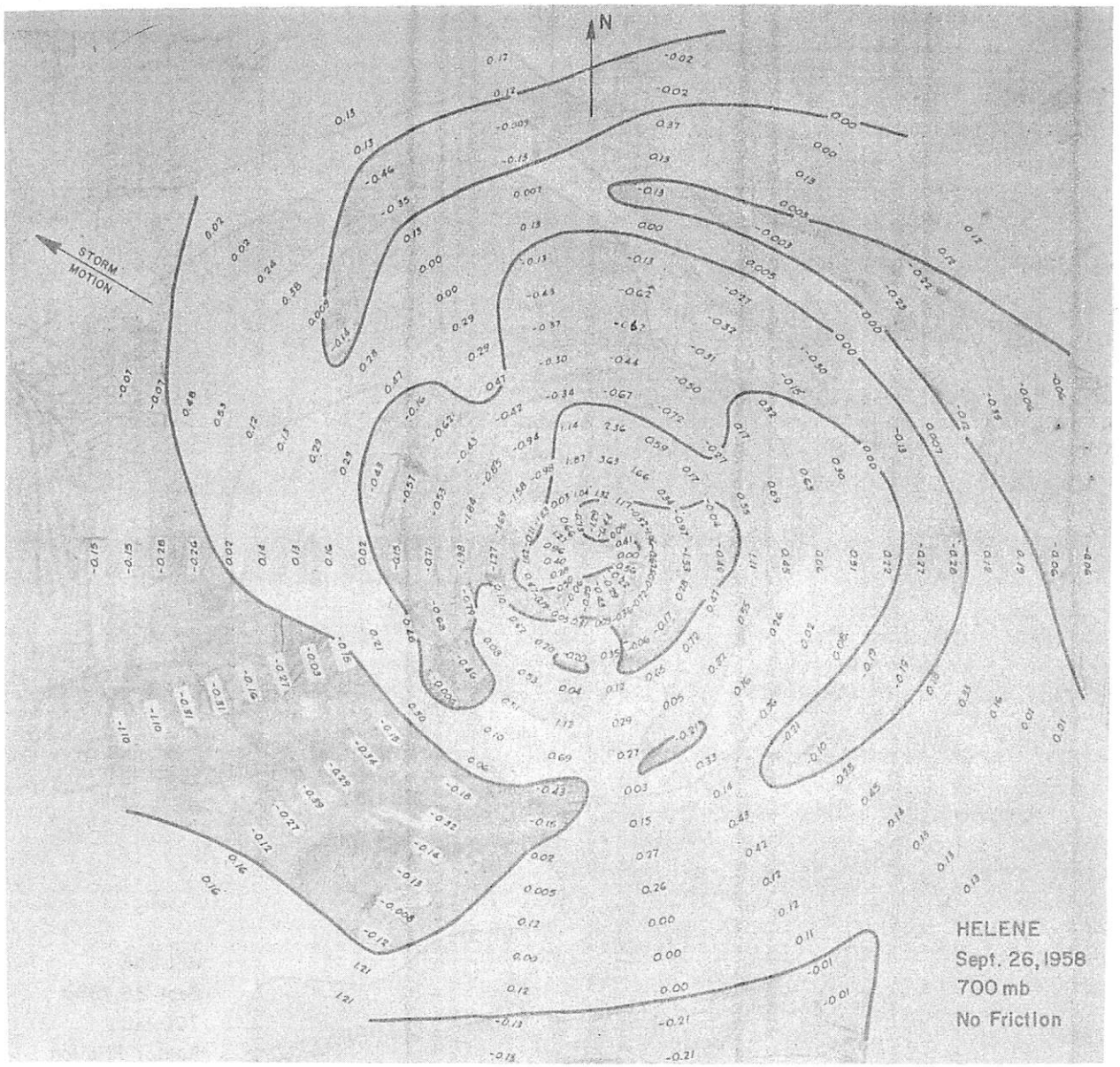

Figure 5. - Non-dimensional vertical velocity field for hurricane Helene for the case where no friction terms are included. To obtain the vertical velocities in units of millibars/hour, multiply by 131.22.

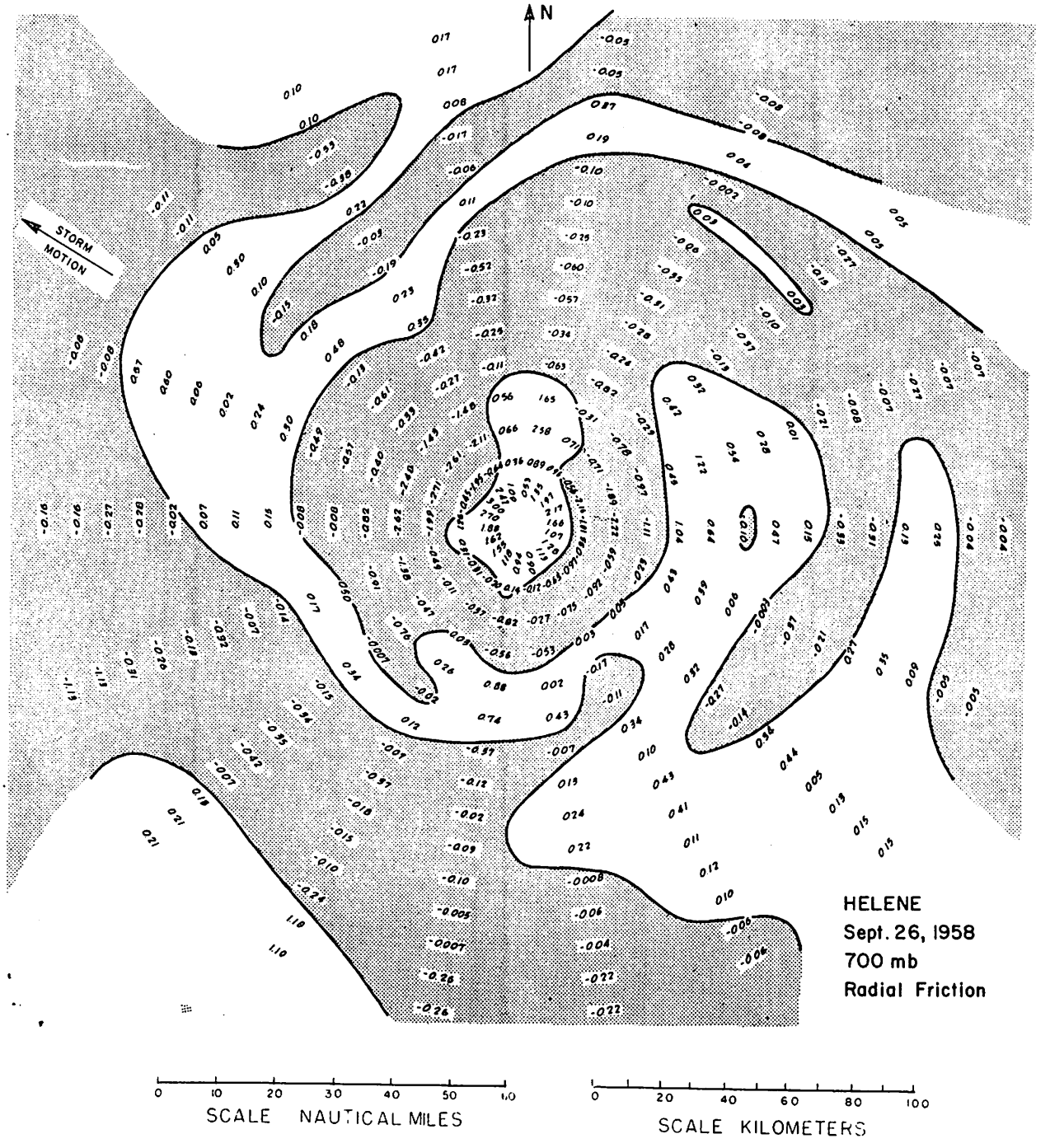

Figure 6. - Non-dimensional vertical velocity field for hurricane Helene for the case where the friction term due to the radial stress of the tangential wind is included. To obtain the vertical velocity in units of millibars/hour, multiply by 131.22.

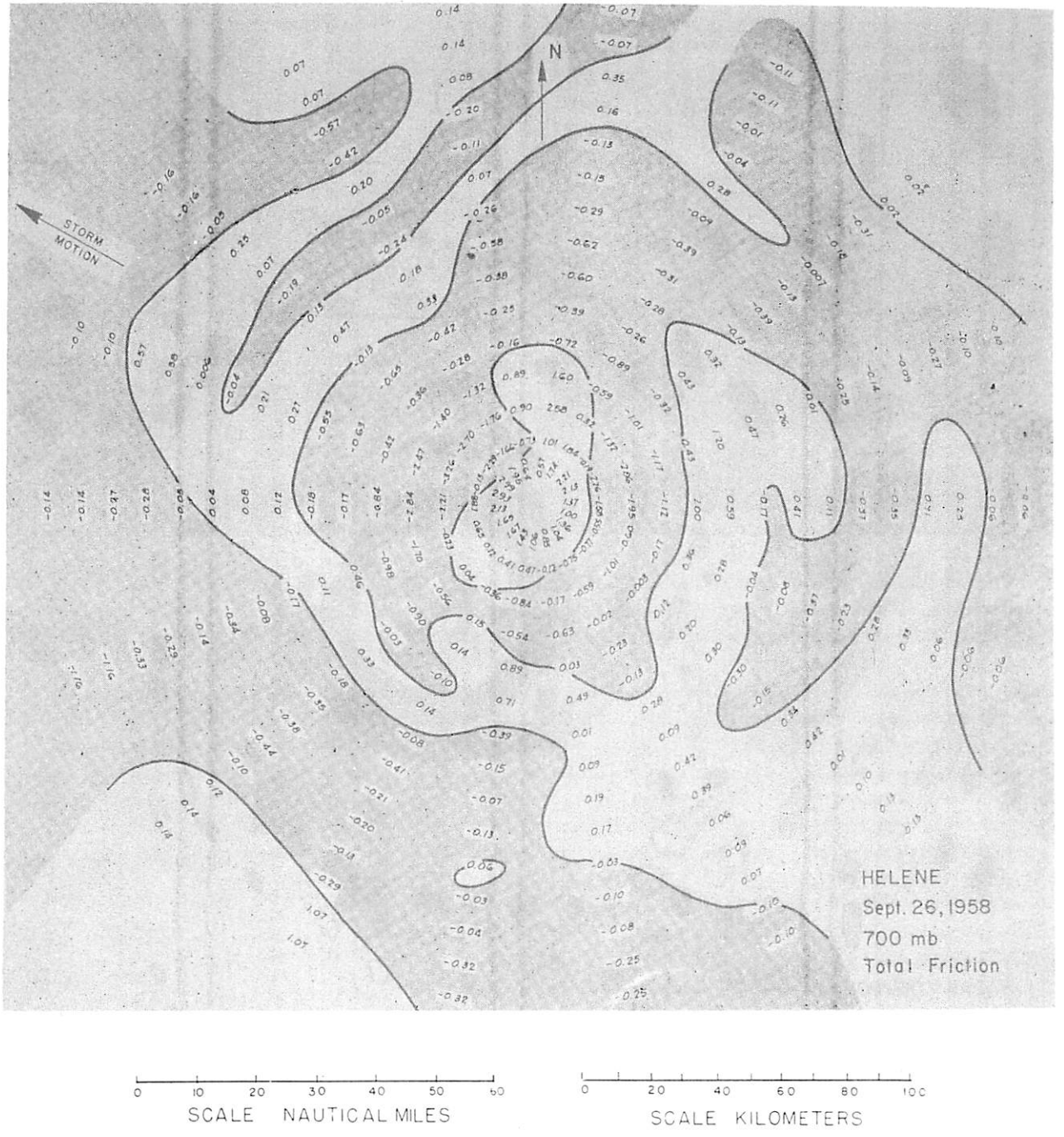

Figure 7. - Non-dimensional vertical velocity field for hurricane Helene for the case where all of the friction terms are included. To obtain the vertical velocities in units of millibars/hour, multiply by 131.22.

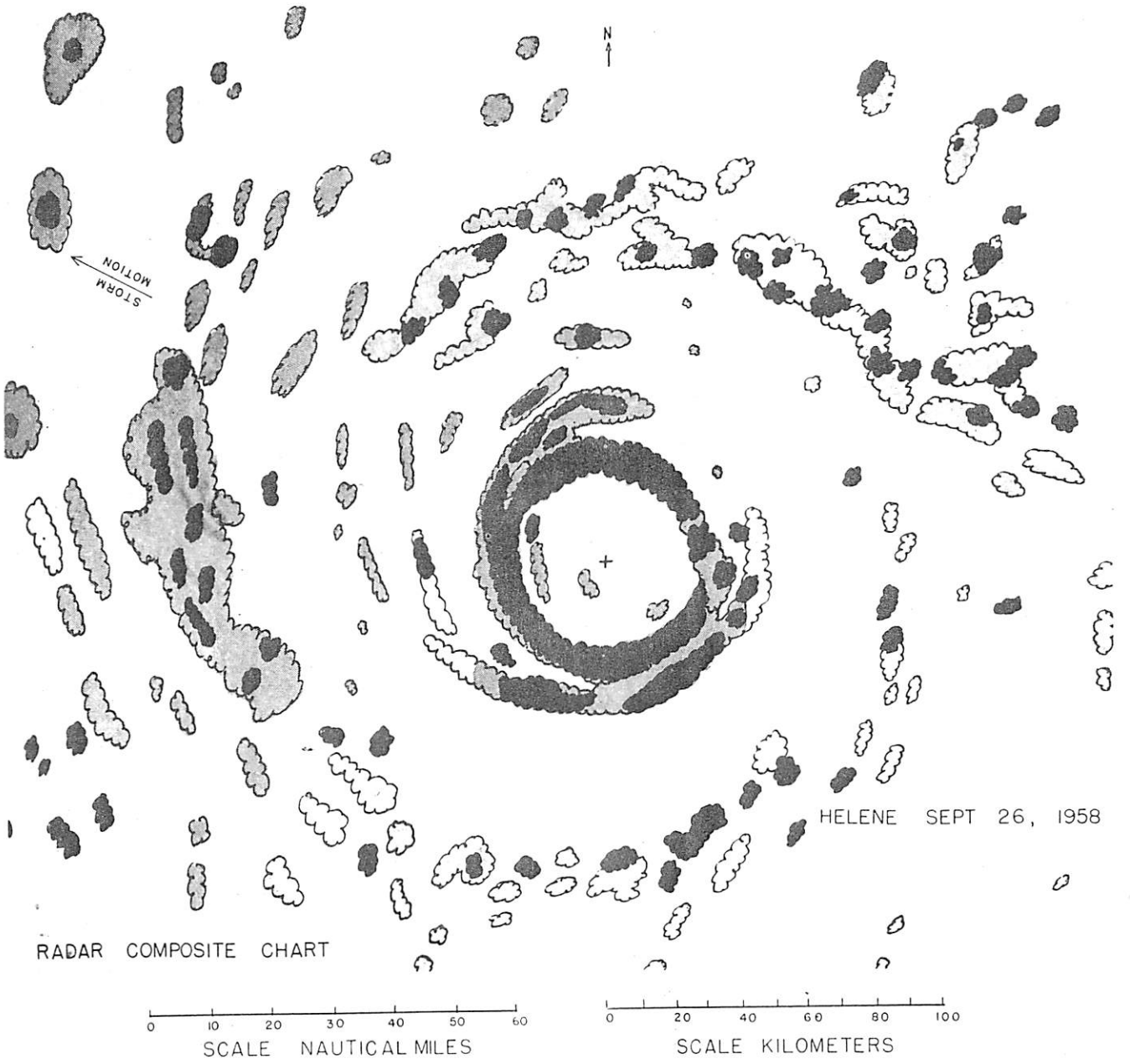

Figure 8. - Radar composite chart for hurricane Helene. The strong and weaker echoes are shown by different shading. [Note: Since the 2-cm. radar covers a small area, the final picture presented here is not very reliable for $r > 60$ km.]

REFERENCES

1. L. Berkofsky, "A Numerical Model for the Prediction of Hurricane Formation," Geophysical Research Papers, No. 67, 1960.

2. A. Kasahara, "A Numerical Experiment on the Development of the Tropical Cyclone," Technical Report, No. 12 on Contract Cwb 9718, Department of Meteorology, University of Chicago, 1960, 85 pp.

3. T. N. Krishnamurti, "On the Vertical Velocity Field in a Steady Symmetric Hurricane," Tellus, vol. 13, No. 2, May 1961, pp. 171-180.

4. T. N. Krishnamurti, "Some Numerical Calculations of the Vertical Velocity Field in Hurricanes," Technical Report, Department of Meteorology, University of California, Los Angeles, 1961.

THE "DOUBLE EYE" OF HURRICANE DONNA

C. L. Jordan
Department of Meteorology, Florida State University

and

Lt. Frank J. Schatzle, USN
Airborne Early Warning Squadron Four, Roosevelt Roads, Puerto Rico

On the afternoon of September 6, 1960, hurricane Donna presented a striking picture on the radar scope of a U. S. Navy hurricane reconnaissance aircraft[1] as illustrated by figure 1. The structure of the inner portion of the storm as indicated by the radar was very unusual in that not only was the exact center of the storm clear of precipitation echoes but there was also a relatively wide ring in the storm interior with little or no radar return. Descriptions of the core of this storm given to the press following the flight led to newspaper stories of a "double eye", and at least one newspaper headline referred to "two-eyed" Donna. These accounts were misleading since they failed to mention that the "eyes" were concentric. In the transmitted weather reports, the storm core was described in terms of two concentric wall clouds and the inner diameter of each of the radar rings was given. As will be discussed below, this "double eye" structure persisted for at least several hours and connections between the inner and outer rings, if present, were very weak.

A low-level penetration of the storm core was attempted from the south-southwest shortly after the time of the photograph presented in figure 1. The aircraft[2] was at an altitude near 1000 ft. and penetrated to a point about 32 mi. from the center of the inner ring or just outside the edge of the outer ring. At this point the penetration attempt was abandoned because of excessive engine cooling due to the heavy rain. Surface wind speed estimates based on the state of the sea reached 100 kt. at 45 mi. from the storm center and the maximum value was entered as "120+". The central sea level pressure of the storm at this time was near 940 mb.

A photograph of the scope of the vertically scanning radar taken during the attempted low-level penetration (fig. 2) gives additional information on the structure of the storm core. This range-height view, taken from a relative position indicated by the "x" in figure 1, was directed across the eye from south-southwest toward north-northeast. The cross-section of the inner ring is clearly shown but, because of attenuation, the outer ring on the opposite side is barely discernible. This radar, the APS-45, is subject to much greater attenuation than the APS-20E, from which figure 1 was obtained, because of the shorter wavelength which is used. The inner wall cloud is shown on the range-height scope as nearly vertical and the echoes extend above 30,000 ft. The diameter of this inner "eye" varied from about 10 mi. at the lower level to about 13 mi. at the higher levels.

---

[1] Of the Airborne Early Warning Squadron Four then located at the Naval Air Station, Jacksonville, Florida.

[2] The aircraft was of the Super Constellation type, U.S.Navy designation WV-3.

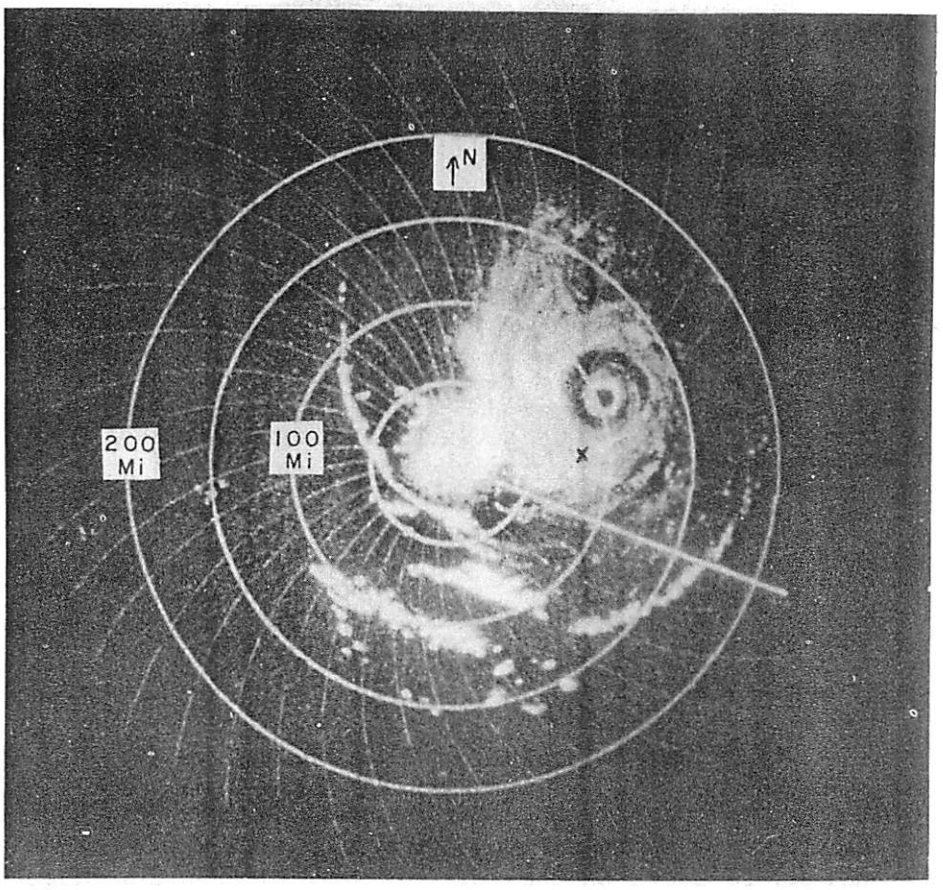

Figure 1. - A photograph of the scope of an APS-20E radar from a U. S. Navy hurricane reconnaissance aircraft taken at approximately 2100 GMT, September 6, 1960. The aircraft position (at the center of the photograph) was about 10 mi. south of Grand Turk Island and about 105 mi. west-southwest of the center of the hurricane. The aircraft was at an altitude of about 1500 ft. and on the heading of 110°. Some of the echoes to the south and southwest of the aircraft at a range of 75-150 mi. were from the mountains of Hispaniola. The APS-20E is an S band (10.4 cm.) radar with a peak power of 2.0 megawatts. The beam width, as defined by the half-power points, is approximately 1.5° in the horizontal and 6.0° in the vertical. The symmetrical spiralling pattern of light lines was caused by interference from other electronic equipment.

The "clear" zone between the inner and outer rings on figure 2 is confused to some extent on the side nearest the aircraft by return from the sea which shows up in the form of a horizontal fanshaped pattern. The small faint echo in the "clear" space on the far side of the inner ring should perhaps be associated with the small echo in the same region on figure 1. The time difference of the two photographs is only about 30 minutes.

The radar appearance of the inner ring was more characteristic of convective type echoes than the outer one and it extended to somewhat greater heights The maximum height of the inner ring during the several hours that it could be seen on this flight was about 45,000 ft. while the clouds forming the outer

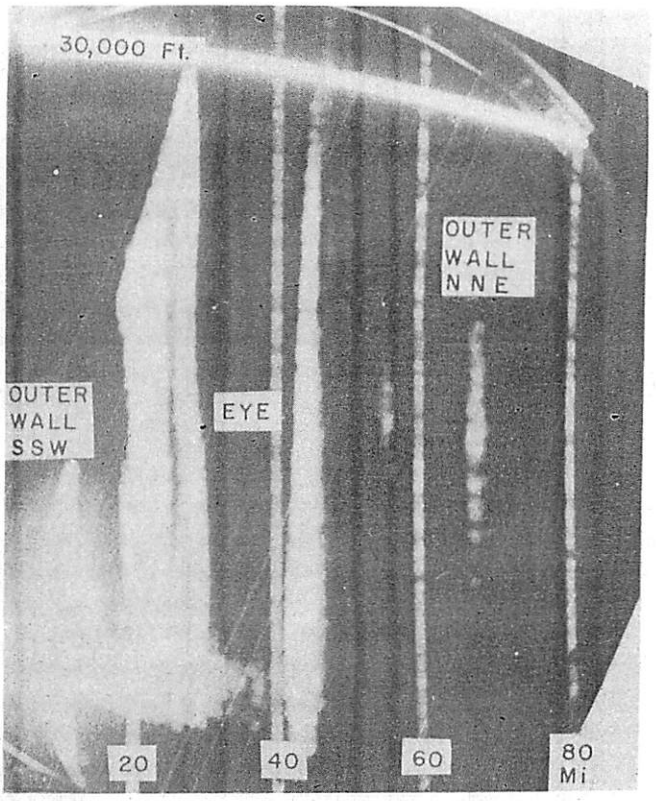

Figure 2. - A photograph of the range-height scope of the APS-45 radar from a U. S. Navy hurricane reconnaissance aircraft taken about 30 minutes after figure 1. Height is shown on the vertical scale and slant range from the aircraft on the horizontal scale. The aircraft was at a relative position given approximately by the "x" on figure 1 and was at an altitude of about 1,000 ft. The view is directly across the storm center toward the north-northeast. The APS-45 is an X band radar (3.2 cm.) with a peak power of 450 kilowatts. The beam width, as defined by the half-power points, is approximately 3.0° in the horizontal and 1.0° in the vertical.

ring appeared to be more stratiform in character and gradually died out on the range-height scope above 30,000 ft. In view of the greater strength and height of the inner echo, it could be argued that, at this time the inner radar ring should be considered as the true wall cloud of the eye.

Following the low-level penetration attempt, a climb to the 700-mb. level was made and the storm core was penetrated from the northeast with relatively little difficulty. The space between the radar rings was free of clouds in a layer which was estimated to extend from about 3,000 ft. to about 25,000 ft. However, only a limited area was visible during the penetration and, unfortunately, the exit was made after dark. The stratocumulus between the two radar rings consisted of well-formed concentric horizontal rolls and appeared to be unusually low. The ocean surface was not visible through the stratocumulus so that we have absolutely no information on the distribution of wind between the inner and outer rings. Unfortunately, the research aircraft of the National Hurricane Research Project did not enter Donna on this day.

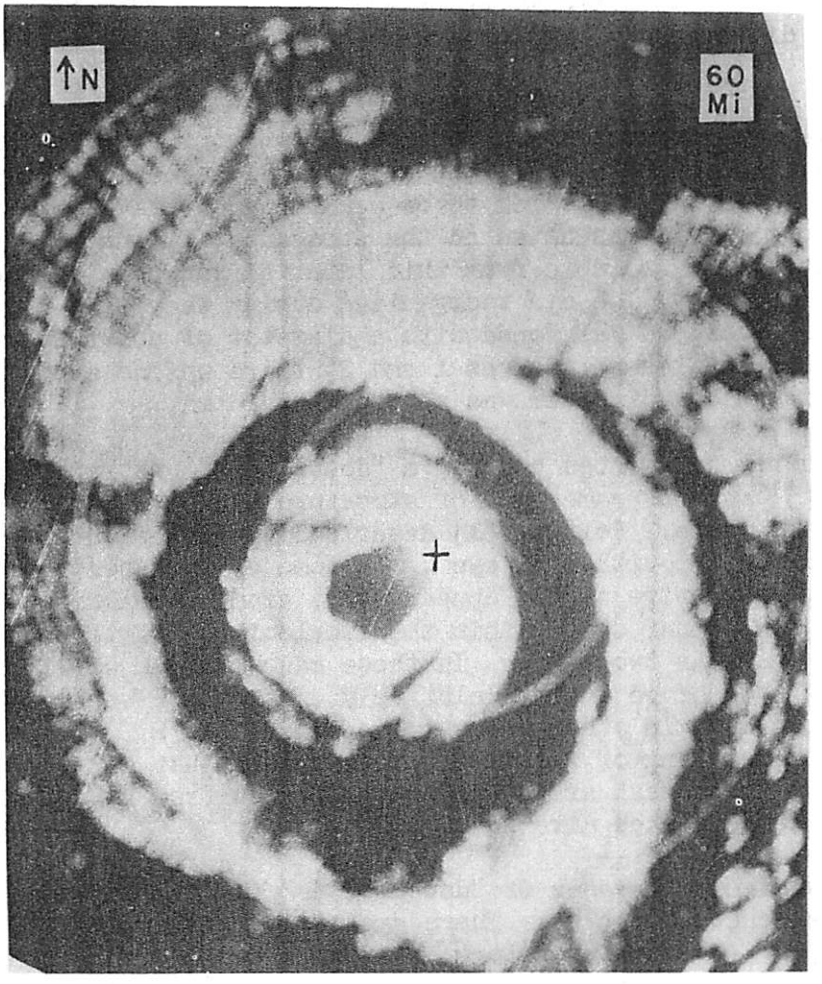

Figure 3. - A photograph of the plan-position scope of the APS-45 radar taken at approximately 2215 GMT, September 6, 1960. The aircraft was at the position indicated by the "+" and at an altitude of about 8,300 ft. The 20-mi. and 40-mi. range circles to the southeast of the center and the 60-mi. circle in the north-northeast sector can be seen faintly.

There was a thick layer of cirrus or high altostratus extending out from the inner core and covering the area between the two rings. The inner core of the storm was described by one of the pilots as resembling a giant "tastee freeze". Inside the inner ring, the stratocumulus was nearly overcast but the sea surface could be seen in spots. Cirrus was absent over most of the inner "eye" and there were no clouds above the stratocumulus which, in this area, extended to about 6,000 ft.

A photograph of the APS-45 scope taken during the penetration of the inner radar ring (while the radar was on horizontal scan) is shown in figure 3. The "clear" ring shows up nicely but it is shown as being somewhat narrower than indicated in figure 1. This difference is not surprising in view of the shorter wavelength of this radar and the fact that the aircraft was much closer to the cloud systems. The narrowest portion of the "clear" ring and the greatest suggestion of a connection is shown on the north side of the center. This is almost directly opposite to what was shown in figure 1 but

there is a time difference of a little more than an hour between these two photographs.

The "double eye" structure was observed throughout a period of about 5 hours during which the afternoon flight of September 6 had the hurricane on its radar. The inner ring appeared to be weakening as the aircraft moved away from the storm but it was noted on the subsequent flight a few hours later. Limited information is available from this later flight because the radar was not functioning properly. The eye reorganized during the night and on the following day an orthodox eye was found with a diameter of about 25 mi. About 12 hours prior to the time of figures 1 and 2, there was no evidence of a "double eye" and the eye diameter was reported as 20 mi.

A rather poorly documented case of a "double eye" was reported in a hurricane of 1947 [3] and the same type of structure has been reported in several typhoons in recent years. Fortner [1] described typhoon Sarah of 1956 at the time when it had "an eye within an eye". In some of the spectacular typhoon cases, the inner convective system appears as a giant cumulonimbus center in a large "eye." The "inner eye" within the cumulonimbus vortex has been observed to be as small as two miles. In these cases, winds well in excess of typhoon force were observed in the relatively clear space separating the inner and outer wall clouds. In other cases in recent years [2], the radar has indicated a very narrow ring of relatively weak return just outside a ring-shaped wall cloud but these weak areas were not apparent from visual observations made from the reconnaissance aircraft.

To our knowledge, all cases of "double eyes" in intense tropical cyclones have been of the concentric type. There are often radar features, the so-called "false eyes", outside the storm core which could be misinterpreted as the eye of the storm by inexperienced observers. These however, do not have closed circulations about them and are hardly detectable, if at all, in the wind and pressure fields.

REFERENCES

1. L. E. Fortner, Jr., "Typhoon Sarah, 1956," Bulletin of the American Meteorological Society, vol. 39, No. 12, Dec. 1958, pp. 633-639.
2. C. L. Jordan, D. A. Hurt, Jr., and C. A. Lowrey, "On the Structure of Hurricane Daisy on August 27, 1958," Journal of Meteorology, vol. 17, No. 3, June 1960, pp. 337-348.
3. U. S. Navy, "A Note on the Double Eye Phenomena as observed during Hurricane 11-20 Sept, 1947," NAVAER 50-IR-207, Office of Chief of Naval Operations, Washington, D. C. 11 pp.

VERIFICATION OF FORECASTS OF HURRICANE MOTION USING VARIOUS TECHNIQUES

Jack D. Tracy
National Hurricane Research Project, Miami, Florida

ABSTRACT

A number of techniques for forecasting hurricane motion for periods of 24 and 36 hours have been verified. These techniques were applied to the hurricanes which occurred during the 1959 and 1960 seasons.

From this appreciable sample of independent data, a sub-set of "homogeneous" data was selected. This sub-set is homogeneous in that only forecasts that were made at the same initial times by each technique are considered. For forecasts of 24-hour motion, the 1960 Travelers prediction equations (designated the "T-60" technique) developed in a cooperative effort with the National Hurricane Research Project, yielded the smallest median vector error of 68 n.mi. next smallest were the Riehl-Haggard-Sanborn (or AROWA) and 1959-Travelers methods with median vector errors of 104 and 106 n.mi., respectively. NWP was next with 122 n. mi.

For the forecasts of 36-hour motion, the T-60 technique had the lowest median vector error of 136 n. mi.

This study demonstrated (a) that the median vector errors were reduced as data became more plentiful, (b) the same techniques produced wide ranges in median errors from one storm to another, and (c) errors made by the T-60 technique became significantly less when the initial and persistence positions were accurately known.

INTRODUCTION

The purpose of this paper is to assess the performance of various forecasting techniques in determining the future course of hurricanes. The point of view taken by this investigation in achieving the above purpose has been that of the verification of operational forecasts of hurricane motion. The technical performance of these techniques will probably be considered at some future date.

In verifying the forecasts provided by the several objective techniques available to the forecaster on an operational basis, the forecast positions for 24 and 36 hours were verified against the actual location of the storm center at the end of these forecast periods. The parameter used as the verification measure is the vector error in units of nautical miles. The storm tracks

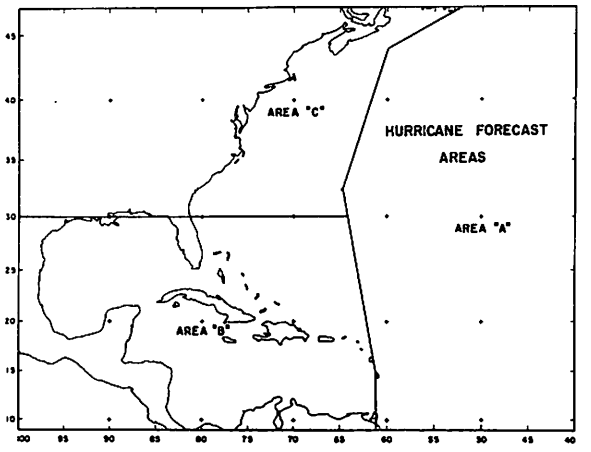

Figure 1. - Areas in which tropical storms were located at time of forecast; used for classifying the verifications.

against which the verifications were made are the official Weather Bureau tracks as published in [1, 2, 3][1].

The writer made all of the forecasts using the 1960 Travelers prediction equations [4] on a simulated operational basis. These equations are defined collectively as the "T-60" technique. They were developed in a cooperative effort between the National Hurricane Research Project and The Travelers Research Center, Inc.

As this technique was applied to the storms for which forecasts were made, a scrupulous attempt was made to prohibit hindsight knowledge of the storm's motion from influencing the selection of the initial and persistence positions that were used in the computations.

For this paper, the presentation of a "homogeneous" set of data has been undertaken. Except for the comments about the District Meteorological Office Operational Forecasts, only those forecasts which were made at the same initial times by each method for each storm are considered. These data have been extracted from a much larger and heterogeneous compilation of verification data, publication of which is expected in the future.

VERIFICATION OF DISTRICT METEOROLOGICAL OFFICES OPERATIONAL FORECASTS

For a paper that was presented by Gentry [5] at the First Technical Conference on Hurricanes in November 1958, the writer verified a number of the operational forecasts made by the Weather Bureau District Meteorological Offices. The verifications were classified according to the area in which the tropical cyclone was located at the time the forecast was made. These areas are shown in figure 1. These areas were selected for they roughly delineate the areas of data density. That is, the most data are usually obtained in Area "B", followed by Area "C", with the smallest amount of data coming from Area "A".

As a logical extension to this earlier work, the verification of these operational forecasts has been continued through the hurricane season of 1960. Table 1 presents these data.

Area "A" has the largest median error for all combinations of years except 1960 when only 8 cases were verified. This median error is 164 n. mi. for the years 1955-1960 and represents 173 cases.

[1]The writer had access to many of the large-scale maps of these storm tracks before they were reduced for inclusion in these publications.

Table 1. - Verification of District Meteorological Office operational forecasts considering the geographical location of the tropical cyclone at the initial time. Forecasts for 24 hours.

Year	Area A		Area B		Area C		A + B + C	
	Median Error (n.mi.)	No. Cases	Median Error (n.mi.)	No. Cases	Median Error (n.mi.)	No. Cases	Median Error (n.mi.)	No. Cases
1955-1957	145	118	93	131	131	84	118	333
1958	165	7	96	52	122	26	104	85
1959	307	40	125	59	127	27	152	126
1960	63	8	77	32	203	19	109	59
1958-1960	208	55	99	143	143	72	129	270
1955-1960	164	173	95	274	137	156	122	603

35 tropical cyclones were considered for the above results.

Area "C" has the next largest median error, 137 n.mi. for the years 1955-1960 representing 156 forecasts.

Area "B" has the least median error of 95 n.mi. for the years 1955-1960 and represents the median of 274 cases. These data clearly demonstrate the dramatic reduction in forecast errors when data become more plentiful.

Although the sample sizes are different from year to year, there appears to be a significant variability in the median error from one hurricane season to the next. This is particularly true if the median errors from area "B" are examined. The writer believes that this variability is due primarily to the accumulated forecast difficulties of the storms themselves.

The forecasts for 35 tropical storms and hurricanes have been verified. The overall median error for all storms and all areas is 122 n.mi. and represents the median of 603 forecasts. This compares with a median error of 118 n.mi. for 333 cases during the years 1955-1957.

Before leaving this section, it should be mentioned that these forecasts were made by many different people at different hurricane forecast offices.

VERIFICATION OF SEVERAL TECHNIQUES GIVING 24-HOUR FORECASTS

Tables 2 and 3 present the vector errors determined for several methods that were applied to the hurricanes of 1959 and 1960. Table 3 also gives the combined vector errors for 1959 and 1960.

These tables were designed to show the operational performance of the different techniques by individual storms as well as the combined results of

Table 2. - Verification of several forecasting techniques for hurricanes of 1959 in Areas "B" and "C". Vector errors are those resulting from errors in forecasts made by each technique making forecasts from the same initial times. Forecasts for 24 hours.

Method	"Cindy"				"Gracie"				"Hannah"			
	Sum	N	Med	Ran	Sum	N	Med	Ran	Sum	N	Med	Ran
T-60	22	1	22	-	808	10	66	37-187	261	3	78	57-126
1959-Travelers	116	1	116	-	956	10	96	54-128	416	3	132	106-178
AROWA	133	1	133	-	978	10	69	34-317	196	3	77	12-107
JNWP	225	1	225	-	1316	10	126	37-232	153	3	48	27-78
Persistence	102	1	102	-	823	10	86	9-144	407	3	167	12-228

Method	"Judith"				"Combined"			
	Sum	N	Med	Ran	Sum	N	Med	Ran
T-60	219	1	219	-	1310	15	68	22-219
1959-Travelers	127	1	127	-	1615	15	116	54-178
AROWA	130	1	130	-	1437	15	75	12-317
JNWP	612	1	612	-	2306	15	125	27-612
Persistence	247	1	247	-	1579	15	102	9-247

Note: In this and the following tables the abbreviations are:-
Sum = Sum of vector errors in n.mi.
N = Number of forecasts
Med = Median error of sample in n.mi.
Ran = Range of sample in n.mi.

Table 3. - Verification of several forecasting techniques for hurricanes of 1960 in Areas "B" and "C". Vector errors are those resulting from errors in forecasts made by each technique making forecasts from the same initial times. Forecasts for 24 hours.

Method	"Cleo"				"Donna"				"Combined"			
	Sum	N	Med	Ran	Sum	N	Med	Ran	Sum	N	Med	Ran
T-60	258	1	258	-	838	11	55	17-220	1096	12	69	17-258
1959-Travelers	290	1	290	-	973	11	88	27-202	1263	12	89	27-290
AROWA	104	1	104	-	1445	11	130	40-207	1549	12	130	40-207
JNWP	266	1	266	-	1727	11	118	29-369	1993	12	120	29-369

Method	"1959 and 1960 Combined"			
	Sum	N	Med	Ran
T-60	2406	27	68	17-258
1959-Travelers	2878	27	106	27-290
AROWA	2986	27	104	12-317
JNWP	4299	27	122	27-612

Table 4a. - Verification of the T-60, JNWP, and persistence forecasting techniques for hurricanes of 1959 in Areas "B" and "C". Vector errors are those resulting from errors in forecasts made by each technique making forecasts from the same initial times. Forecasts for 36-hours.

Method	"Cindy"				"Debra"				"Gracie"			
	Sum	N	Med	Ran	Sum	N	Med	Ran	Sum	N	Med	Ran
T-60	703	3	257	119-327	384	2	192	114-270	1872	14	127	37-321
Persistence	624	3	202	82-340	283	2	142	92-191	2520	14	200	32-295
JNWP	828	3	238	192-398	187	2	94	66-121	2433	14	189	54-294

Method	"Hannah"				"Judith"				"Combined"			
	Sum	N	Med	Ran	Sum	N	Med	Ran	Sum	N	Med	Ran
T-60	993	5	204	87-294	1189	3	468	237-484	5141	27	159	37-484
Persistence	1416	5	300	150-444	1365	3	438	288-639	6208	27	207	32-639
JNWP	671	5	133	99-174	2516	3	693	497-1326	6635	27	184	54-1326

Table 4b. - Verification of the T-60, JNWP, and persistence forecasting techniques for hurricanes of 1960 in Areas "B" and "C". Vector errors are those resulting from errors in forecasts made by each technique at the same initial times. Forecasts for 36-hours.

Method	"Cleo"				"Donna"				"Ethel"			
	Sum	N	Med	Ran	Sum	N	Med	Ran	Sum	N	Med	Ran
T-60	158	1	158	-	1370	12	77	17-327	325	1	325	-
Persistence	222	1	222	-	2485	12	184	122-452	354	1	354	-
JNWP	364	1	364	-	2925	12	189	26-658	191	1	191	-

Method	"Combined"				"1959 and 1960 Combined"			
	Sum	N	Med	Ran	Sum	N	Med	Ran
T-60	1853	14	111	17-327	6994	41	136	17-484
Persistence	3061	14	193	77-452	9269	41	202	32-639
JNWP	3480	14	190	26-658	10115	41	189	26-1326

each technique. Because of the restriction imposed by considering these forecasts which were made by each technique at the same initial times, the sample size has been reduced greatly. However, this restriction does permit a good homogeneous set of data to be presented for analysis and study.

Tables 2 and 3 indicate the variability in the vector errors resulting from the forecasts made by these techniques from one storm to another. It is suggested that no technique had a stable performance. For example, the T-60 method for Gracie has a median error of 66 n. mi. whereas for Donna the error is 55 n. mi. The Riehl-Haggard-Sanborn (or AROWA) method for Gracie has a median error of 69 n.mi. whereas for Donna the error is 130 n.mi.

When the combined errors for each year are inspected, it is seen that the T-60 and JNWP techniques maintained about the same medians. The others exhibited wide variations.

When the overall performances of 1959 and 1960 are combined, the T-60 method has the smallest median error of 68 n.mi. Next were the Riehl-Haggard-Sanborn and 1959 Travelers methods with 104 and 106 n.mi., respectively. They were followed by the JNWP technique with 122 n.mi. Twenty-seven forecasts were verified for each of these medians.

VERIFICATION OF 36-HOUR FORECASTS USING THE T-60, JNWP, AND PERSISTENCE TECHNIQUES

Tables 4a and 4b present the vector errors for the T-60, JNWP, and persistence techniques for the hurricanes of 1959 and 1960. Table 4b gives the combined vector errors for 1959 and 1960.

These tables also illustrate the fact that the 36-hour forecast techniques show variability in performance from one storm to another as did the 24-hour forecast techniques. Not considering the data for hurricane Judith, the T-60 method has median errors ranging from 77 to 204 n.mi. Similar statements can be made for the other two methods.

When the combined errors for each year are inspected, it is seen that the errors for each technique varied but the JNWP method had the least variability.

When the overall performances of 1959 and 1960 are combined, the T-60 method has the least median error of 136 n.mi. followed by JNWP with 189 n.mi. Next was persistence with 202 n.mi. Forty-one forecasts were verified for each of these medians.

A further breakdown of this verification data into areas "B" and "C" and by storm intensity was undertaken. These tables will not be presented but the significant points contained in them showed essentially the same information as given in tables 2, 3, and 4 except that the magnitudes of the median errors were somewhat less.

SUMMARY, CONCLUSIONS, AND SUGGESTIONS

For those forecasts of 24-hour motion, the T-60 technique has the smallest median error of 68 n.mi. followed by the Riehl-Haggard-Sanborn and 1959 Travelers methods with 104 and 106 n.mi. respectively. JNWP followed with 122 n. mi.

For those forecasts of 36-hour motion, the T-60 technique has the least median error of 136 n.mi. Next was JNWP with 189 n.mi. followed by persistence with 202 n.mi.

All median errors for these techniques appeared to become smaller as the data became more plentiful.

The writer believes that this study enables him to endorse a suggestion made by Veigas, Miller, and Howe [6]. This suggestion is "... Reduction in the size of the zones or a stratification of storms according to structure should be attempted in order to provide more homogeneity in the storms for which a given equation [or technique][2] is used ..."

As an attempt to predict the track of a hurricane more accurately during recurvature or a change in course, parameters could be developed from the dependent data which (a) give the radii of curvature exhibited by known storm tracks as a function of the motion of the storm center, and (b) give the rates of change of these radii of curvature as a function of observed accelerations and decelerations in the motion of the storm center. This information would be incorporated in statistically determined prediction equations by suitable means.

Present and future prediction techniques might be modified so as to "monitor themselves" by considering the latest vector error made by each technique during a particular storm.

An experiment conducted using hurricane Donna has highlighted the importance of having accurate information as to the initial and persistence positions of a hurricane in applying the T-60 technique. When the initial and persistence positions that were determined operationally are used, the average vector error is 90 n.mi. If the initial and persistence positions as determined from the official tracks are used, the average vector error becomes 73 n.mi. Thirty-seven forecasts were verified in each case.

Of course the accuracy of all techniques would probably improve as suitable data necessary for their application became more plentiful.

---

[2] Added by writer.

REFERENCES

1. G. W. Cry, W. H. Haggard, and H. S. White, "North Atlantic Tropical Cyclones," Technical Paper No. 36, U. S. Weather Bureau, Washington, D. C., 1959, 214 pp.
2. G. E. Dunn, and Staff Weather Bureau Office, Miami, "The Hurricane Season of 1959," Monthly Weather Review, vol. 87, No. 12, Dec. 1959, pp. 441-450 (see p. 442.).
3. G. E. Dunn, "The Hurricane Season of 1960," Monthly Weather Review, vol. 89, No. 3, Mar. 1961, pp. 99-108.
4. K. W. Veigas, "Prediction of Twelve, Twenty-four and Thirty-six Hour Displacement of Hurricanes by Statistical Methods," Final Report , Contract No. Cwb-9807, The Travelers Research Center, Inc., Hartford, Conn., 1961, 36 pp.
5. R. C. Gentry, "A Re-Evaluation of the Problem of Predicting Hurricane Movement," Proceedings of the Technical Conference on Hurricanes, American Meteorological Society, Miami, Fla. 1958.
6. K. W.Veigas, R. G. Miller, and G. M. Howe, "Probabilistic Prediction of Hurricane Movements by Synoptic Climatology," Occasional Papers in Meteorology, No. 2, Travelers Weather Research Center, Hartford, Conn., 1959.

USE OF VERTICALLY INTEGRATED FLOW IN PREDICTION OF HURRICANE DISPLACEMENT[1]

(Condensed Version)

Frederick Sanders
Massachusetts Institute of Technology, Cambridge, Mass.

INTRODUCTION

In view of the crucial nature of the prediction of hurricane position it seems worthwhile to investigate the possible advantages of barotropic prediction of vertically averaged flow in this respect. Previous attempts at barotropic prediction of hurricane tracks by application at mid-tropospheric levels have been reported by Kasahara [1] and by Birchfield [2], among others, with some success. It is reasonable to hope, therefore, that a significant improvement in the accuracy of these forecasts can be achieved by use of vertically averaged data in lieu of data at a single level or a simple combination of data at a few levels.

THE BASIS OF THE PREDICTION METHOD

The development of the prediction method starts with a pressure-averaged form of the simplified vorticity equation, derived on the assumption that ω, the substantial derivative of pressure, vanishes at 1000 mb. and at 100 mb., the boundaries of the layer over which the averaging is performed. Thus,

$$\frac{\partial h_m}{\partial t} = - \mathbf{V}_m \cdot \nabla (h_m + f) - (\mathbf{V}' \cdot \nabla h')_m \qquad (1)$$

where

$$( )_m \equiv \frac{1}{900\ (\text{mb.})} \int_{100(\text{mb.})}^{1000(\text{mb.})} ( )\ dp$$

$$( )' \equiv ( ) - ( )_m$$

The second term on the right-hand side of equation (1) is neglected in the present work, though it may be important to the extent that there is an organized pattern of vertical wind shear.

Application of the principles of Fjørtoft's [3] graphical technique indicates that the displacement velocity of the hurricane, $\mathbf{C}$, is given by the velocity of a "steering" flow evaluated at the hurricane center. Specifically,

---

[1]The work reported herein was sponsored by Geophysics Research Directorate, Air Force Cambridge Research Laboratories under Contract Nos. AF 19(604)-1305, AF 19(604)-5491, and AF 19(604)-8373.

Table 1. - Summary of results.

Period	RMS Position Error (n.m.) 12-hr Fcst	RMS Position Error (n. m.) 24-hr Fcst	RMS Position Error (n. m.) 36-hr Fcst	RMS Magnitude of Vector Diff. $\lvert\mathbb{C} - \overline{\overline{\mathbb{W}}}\rvert$ (Knots)	Mean Vector Diff. (Deg & kts) Geographical	Mean Vector Diff (Deg & kts) Relative	
1954-1958	—	156	—	3.3	129/0.8	126/LQ	
N		41		42	42	42	
1959-1960	58	126	257	4.1	140/1.4	130/1.5	
N	27	25	22	27	27	27	
Gracie (1959)	46	98	200	44	150/2.9	145/1.7	
N	6	6	6	7	7	7	
Donna (1960)	55	95	228	3.9	120/1.3	160/2.4	
N	7	6	6	7	7	7	

$$\mathbb{C} = \overline{\mathbb{V}_m} + \mathbb{V}_G \qquad (2)$$

where

$$\mathbb{V}_m = (g/f)\ \mathbb{k} \times \nabla \overline{Z}_m$$

$$\mathbb{V}_G = (g/f)\ \mathbb{k} \times \nabla G$$

$$G \equiv \int_0^{\phi} (f^2 \Delta^2 \operatorname{cotan} \phi / gm.^2)\, d\phi$$

Here $\overline{Z}_m$ is a horizontally averaged height. The selected value of the averaging distance, Δ, was 180 n.mi., half that recommended by Fjørtoft. This choice, however, is appropriate for the relatively small size of the tropical cyclone. The velocity, $\mathbb{V}_G$, carries the influence of the variation of Coriolis parameter. It is an east wind of about 1 kt. and was neglected in the results to be presented. The intense inner portion of the hurricane vortex was intentionally omitted from the initial analysis.

RESULTS

Table 1 contains a summary of results obtained in application of the method to numerous hurricanes over the period from 1954 to 1960. These results are of two types. The three right-hand columns of the table afford com-

parisons of the hurricane displacement velocity and the concurrent steering velocity,[2] and thus a test of the validity of equation (2). The vector differences are quite small and quite consistent from year to year and from storm to storm. The two right-hand columns indicate the presence of a significant bias. The direction of the difference is the direction from which the vector emanates. Thus, storms move more rapidly northwestward than indicated by the steering flow. The mean relative difference (with 360° being taken as the direction toward which the storm is moving) indicates that the storm moves to the left of the direction of the steering flow and more rapidly than its speed. The zonal bias is attributable to the failure to include V_G in the actual determinations of steering flow. Analysis error and the effect of organized vertical wind shear probably both contribute to the bias along the storm track.

A number of forecasts of storm position were made by displacing the hurricane for 12, 24, or 36 hours in the initial field of steering flow, on the assumption that the field remains steady. The results of these forecasts are summarized in the first three columns of table 1. The relatively high root-mean-square error in the 24-hour forecasts for 1954-1958 is attributable to the ten predictions made for Hazel 1954, which yielded a RMS error of 253 n.mi. The error for the remaining forecasts during this period was 107 n.mi. In the case of Hazel, and indeed with all other cases of spectacular error, there were pronounced temporal changes in the steering flow. Recomputation of selected trajectories, based upon either observed or barotropically computed changes of the steering flow, eliminated about half of the error in these cases of forecast failure.

ADVANTAGES OF THE USE OF VERTICALLY AVERAGED DATA

These results are not significantly better than those obtained by any of several other methods. To demonstrate the efficacy of the use of vertically averaged winds a direct study was made of the difference between this flow and 500-mb. flow. A typical result, for Carol 1954, is shown in figure 1. In this figure the vertically averaged and 500-mb. heights are expressed as $\tilde{D}$ and D_5, their respective departures from standard atmosphere values. A hub of excessive averaged heights, due to relative warmth in the upper troposphere, lies to the right of the track of this northward-moving storm. The averaged wind contains a stronger southerly component than does the 500-mb. wind at all coastal locations. In view of the deficit in predicted speed yielded by the averaged data it is apparent that a forecast based upon 500-mb. data alone must be inferior.

Similar patterns of difference were found for many of the other cases investigated, but not for all. A similar pattern, unusually well documented by

---

[2] The wavy bar refers to an approximation to the vertically averaged value, derived from use of data at mandatory levels. Thus, $(\tilde{\ }) \equiv \frac{1}{12}(\ )_{1000} + \frac{1}{6}(\ )_{850} + \frac{1}{5.14}(\ )_{700} + \frac{1}{6}(\ )_{500} + \frac{1}{9}(\ )_{400} + \frac{1}{12}(\ )_{300} + \frac{1}{18}(\ )_{250} + \frac{1}{18}(\ )_{200} + \frac{1}{18}(\ )_{150} + \frac{1}{36}(\ )_{100} \approx (\ )_m$

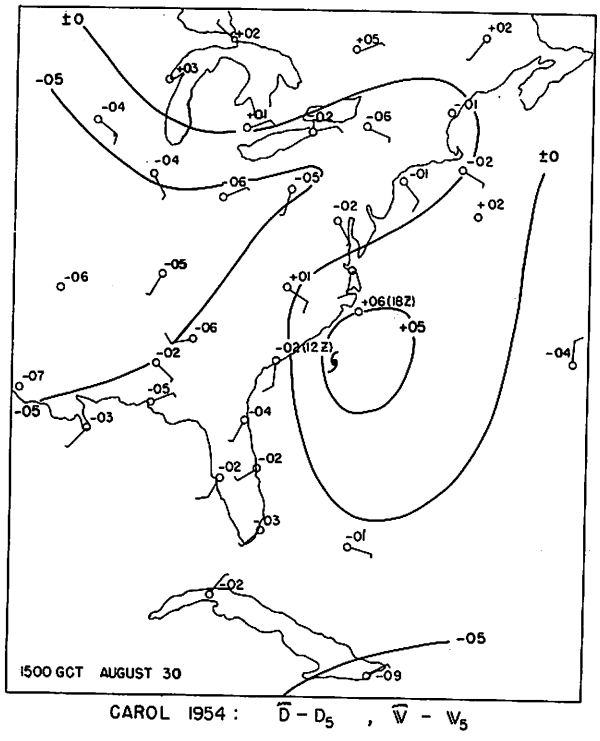

Figure 1. - Difference between vertically averaged and 500-mb. flow. Carol, 1500 GMT Aug. 30, 1954.

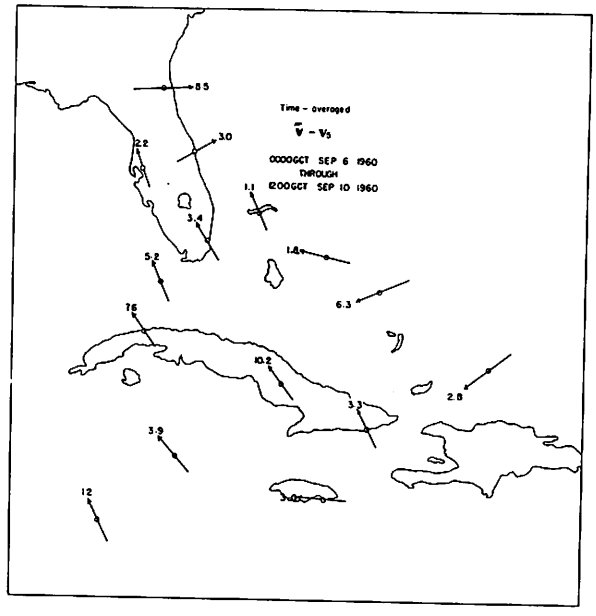

Figure 2. - Time-averaged 500-mb. wind, Donna, Sept. 6-10, 1960.

wind data, was found for Donna 1960 over the period September 6 to 10, as shown in figure 2. The track of the storm lay from a short distance northeast of Hispaniola through the Bahamas to southern Florida. Again the averaged data contain a few more knots along the track than do the 500-mb. data, so that the former must yield a superior forecast.

These results suggest the presence of vertical wind shear sufficiently well organized to raise some doubt whether the neglect of the second term on the right-hand side of equation (1) is justifiable. In an attempt to answer this question, a dynamic analysis was performed of the winds in the vicinity of Donna 1960 from September 6 to 10. To avoid the cumbersome analysis of vorticity gradients, the treatment was carried out in analogous terms of momentum transport, along lines suggested by Starr [4]. With reference to figure 3, consider a cylinder with a locally fixed vertical axis and a radius R, bounded at the base and top by the 1000-mb. and 100-mb. surfaces, respectively. On the assumption that ω vanishes at these levels, and with the neglect of friction, the time rate of change of M, the angular momentum of flow within the cylinder about the local axis is given approximately by the transport of momentum across its surface. Thus,

$$\frac{\partial M}{\partial t} \approx R \int_S \rho \; c_T \; c_R \; dS = \frac{R \; 900(\text{mb.})}{g} \int_0^{2\pi} (c_T \; c_R)_m \; d\theta \qquad (3)$$

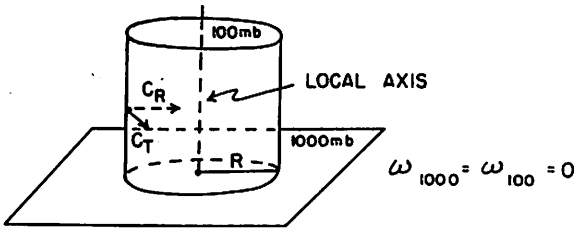

Figure 3. - Diagram illustrating angular momentum computations.

where $M \equiv \int_V \rho\ r\ c_T\ dV$.

Note that momentum transport is proportional to the product of the tangential and radial components of the wind, c_T and c_R, respectively. As in the case of vorticity advection, it is convenient to write

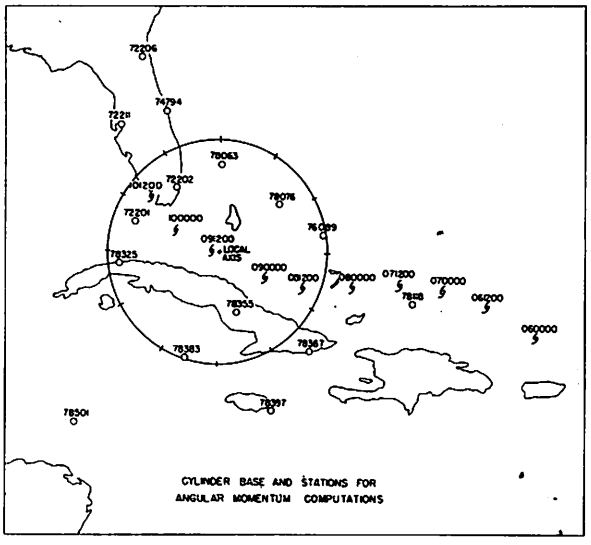

Figure 4. - Cylinder base and stations for angular momentum computations with track of hurricane also shown.

$$(c_T\ c_R)_m = (c_T)_m\ (c_R)_m + (c_T'\ c_R')_m \qquad (4)$$

Similarly the second term on the right-hand side of equation (4) represents the effect of organized vertical wind shear. The selected local axis and the stations for which data were considered are shown in figure 4, along with positions of the storm center.

Values of $\widetilde{\widetilde{c_T\ c_R}}$, $\widetilde{c_T}\ \widetilde{c_R}$, and $(c_T\ c_R)_5$ were evaluated for each available wind sounding. An analysis of the results is presented in figure 5. It is evident that the value of the mean product, $\widetilde{\widetilde{c_T\ c_R}}$, can be better represented by the product of the means, $\widetilde{c_T}\ \widetilde{c_R}$, than by the product at 500 mb., the level most frequently used for barotropic prediction. Cursory examination of the data indicated that the mean product was most closely approximated by the data at 700 mb. and at 500 mb. more frequently than by data at other levels, but not by a wide margin.

For more direct implications concerning vorticity advection than can be given by analysis of individual soundings, estimates of momentum transfer across the vertical wall of a cylinder with radius 240 n.mi., the base of which is shown in figure 4, were made by summations of analyzed values of $\widetilde{\widetilde{c_T\ c_R}}$ and $\widetilde{c_T}\ \widetilde{c_R}$ at twelve points on the circumference. The summations of these two quantities were highly correlated ($r = 0.984$) and the regression equation was given by

$$\sum \widetilde{\widetilde{c_T\ c_R}} = 87 + 1.09\ \widetilde{c_T}\ \widetilde{c_R}\ (\text{kt.})^2 \qquad (5)$$

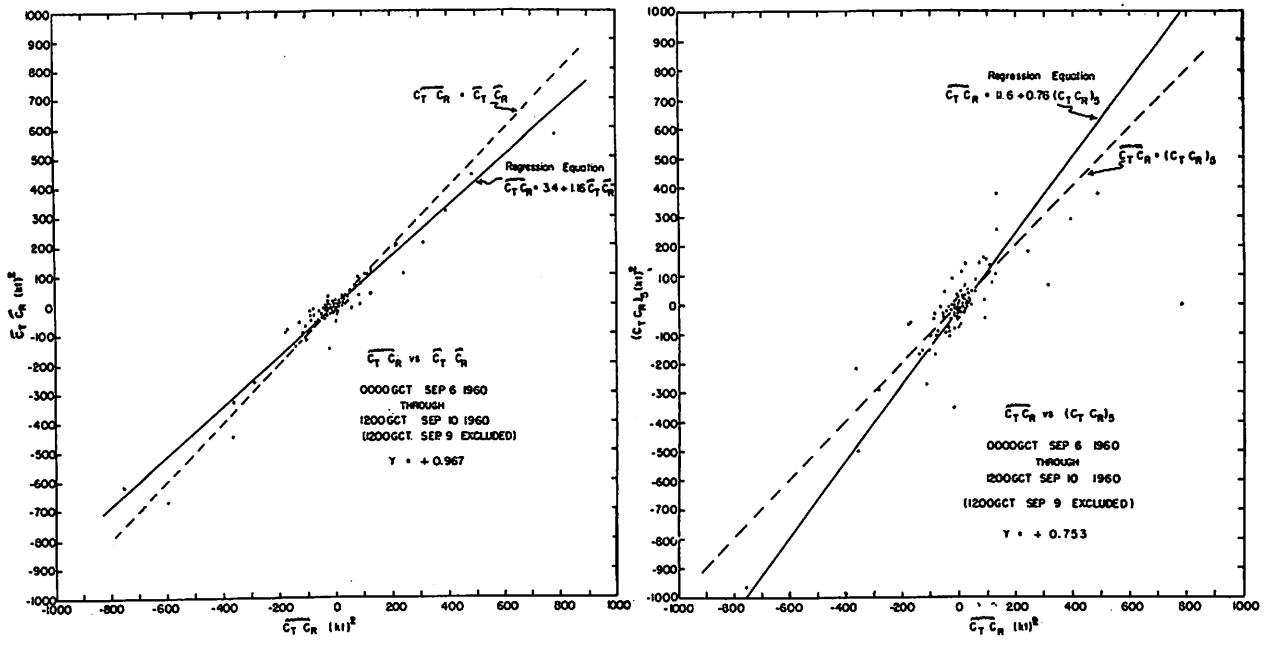

Figure 5. - Comparisons of evaluation of $\widetilde{c_T\, c_R}$, $\widetilde{c}_T\, \widetilde{c}_R$, and $(c_T\, c_R)_5$ for each available wind sounding.

The fact that the product of the means underestimated the mean product by almost 10 percent suggests that the deficit in predicted forward speed for this hurricane (see table 1) can be partly accounted for by the neglect of $(\mathbb{V}' \cdot \nabla h')_m$ in equation (1).

At this point, however, a curious paradox arises. Because of the high correlation mentioned above, it is evident that $\widetilde{c_T'\, c_R'}$ is nearly proportional to $\widetilde{c}_T\, \widetilde{c}_R$. This feature is specifically characteristic of the equivalent-barotropic model atmosphere, as propounded by Charney and Eliassen [5]. Yet no "equivalent-barotropic level" can be found at which the product represents the mean product as well as does the product of the means. The reason appears to be that substantial irregular, and largely random, vertical variation of wind is present along with the organized large-scale shear, rendering the wind at any single level nonrepresentative to a greater or lesser degree. There seems to be no short-cut around use of the vertically integrated data.

A CONCLUDING RECOMMENDATION

A suggested optimum forecasting procedure might be:

1. Compute vertically averaged data over the region within perhaps 1000 miles of the hurricane.

2. Remove the intense inner portion of the vortex by ignoring it, or perhaps by some better way.

3. Determine a hurricane steering flow by suitable horizontal averaging of the rest of the field of flow. Perhaps the hurricane could be displaced with a percentage of the speed of the steering flow, as determined by a regression analysis of momentum transports in the initial data.

4. Predict temporal changes of the steering flow barotropically, using convential 500-mb. results as a boundary condition along the periphery of the inner environmental region.

Through use of a procedure such as this it would not be unreasonable to hope that the error in short-range prediction of hurricane displacement could be reduced to about 60 percent of its present value.

REFERENCES

1. A. Kasahara, "The Numerical Prediction of Hurricane Movement with the Barotropic Model," Journal of Meteorology, vol. 14, No. 5, Oct. 1957, pp. 386-402.
2. G. E. Birchfield, "Numerical Prediction of Hurricane Movement With the Use of a Fine Grid," Journal of Meteorology, vol. 17, No. 4, Aug. 1960, pp. 406-414.
3. R. Fjørtoft, "On a Numerical Method of Integrating the Barotropic Vorticity Equation," Tellus, vol. 4, No. 3, Aug. 1952, pp. 179-194.
4. V. P. Starr, "Some Aspects of the Dynamics of Cyclones," Geophysical Research Papers, No. 24, Air Force Cambridge Research Center, 1953, pp. 9-17.
5. J. G. Charney and A. Eliassen, "A Numerical Method for Predicting the Perturbations of the Middle Latitude Westerlies," Tellus, vol. 1, No. 2, May 1949, pp. 38-54.

INTERACTION OF A HURRICANE WITH THE STEERING FLOW AND ITS EFFECT UPON THE HURRICANE TRAJECTORY

Akira Kasahara

and

George W. Platzman

The University of Chicago, Chicago, Ill.

ABSTRACT

If the steering flow is defined at all times as the residual after subtraction of an axially-symmetric vortex which moves with variable speed but invariant shape, then as shown by Morikawa, interaction terms appear in the prediction equation which governs the steering flow.

The vortex is taken here as in previous work by Kasahara [1] as one which minimizes the variance of the steering flow in the initial data, rather than as the singular vortex used by Morikawa [3]. The propagation velocity of the vortex, defined in such a way as to minimize individual changes of the steering-flow vorticity or potential vorticity, includes small dynamical terms dependent upon the steering-flow vorticity gradient and upon the scale of the vortex.

Numerical computations are made for hurricane Betsy 1956; the results are compared with those obtained earlier (Kasahara [2]) and with those of Morikawa.

REFERENCES

1. A. Kasahara, "The Numerical Prediction of Hurricane Movement with the Barotropic Model," Journal of Meteorology, vol. 14, No. 5, Oct. 1957, pp. 386-402.
2. A. Kasahara, "A Comparison between Geostrophic and Nongeostrophic Numerical Forecasts of Hurricane Movement with the Barotropic Steering Model," Journal of Meteorology, vol. 16, No. 4, Aug. 1959, pp. 371-384.
3. G. K. Morikawa, "Geostrophic Vortex Motion," Journal of Meteorology, vol. 17, No. 2, Apr. 1960, pp. 148-158.

AN IMPROVED NWP MODEL FOR FORECASTING THE PATHS OF TROPICAL CYCLONES

(Condensed Version)

Lloyd W. Vanderman, Major USAF
Joint Numerical Weather Prediction Unit, Suitland, Md.

An improved numerical prediction model for forecasting the paths of hurricanes and typhoons is presented. The barotropic flow is assumed as the steering flow for the tropical cyclone. The tropical cyclone is eliminated from the initial height analysis and a steering wind, determined by the recent past movement of the cyclone, is analyzed in its region. The tropical cyclone is then represented by a constant circular vortex stream described in terms of the cyclone's eye radius, maximum wind speed, and outside mean radius which are available from reconnaissance and other data and analyses. The equation for the vortex stream is:

$$\psi_1 = \frac{8}{3} v_m R_o^{5/8} [r^{3/8} - R^{3/8}], \qquad R_o \leq r \leq R; \tag{1a}$$

$$\psi_2 = \frac{v_m}{2 R_o} [r^2 - R_o^2] + \psi_1 (r = R_o), \qquad 0 \leq r \leq R_o; \tag{1b}$$

in which; v_m is the maximum wind speed of the cyclone; R_o is the eye radius of the cyclone; R is the mean outside radius of the cyclone circulation; r is radius distance from the vortex center. Equation (1a) is for a $C = vr^{5/8}$ vortex between the eye radius and the outside radius and equation (1b) is for a $c = vr^{-1}$ vortex for the region of the eye. v_m is assigned to the edge of the eye, $\psi_1 = 0$ at $r = R$, and $\psi_2 = \psi_1$ at $r = R_o$. Figure 1 shows wind speed and stream curves, representing a typical hurricane with respect to values of v_m, R_o, and R, for several wind speed profiles of the vortex in the region between the eye radius and the outside radius. To insure that the vortex is well defined around its center, R, the outside radius, is greater than $\sqrt{10/2}$ grid lengths (See fig. 2) so that eight or more grid point values other than zero always represent it. A grid length is 381 km. at 60°, the true latitude of the polar sterographic map projection used.

The modified barotropic forecast equation employed is:

$$(\nabla^2 - K\bar{\eta}) \frac{\partial \bar{\psi}}{\partial t} = J(\bar{\eta}, \bar{\psi} + \psi) + \bar{\eta} G \tag{2}$$

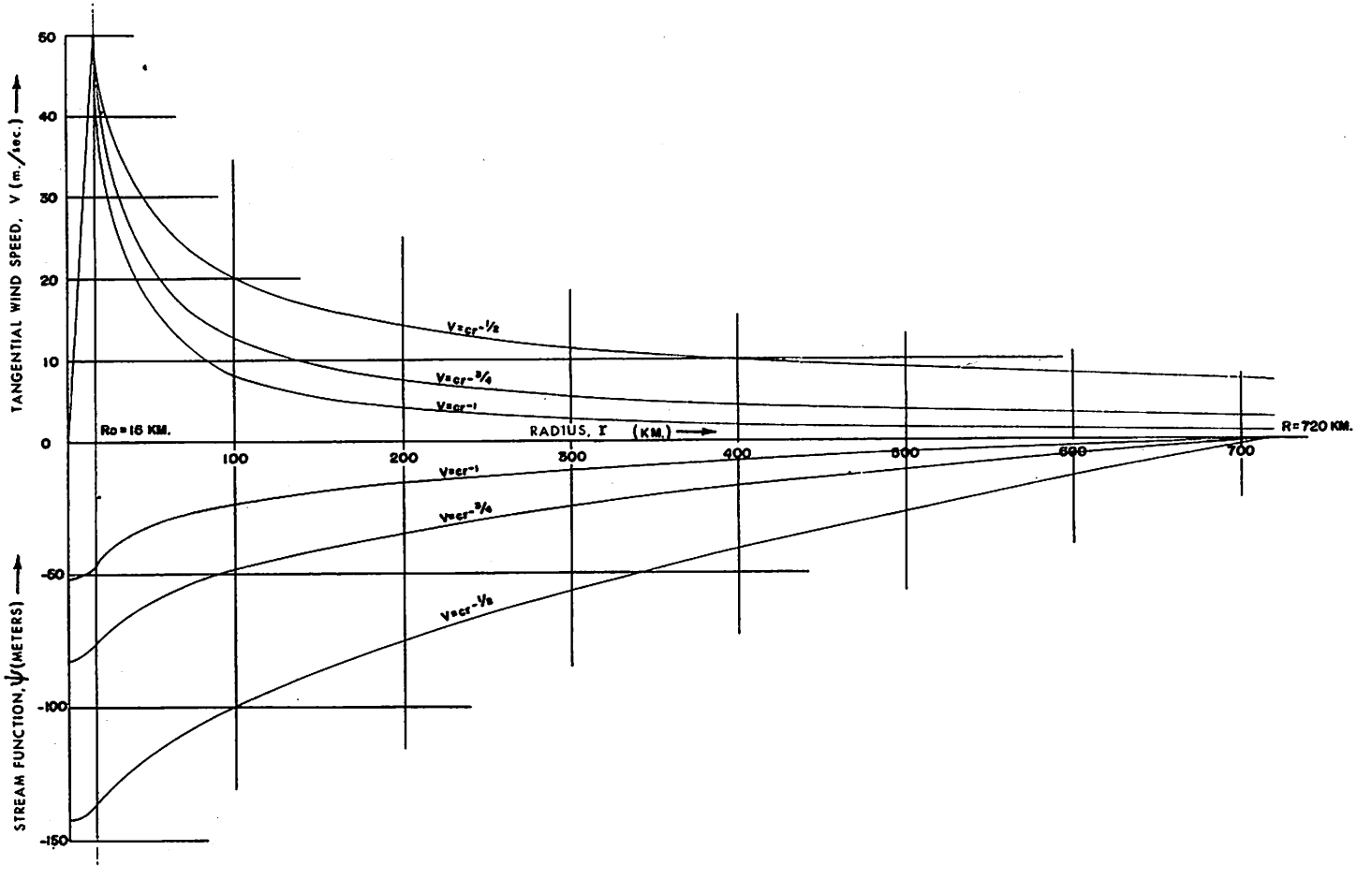

Figure 1. - Wind speed and stream function curves of the several definitions of wind speed for the region outside the vortex eye. Maximum speed 50 m.p.s., radius of the eye 16 km.; outside radius 720 km.

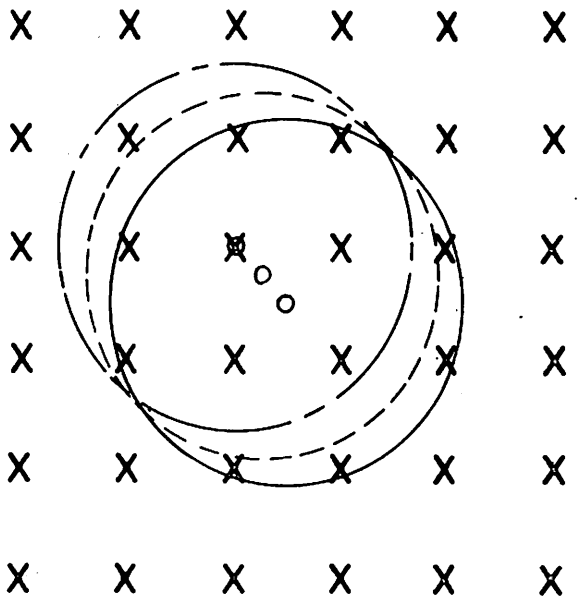

Figure 2. - Grid representation of the vortex with 8 or more grid point stream values. Outside radius $R > \sqrt{10}/2$ grid lengths.

in which t is time; K is a constant; $\bar{\psi}$ is the barotropic steering stream; $\bar{\eta}$ is the absolute vorticity of the barotropic steering stream; ψ is the vortex stream, and $\bar{\eta}$ G is a combined mountain and friction term. Two terms, apparently missing from the advection Jacobian, are $J(\zeta, \psi)$, the advection of the relative vorticity of the vortex with the vortex flow, which is equivalent to zero since the vortex is steady and circular, and $J(\zeta, \bar{\psi})$. The latter term is accounted for by mechanically moving the vortex stream with its center point which is tracked in the barotropic steering flow thereby complementing the barotropic forecast equation (2).

Figure 3 shows several forecasts for different wind speed profiles and the same values of v_m, R_o, and R. A point track in the barotropic steering flow, with no vortex, is included for comparison. Figure 4 shows two forecasts for the definition $c = vr^{5/8}$ between the eye and the outside radius. One forecast employed the 500-mb. barotropic steering flow and the other a vertically weighted mean barotropic flow. This forecasting model seems to be more sensitive to the wind speed profile employed for the vortex than to the values of v_m, R_o, and R. The best average wind speed profile for the vortex appears to be $c = vr^{5/8}$ in the region $R_o \leq r \leq R$.

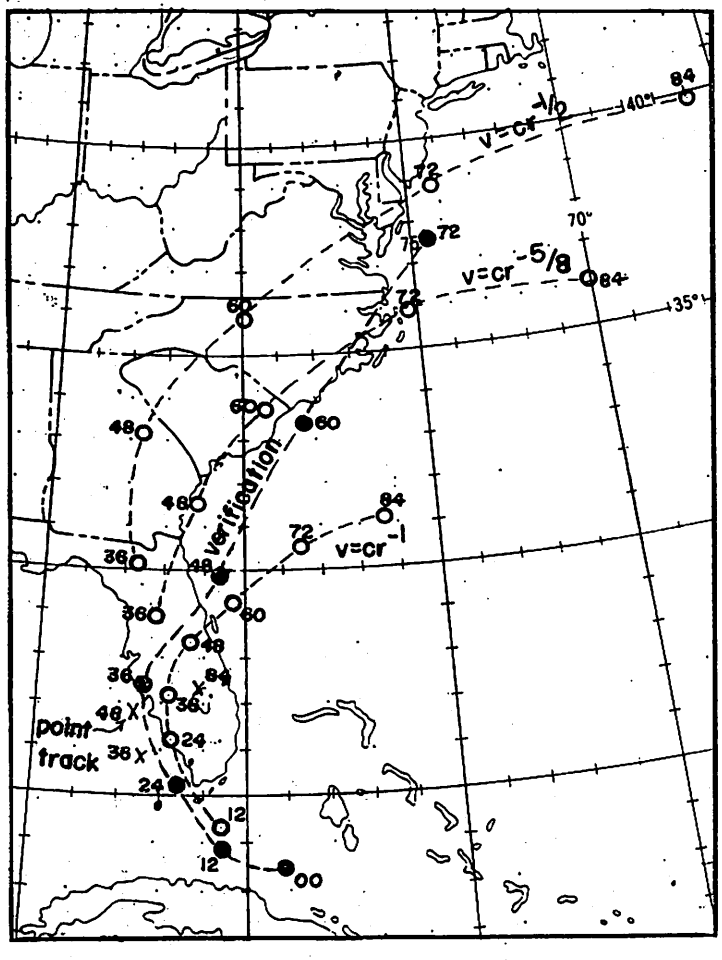

Figure 3. - Forecasts for hurricane Donna from 1200 GMT Sept. 9, 1960. Solid dots, actual track; open circles, forecast tracks; x's, point track.

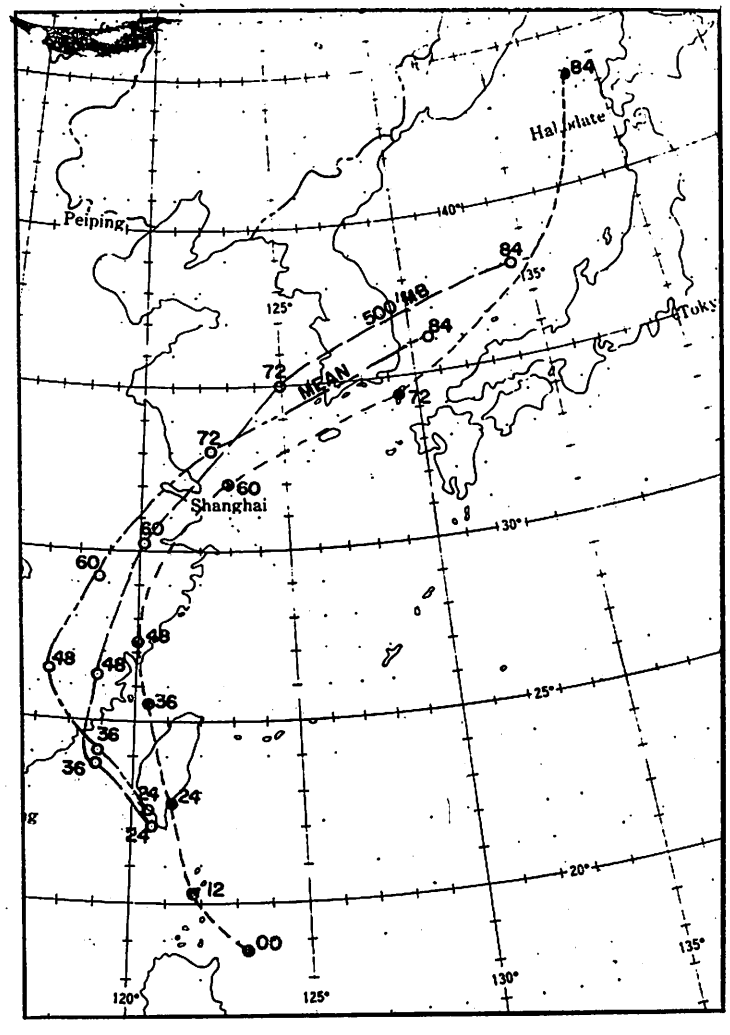

Figure 4. - Forecasts for typhoon Betty from 1200 GMT, May 25, 1961. Solid dots, actual track; open circles, forecast tracks using $v = cr^{-5/8}$.

PREDICTION OF TWELVE, TWENTY-FOUR, AND THIRTY-SIX HOUR DISPLACEMENT OF HURRICANES BY STATISTICAL METHODS

(Extended Abstract)

Keith W. Veigas
Travelers Research Center, Inc., Hartford, Conn.

INTRODUCTION

The development of statistically-derived objective procedures for the prediction of hurricane movement has been the object of a series of extensive experiments carried out during the past four years both by the Travelers Research Center (Veigas et al. [3]) and at AROWA (Riehl, et al. [2]). In these experiments the statistical analyses were based, in general, on various regression techniques, and the prediction problem was formulated in terms of a moving coordinate system - i.e., parameters were measured at positions fixed with respect to the center of the hurricane rather than at positions fixed with respect to the earth.

The encouraging measure of success achieved in these early experiments for predicting the 24-hr. displacement of hurricanes suggested the possibility of extending the analyses to prediction of 12- and 36-hr. displacements. The availability of a greatly-improved set of data (gathered during the post-war years and including upper-air observations) added impetus to the undertaking of such a study, for these data would not only lead to a reasonable extension of the forecast time interval but also would permit a direct re-evaluation of the earlier 24-hour experiments.

With these objectives in mind, a joint project was established between the United States Weather Bureau and the Travelers Research Center. The primary concern of the project was the development and testing of a new set of 12-, 24-, and 36-hr. statistical prediction equations with the analysis to be based on the best set of hurricane observations currently available.

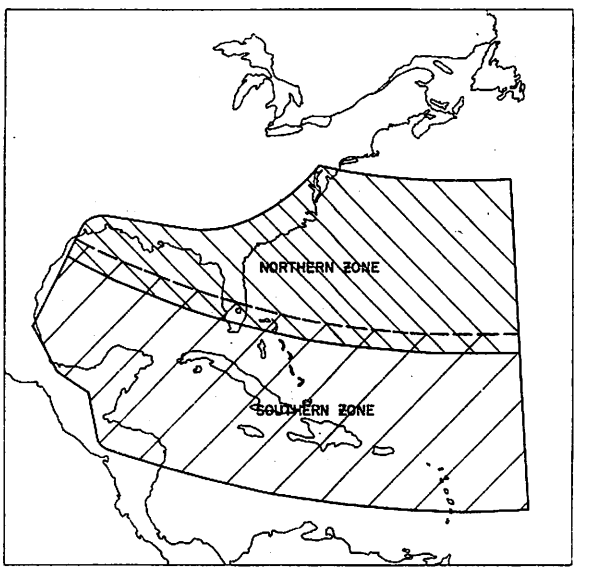

Figure 1. - Hurricane areas, southern and northern zones.

RESULTS - DEPENDENT DATA

The screening regression procedure (Miller [1]) was used to derive prediction equations for the east-west and north-south components of the 12-, 24-, and 36-hr. displacement of hurricanes in both the southern and northern zones (see fig. 1). All the necessary computations were carried out by the IBM 704

Table 1. - Sample size and number of possible predictors: the southern zone and the northern zone.

Zone	Sample size	Number of possible predictors
Southern	129 cases	99 (sea level predictors)
Northern	150 cases	154 (sea level and 500-mb. predictors)

Table 2. - Summary of results, dependent data, southern zone.

Sample size	Forecast interval	RMSE (n. mi.)		
		N-S component	E-W component	Vector
129	12-hr.	33	33	47
129	24-hr.	69	67	96
129	36-hr.	118	110	162

Table 3. - Summary of results, dependent data, northern zone.

Sample size	Forecast interval	RMSE (n. mi.)		
		N-S component	E-W component	Vector
150	12-hr.	35	36	51
150	24-hr.	78	77	110
150	36-hr.	115	123	169

The sample size and the number of predictors used are summarized in table 1.

A summary of the southern zone dependent data results, in terms of the RMSE for each component and for the total vector change is given in table 2. These results indicate that some improvement may have been achieved over the results reported in 1959 [3]. For example, the 24-hr. RMSE in this study was 96 n. mi., compared with 120 n. mi. in the 1959 experiments. The validity of this improvement, of course, must be checked with independent data.

A summary of the dependent data results for the northern zone, in terms of RMSE for each component and for the total vector change, is given in table 3. The northern zone results (as did the southern zone) suggested some improvement over the earlier studies. For example, the 24-hr. RMSE was 110 n.mi. compared with 180 n.mi. in the 1959 experiment. Again, of course, the validity of any improvement must be tested with independent data.

Table 4. - Summary of operational forecasts for hurricane Donna.

Number of forecasts	Forecast interval	Vector RMSE (n. mi.)
5	12-hr.	45
11	24-hr.	114
11	36-hr.	190

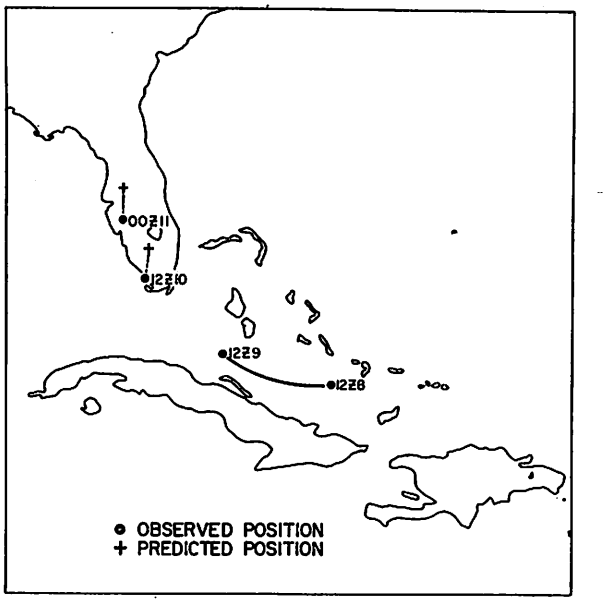

Figure 2. - Forecast and observed tracks for hurricane Donna 1200 GMT, September 9, 1960.

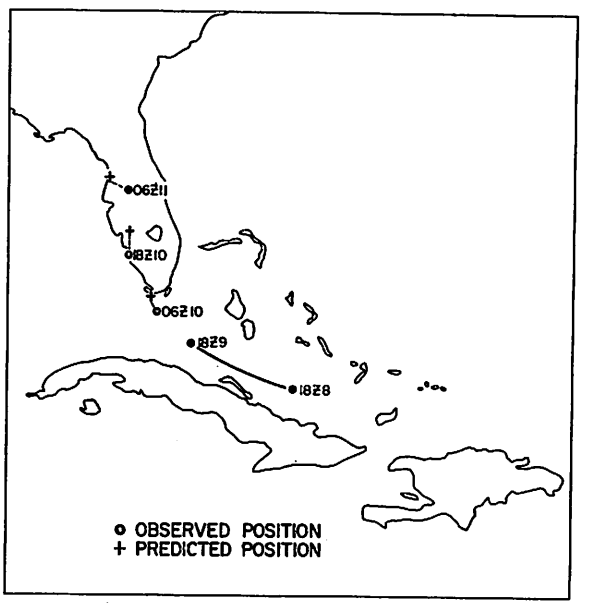

Figure 3. - Forecast and observed tracks for hurricane Donna 1800 GMT, September 9, 1960.

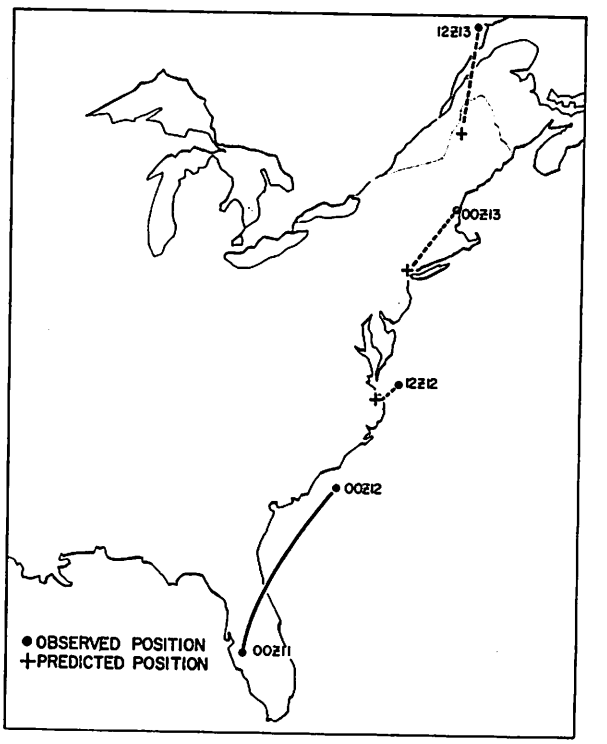

Figure 4. - Forecast and observed tracks for hurricane Donna 0000 GMT, September 12, 1960.

RESULTS - INDEPENDENT DATA

The author was fortunate to be in Miami in September 1960 when hurricane Donna was threatening the Caribbean and the eastern portions of the United States. This provided the opportunity to prepare several forecasts of Donna's displacement under operational conditions. A summary of the results of these operational forecasts is given in table 4. In all, five 12-hr. forecasts, eleven 24-hr. forecasts, and eleven 36-hr. forecasts were prepared. The vector RMSE's obtained for this small but independent sample suffered only minor shrinkage when compared with the RMSE's of the dependent data. For example, the RMSE OF 114 n.mi. for the eleven 24-hr. forecasts compares very favorably with the RMSE's of 96 and 110 n. mi. obtained with the southern and northern zone dependent data, respectively.

Three forecasted and observed tracks for Donna are illustrated in figures 2, 3, and 4. In the 24-hr. period prior to 1200 GMT, September 9, hurricane Donna had been moving in a westerly direction parallel to the northern coast of Cuba. At 1200 GMT, forecasts for 24-hr. and 36-hr. intervals were made, both of which indicated a tendency for the storm to recurve (see fig. 2). Hurricane Donna did in fact recurve, and the vector error for both the 24-hr. and the 36-hr. forecasts was only 60 n. mi.

Six hours later, at 1800 GMT, September 9, 12-, 24-, and 36-hr. forecasts were prepared (see fig. 3). Again the change in direction of motion was correctly forecasted. The vector errors for the 12-, 24-, and 36-hr. forecasts were only 30, 48, and 60 n.mi. respectively.

Donna continued to move up the east coast and passed into the northern zone. The northern zone 12-, 24-, and 36-hr. forecasts computed at 0000 GMT September 12 are shown in figure 4. Despite the fact that in this case the equations failed to account for all of the storm's accelerated motion and resulted in rather large forecast errors of 60, 180, and 252 n.mi. for the three forecast intervals respectively, the forecasted track was notably close to the subsequently observed track.

REFERENCES

1. R. G. Miller, "A Statistical Procedure for Screening Predictors in Multiple Regression," Studies in Statistical Weather Prediction, AFCRC-TR-58-272, The Travelers Weather Research Center, Final Report on Contract No. AF19 (604)-1590, Dec. 1958, pp. 86-95.
2. H. Riehl, W. H. Haggard, and W.R. Sanborn, "On the Prediction of 24-Hour Hurricane Movement," Journal of Meteorology, vol. 13, No. 5, Oct. 1956, pp. 415-420.
3. K. W. Veigas, R. G. Miller, and G. M. Howe, "Probabilistic Prediction of Hurricane Movements by Synoptic Climatology," Occasional Papers in Meteorology, No. 2, Travelers Weather Research Center, 1959, 54 pp.

THREE SETS OF REGRESSION EQUATIONS TO FORECAST THE MOVEMENTS AND SURFACE PRESSURES OF TYPHOONS

H. Arakawa
Meteorological Research Institute, Tokyo, Japan

INTRODUCTION

Forecasting the tracks and the intensities of typhoons is a very important problem in Japan, for the estimated annual mean damage attained some 2/3 billion dollars after the 1946-1958 census. Although synoptic forecasters can predict the movement of typhoons with moderate skill, there exists a need for more accurate forecasts. Recent advances in numerical weather predictions provide unique forecasting techniques that seem to be very promising. Another promising alternative is the statistical forecasting of the movement of hurricanes proposed by Veigas and Miller in 1958. The present author intends to present summaries of his statistical study on the movements and the central surface pressures of typhoons by means of the Veigas-Miller screening procedure. This study is to be classified into three categories as follows:

1. REGRESSION EQUATIONS FOR THE MOVEMENT AND THE CENTRAL SURFACE PRESSURE OF TYPHOONS SITUATED IN THE AREA 120°E.- 180°E., 20°N.- 34°N.

Almost all typhoons which hit Japan proper advance through the area (120° E.-180°E., 20°-34°N.) shown in figure 1. To obtain the pressure patterns relative to the typhoon center, the author took the grid points provided by 5-degree east latitude and 5-degree north latitude intersections. Eighty-four grid point pressures were read from the surface weather map to give the pressure pattern relative to each typhoon center, as shown by figure 2.

Using daily weather maps covering 11-year periods (1949-1959), the author found the number of typhoon days (shown in table 1) and stratified these cases by time of day and by months. Here tropical storms are also included in the data sample.

The number of possible predictors total 89 and are as follows:

$x_1 \ldots\ldots x_{84}$: surface pressure values at chart time ($x_{46} = p_o$)

λ_o : east longitude at chart time

ϕ_o : north latitude at chart time

λ_{-24} : east longitude 24 hours prior to chart time

ϕ_{-24} : north latitude 24 hours prior to chart time

p_{-24} : central pressure 24 hours prior to chart time

The predictands are:

$\lambda_{24)_{pred.}}$: east longitude 24 hours after the chart time

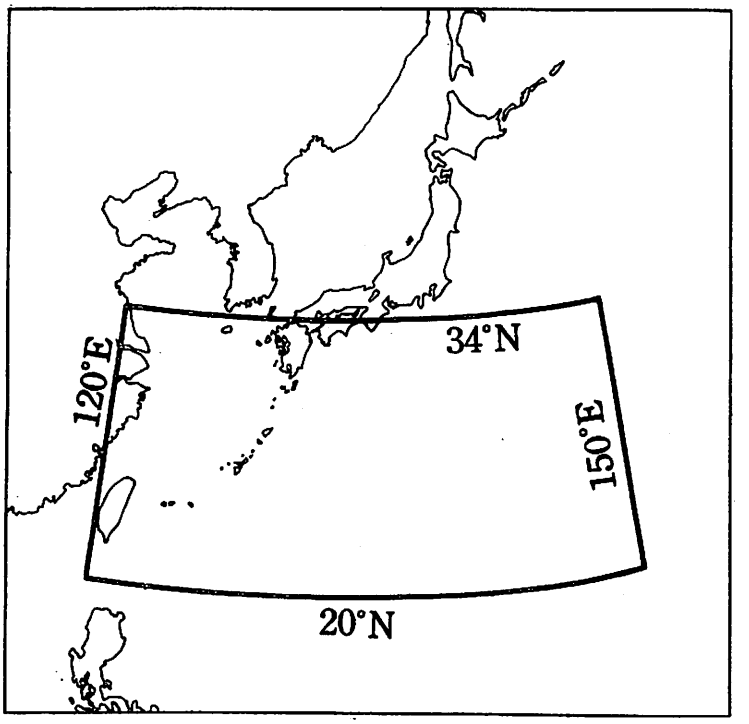

Figure 1. - If the current location of the storm center was in the zone outlined, 84 surface pressure values were read at the points shown in figure 2.

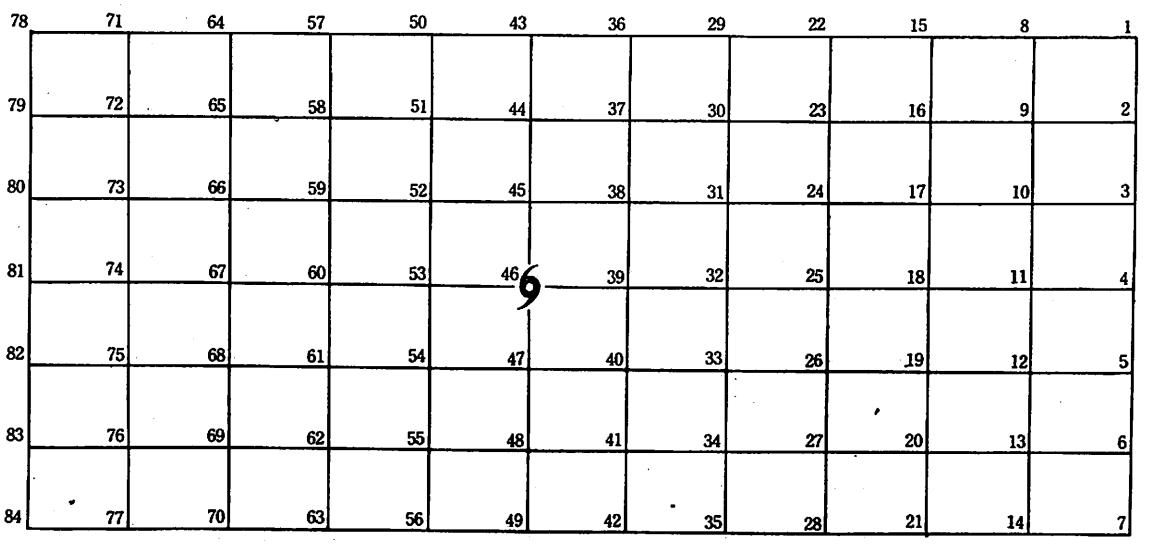

Figure 2. - The 5° grid used for reading surface pressures. Center of grid was placed at nearest 1° point to center of storm and pressures were read at the numbered intersections.

Table 1. - Number of tropical storm and typhoon days within the zone of figure 1 during the years 1949-1959.

	Aug.	Sept.	Oct.	Nov.	Dec.	Jan.	Feb.	Mar.	Apr.	May	June	July
0300 I	144	119	61	42	13	4	—	—	10	7	21	92
						250						
1500 I	140	126	58	42	9	5	—	—	11	8	24	90
						247						

$\phi_{24})_{pred.}$: north latitude 24 hours after the chart time

$p_{24})_{pred.}$: central pressure 24 hours after the chart time

Seven sets of the regression equations (table 2) were computed by the IBM 704. P.R. stands for the percentage reduction of variance.

Table 2. - Regression equations based on surface data (all tropical cyclones).

For July (chart time 0300 I)

$\lambda_{24})_{pred.} = -276.3 + 1.4833\lambda_0 - 0.5973\lambda_{-24} - 0.1236X_1 + 0.3622X_{\cdot} + 0.3242X_{\cdot} - 0.2717X_{\cdot}$, P.R.=93.9 %

$\phi_{24})_{pred.} = +219.9 + 1.4798\phi_0 - 0.5118\phi_{-24} - 0.2340X_{\cdot} + 0.2391X_{\cdot} - 0.4956X_{\cdot} + 0.2731X_{\cdot}$, P.R.=89.9 %

$p_{24})_{pred.} = -1523.8 + 1.0105p_0 - 0.3539p_{-24} + 0.7173\phi_0 + 0.9589X_{\cdot} - 1.0234X_{\cdot} + 1.8877X_{\cdot}$, P.R.=85.0 %

For August (chart time 0300 I)

$\lambda_{24})_{pred.} = -316.7 + 1.5586\lambda_0 - 0.6123\lambda_{-24} + 0.1881\phi_0 + 0.1620X_{\cdot} - 0.1390X_{\cdot} + 0.2937X_{\cdot}$, P.R.=95.5 %

$\phi_{24})_{pred.} = +14.6 + 1.7323\phi_0 - 0.6183\phi_{-24} + 0.1312X_{\cdot} - 0.0998X_{\cdot} - 0.1806X_{\cdot} + 0.1329X_{\cdot}$, P.R.=86.2 %

$p_{24})_{pred.} = +874.1 + 0.6576p_0 + 0.5581\phi_0 + 1.5124X_{\cdot} - 0.8831X_{\cdot} - 2.2906X_{\cdot} + 1.1162X_{\cdot}$, P.R.=78.3 %

For August (chart time 1500 I)

$\lambda_{24})_{pred.} = -541.3 + 1.3098\lambda_0 - 0.3330\lambda_{-24} + 0.4646X_{\cdot} - 0.0992X_{\cdot} + 0.3825X_{\cdot} - 0.2086X_{\cdot}$, P.R.=93.1 %

$\phi_{24})_{pred.} = -209.4 + 1.6726\phi_0 - 0.6339\phi_{-24} + 0.1155X_{\cdot} - 0.3007X_{\cdot} + 0.2195X_{\cdot} + 0.1729X_{\cdot}$, P.R.=88.2 %

$p_{24})_{pred.} = +3273.5 + 0.5652p_0 + 1.4361\phi_0 - 2.4604X_{\cdot} + 1.5315X_{\cdot} - 1.2413X_{\cdot} - 0.6845X_{\cdot}$, P.R.=76.8 %

For September (chart time 0300 I)

$\lambda_{24})_{pred.} = -348.0 + 1.7476\lambda_0 - 0.8224\lambda_{-24} + 0.7999\phi_0 - 0.5708\phi_{-24} + 0.4760X_{\cdot} - 0.1262X_{\cdot}$, P.R.=94.5 %

$\phi_{24})_{pred.} = -375.6 + 2.1619\phi_0 - 0.9940\phi_{-24} - 0.2527X_{\cdot} + 0.2326X_{\cdot} + 0.2091X_{\cdot} + 0.1801X_{\cdot}$, P.R.=95.3 %

$p_{24})_{pred.} = -669.5 + 0.8388p_0 - 0.2225p_{-24} + 1.3751\phi_0 - 0.6306\lambda_{-24} + 2.5399X_{\cdot} - 1.4545X_{\cdot}$, P.R.=70.7 %

For September (chart time 1500 I)

$\lambda_{24})_{pred.} = -66.9 + 1.6243\lambda_0 - 0.6736\lambda_{-24} + 0.7432\phi_0 - 0.4778\phi_{-24} - 0.2977X_{\cdot} + 0.3655X_{\cdot}$, P.R.=94.9 %

$\phi_{24})_{pred.} = -200.0 + 1.7050\phi_0 - 0.5798\phi_{-24} - 0.3738X_{\cdot} + 0.2615X_{\cdot} + 0.3094X_{\cdot}$, P.R.=90.4 %

$p_{24})_{pred.} = -416.5 + 0.7966p_0 - 0.1391p_{-24} + 3.2742\phi_0 - 0.5289\lambda - 2.2213\phi_{-24} + 0.7838X_{\cdot}$, P.R.=73.3 %

For October ~ July (chart time 0300 I)

$\lambda_{24})_{pred.} = -614.2 + 1.4185\lambda_0 - 0.6007\lambda_{-24} + 0.5920\phi_0 - 0.4430\phi_{-24} + 0.4888X_{\cdot} + 0.3666X_{\cdot} - 0.2253X_{\cdot}$, P.R.=90.8 %

$\phi_{24})_{pred.} = -146.4 + 1.5589\phi_0 - 0.6309\phi_{-24} - 0.2879X_{\cdot} + 0.1678X_{\cdot} + 0.0686X_{\cdot} + 0.1502X_{\cdot} + 0.1387X_{\cdot} - 0.0902X_{\cdot}$, P.R.=85.0 %

$p_{24})_{pred.} = -149.3 + 0.9228p_0 - 0.2971p_{-24} + 1.4303\phi_0 - 0.8196\phi_{-24} + 0.7493X_{\cdot} + 0.7428X_{\cdot} - 0.5448X_{\cdot} - 0.4499X_{\cdot}$, P.R.=77.7 %

For October ~ July (chart time 1500 I)

$\lambda_{24})_{pred.} = -708.1 + 1.5328\lambda_0 - 0.7014\lambda_{-24} + 0.3516X_{\cdot} + 0.5713X_{\cdot} - 0.2875X_{\cdot} + 0.0898X_{\cdot}$, P.R.=88.9 %

$\phi_{24})_{pred.} = -39.2 + 1.5673\phi_0 - 0.6772\phi_{-24} - 0.1219X_{\cdot} + 0.2094X_{\cdot} + 0.1067X_{\cdot} - 0.0672X_{\cdot} - 0.0844X_{\cdot}$, P.R.=84.0 %

$p_{24})_{pred.} = -596.2 + 0.8094p_0 - 0.1753p_{-24} + 1.6671\phi_0 - 1.1828\phi_{-24} - 0.2186\lambda_{-24} + 0.9655X_{\cdot}$, P.R.=74.7 %

An operational independent test is now under way by the staff of the Forecasting Division, Japan Meteorological Agency, using the data of the current typhoon season, 1961.

2. REGRESSION EQUATIONS FOR THE MOVEMENT AND THE CENTRAL SURFACE PRESSURE OF TYPHOONS IN THE WESTERN NORTH PACIFIC

Typhoons located in the whole western North Pacific were tested. Here the area discussed is confined to the North Pacific from 0°N. to 34°N. and from the coasts of China, Formosa and the Philippines to 180°E., excluding the southern China Sea. The pressure pattern relative to the typhoon center was expressed by the surface pressure values at 91 grid points as shown in figure 3.

Regression equations were derived for the full-grown typhoons which occurred in the 5-year period 1956-1960. The numbers of typhoon data samples were: 1956, 55; 1957, 88; 1958, 91; 1959, 71; 1960, 69. The total number was 374. (Total number of data samples in IBM card form was 3366.) The set of predictors was 99, as follows:

$x_1 \cdots\cdots x_{91}$: surface pressure values at chart time ($x_{47} = p_o$)

λ_{-12} : east longitude 12 hours prior to chart time

ϕ_{-12} : north latitude 12 hours prior to chart time

p_{-12} : central surface pressure 12 hours prior to chart time, and

λ_o, ϕ_o, λ_{-24}, ϕ_{-24} and p_{-24} have the same meaning as in section 1, respectively. The set of predictands is as follows:

$\lambda_{12)_{pred.}}$: east longitude 12 hours after chart time

$\phi_{12)_{pred.}}$: north latitude 12 hours after chart time

$p_{12)_{pred.}}$: central surface pressure 12 hours after chart time

$\lambda_{48)_{pred.}}$: east longitude 48 hours after chart time

$\phi_{48)_{pred.}}$: north latitude 48 hours after chart time

$p_{48)_{pred.}}$: central surface pressure 48 hours after chart time

The set of regression equations computed by the IBM 704 is shown in table 3. The independent test of these sets of regression equations is underway by Prof. C.S. Ramage, University of Hawaii.

3. REGRESSION EQUATIONS IN TERMS OF THE SURFACE MAP AND THE 700-MB. MAP

The process of obtaining the forecasting regression equations is almost the same as stated in section 2 except the pressure pattern was expressed as the combination of the surface map and the 700-mb. map. The surface grid points relative to the full-grown typhoon center are 91 as stated above, while 700-mb. height values were read off at the grid points 92 to 175. The number of predictors was 183. i.e.:

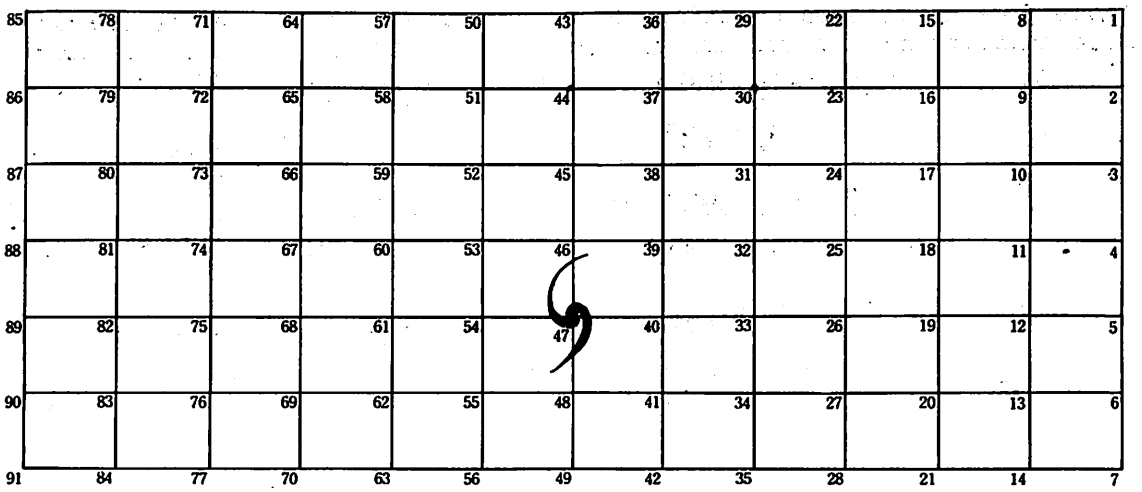

Figure 3. - Grid used for reading surface pressures (typhoons only).

x_1 ..... x_{91} : 91 surface pressure values at chart time

h_{92} .... h_{175} : 84 700-mb. height values at chart time and eight more predictors, λ_o, ϕ_o, λ_{-12}, ϕ_{-12}, p_{-12}, λ_{-24}, ϕ_{-24}, p_{-24}. The grid points relative to the center of a full-grown typhoon are illustrated in figure 4.

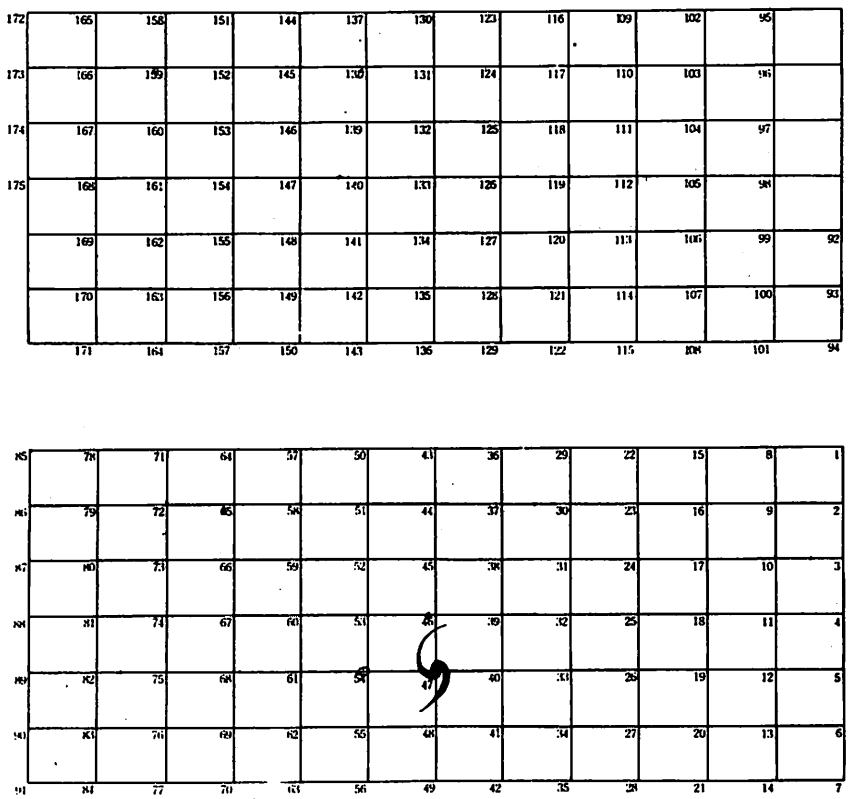

Figure 4. - Grids used for reading surface pressures (bottom) and 700-mb. heights (top).

Table 3. - Regression equations based on surface data (typhoon only).

$$\lambda_{12})_{pred.} = -242.3 + 1.3669\lambda_0 - 0.3951\lambda_{-24} + 0.0682X_{89} + 0.1752X_{13} - 0.0572X_{45} + 0.0575X_{75} \qquad P.R. = 99.2\%$$

$$\Phi_{12})_{pred.} = -57.3 + 1.5595\Phi_0 - 0.3833\Phi_{-12} - 0.1734\Phi_{-24} + 0.0553X_{89} - 0.0733X_{53} + 0.0750X_{26} \qquad P.R. = 98.9\%$$

$$p_{12})_{pred.} = -775.4 + 1.0978p_0 - 0.1470p_{-12} - 0.1457p_{-24} - 0.1046\lambda_{-24} + 0.7267X_6 + 0.2416X_{40} \qquad P.R. = 86.4\%$$

$$\lambda_{24})_{pred.} = -589.6 + 1.6812\lambda_0 - 0.7516\lambda_{-24} + 0.7209\Phi_0 - 0.6155\Phi_{-12} + 0.2443X_{89} + 0.3469X_{21} \qquad P.R. = 97.1\%$$

$$\Phi_{24})_{pred.} = -112.5 + 2.2797\Phi_0 - 1.2540\Phi_{-12} + 0.1284X_{90} - 0.0692X_{52} + 0.1821X_{26} - 0.1293X_{39} \qquad P.R. = 95.9\%$$

$$p_{24})_{pred.} = -1581.9 + 0.8613p_0 - 0.3225p_{-24} - 0.3547\lambda_{-24} + 0.9063X_6 + 1.0163X_{46} - 0.9921X_{63} + 1.1259X_{21} \qquad P.R. = 61.3\%$$

$$\lambda_{48})_{pred.} = -1037.6 + 1.8948\lambda_0 - 1.0458\lambda_{-24} + 2.1311\Phi_0 - 1.7983\Phi_{-12} + 0.6461X_{13} + 0.6245X_{89} - 0.2289X_{17} \qquad P.R. = 89.2\%$$

$$\Phi_{48})_{pred.} = -106.6 + 2.8977\Phi_0 - 1.8073\Phi_{-12} - 0.5396X_{46} + 0.2914X_{40} + 0.2132X_{90} + 0.2034X_{25} - 0.0613X_{50} \qquad P.R. = 88.3\%$$

$$p_{48})_{pred.} = -1790.4 + 0\ 6493p_0 - 0.5141p_{-12} - 0.6288\lambda_{-24} + 2.6177X_6 + 1.4297X_{46} - 1.3597X_{63} \qquad P.R. = 40.7\%$$

The number of typhoon data samples was: 1957,88; 1958, 91; 1959, 71; 1960, 69, and the total number was 319. (Total number of data sample in IBM card form was 5104.)

Regression equations computed for 12 hours, 24 hours and 48 hours after chart time are given in table 4, where $H_o = h_{134}$.

Table 4. - Regression equations based on surface and 700-mb. data (typhoons only).

$$\lambda_{12})_{pred.} = -32.4 + 1.7792\lambda_0 - 0.7922\lambda_{-12} - 0.0076_4\, h_{124} + 0.0576 X_{89}, \quad P.R. = 99.5\%$$

$$\Phi_{12})_{pred.} = -33.0 + 1.7710\Phi_0 - 0.7770\Phi_{-12} - 0.0076_8\, h_{147} + 0.0568 X_{26}, \quad P.R. = 99.1\%$$

$$p_{12})_{pred.} = -117.8 + 0.6989 p_0 - 0.2245 p_{-24} + 0.6052 X_6 + 0.0385_4\, H_0 - 0.0301_1\, h_{132}, \quad P.R. = 86.9\%$$

$$\lambda_{24})_{pred.} = -443.2 + 2.2714\lambda_0 - 1.3341\lambda_{-12} - 0.0130_3\, h_{131} - 0.0131_9\, h_{98} + 0.1648 X_{89} + 0.3640 X_{13}, \quad P.R. = 98.0\%$$

$$\Phi_{24})_{pred.} = -40.2 + 2.2424\Phi_0 - 1.2208\Phi_{-12} - 0.0255_2\, h_{147} + 0.0167_9\, h_{113} + 0.0117_9\, h_{174} + 0.0099_5\, h_{170}, \quad P.R. = 97.2\%$$

$$p_{24})_{pred.} = -172.6 + 0.0949_7\, H_0 - 0.3076 p_{-24} - 0.3304\lambda_{-24} - 0.0384_1\, h_{116} + 1.5687 X_{14} + 1.1770 X_{40} - 1.4217 X_{63}, \quad P.R. = 63.5\%$$

$$\lambda_{48})_{pred.} = -514.7 + 2.9247\lambda_0 - 2.0600\lambda_{-12} + 1.7773\Phi_0 - 1.5491\Phi_{-12} - 0.0237_8\, h_{124} + 0.0662_4\, h_{107} + 0.3896 X_{88}, \quad P.R. = 90.9\%$$

$$\Phi_{48})_{pred.} = +32.5 + 2.6899\Phi_0 - 1.5568\Phi_{-12} - 0.1904 X_{45} + 0.0376_3\, h_{170} + 0.0362_1\, h_{112} - 0.0441_3\, h_{147} + 0.0216_6\, h_{174}, \quad P.R. = 90.2\%$$

$$p_{48})_{pred.} = -1403.7 + 0.0700_6\, H_0 - 0.4249 p_{-12} - 0.5846\lambda_{-24} + 2.4512 X_6 - 0.0791_4\, h_{130} + 0.1376_5\, h_{126}, \quad P.R. = 43.7\%$$

So far, these regression equations show much promise. Data from the 700-mb. chart seem to give prognostic equations with a higher reliability as shown in terms of the percentage reduction of variance.

In conclusion, it should be remarked that values for longitude and latitude are expressed in degrees and tenths, those for surface pressure in millibars, and those for height of the 700-mb. surface in meters, throughout this paper.

List of Those Attending the Conference

Dr. M. A. Alaka	USWB, Miami, Fla.
Dr. H. Arakawa	Meteorological Research Institute, Tokyo, Japan
E. A. Amman	USWB, Cocoa Beach, Fla.
T. M. Anderson	USAF, Silver Spring, Md.
A. B. Arnett	USWB, Miami, Fla.
R. E. Bailey	United Aircraft Corp., Wethersfield, Conn.
J. C. Ballard	USWB, Altanta, Ga.
E. M. Ballenzweig	Fleet Weather Facility, USN, Norfolk, Va.
J. M. Batista	Aeronautica Civil, Bogota, Colombia
Dr. L. Berkofsky	AF Cambridge Research Laboratory, Bedford, Mass.
E. G. Bice	USWB, Brownsville, Tex.
F. G. Boucher	Jersey Production Research, Tulsa, Okla.
R. M. Brown	Brookhaven National Laboratory Brookhaven, N. Y.
W. F. Brown	USWB, Miami, Fla.
Dr. A. Bruinenberg	Meteorological Service, Curaçao Netherlands Antilles
Lt.Col. R. C. Bundgaard	USAF-AWS, Colorado Springs, Colo.
R. S. Bush	Pan American World Airways, Miami, Fla.
J. B. Cambiaso V.	Dominican Weather Bureau, Ciudad Trujillo, Dominican Republic
Capt. R. F. Caracciolo	Brazilian Air Force, Rio de Janeiro, Brazil
V. Carmichael	USWB, Miami, Fla.
C. B. Carney	USWB, Raleigh, N. C.
R. L. Carrodus	USWB, Miami, Fla.
E. Carson	USWB, Galveston, Tex.
V. M. Castro	Servicio Meteorologico Nacional Tegucigalpa, Honduras
D. C. Chalifour	Barnes Engineering Co., Eau Gallie, Fla.
J. A. Channon	West Indies Meteorological Service, Port of Spain, Trinidad
P. P. Chase	USWB, Miami, Fla.
M. Charbonnier	Service Météorologique, Fort de France, Martinique
F. E. Christensen	USWB, Miami, Fla.
H. W. Church	Sandia Corporation, Albuquerque, N. Mex.
P. F. Clapp	USWB, Washington, D.C.
G. B. Clark	USWB, Miami, Fla.
E. Coen	Servicio Meteorologico, San Jose Costa Rica
L. A. Cohen	New York University, New York N. Y.
S. G. Cohen	Ess Gee Inc., Elmsford, N. Y.
L. G. Collett	Key West, Fla.
Dr. J. A. Colón	USWB, Miami, Fla.
L. F. Conover	USWB, Miami, Fla.
E. V. Copeland'	USWB, Miami, Fla.
Cdr. J. A. Cork, Jr.	Fleet Weather Faciltiy, USN, Miami, Fla.
W. M. Cravens	General Electric Co., Bethesda Md.
G. W. Cry	USWB, Washington, D. C.
J. A. Cummings	USWB, Charleston, S. C.
Miss D. K. Daspit	Tulane University, New Orleans, La.
H. W. Davis	USWB, Miami, Fla.
W. R. Davis	USWB, Miami, Fla.
J. L. Dooley	Atlantic Refining Co.-WTVJ, Miami, Fla.
H. W. Dubach	National Oceanographic Data Center, Washington, D. C.
G. E. Dunn	USWB, Miami, Fla.
J. Dunphy	Raytheon Co., Stow, Mass.
O. E. Edrington	USWB, San Antonio, Tex.
Dr. Mariano A. Estoque	University of Hawaii, Kailua, Hawaii
Dr. A. J. Faller	Woods Hole Oceanographic Institution, Woods Hole, Mass.
R. M. Ferry	USWB, Tampa, Fla.
Dr. H. G. Fortak	The Free University of Berlin, Berlin, Germany
Cdr. A. N. Fowler	Fleet Air Wing 11, USN, Jacksonville, Fla.
N. L. Frank	USWB, Miami, Fla.
H. A. Friedman	USWB, Miami, Fla.
Dr. T. Fujita	University of Chicago, Chicago, Ill.
R. C. Fusco	Ess Gee Inc., Elmsford, N. Y.
R. C. Gentry	USWB, Miami, Fla.
J. J. George	Eastern Air Lines, Atlanta, Ga.
H. P. Gerrish	USWB, Miami, Fla.
Prof. F. Gerritsen	University of Florida, Gainesville, Fla.
H. V. Goodyear	USWB, Washington, D. C.
O. A. Gorden, Jr.	USWB, Miami, Fla.
W. M. Gray	University of Chicago, Chicago, Ill.
A. C. Grunenfelder	USWB, Miami, Fla.
J. R. Gulick	USWB, Miami, Fla.
W. H. Haggard	USWB, Asheville, N. C.
Maj. R. E. Hairston	USAF, Miami, Fla.
D. L. Harris	USWB, Washington, D. C.
R. Harris	General Electric Co., Bethesda Md.
Capt. M. G. Hatch	USAF, Miami, Fla.
H. F. Hawkins	USWB, Miami, Fla.
Prof. S. L. Hess	Florida State University, Tallahassee, Fla.
R. Higgs	USWB, San Juan, Puerto Rico
E. C. Hill, Jr.	USWB, Miami, Fla.
H. W. Hiser	University of Miami, Miami, Fla.
H. M. Hoose	USWB, Miami, Fla.
H. Huber	American Institute of Electrical Engineers, Miami, Fla.
L. F. Hubert	USWB, Washington, D. C.
J. L. Hudnall	USWB, West Palm Beach, Fla.
Prof. T. Ichiye	Florida State University, Tallahassee, Fla.
A. W. Johnson	USWB, Washington, D. C.
N. E. Johnson,	USWB, Honolulu, Hawaii
W. O. Johnson	USWB, Lakeland, Fla.
Prof. C. L. Jordan	Florida State University, Tallahassee, Fla.
R. W. Jones	University of Chicago, Chicago, Ill.
R. C. Jorgensen	Dow Chemical Co., Freeport, Tex.
Dr. A. Kasahara	University of Chicago, Chicago, Ill.
Dr. E. Kessler	Travelers Research Center, Inc., Hartford, Conn.
C. G. Knudsen	USWB, New York, N. Y.
R. H. Kraft	USWB, Miami, Fla.
Dr. H.-L. Kuo	Massachusetts Institute of Technology, Cambridge, Mass.
J. P. Kurtzweil	USWB, Key West, Fla.
Prof. J. Langfelder	University of Florida, Gainesville, Fla.
Prof. N. E. LaSeur	Florida State University, Tallahassee, Fla.
Prof. R. L. Lavoie	University of Hawaii, Honolulu, Hawaii
R. Lee	Meteorological Branch, Department of Transport, Toronto, Canada
R. Leep	WTVT Television, Tampa, Fla.

Dr. H. Lessmann	Meteorological Service El Salvador, San Salvador, El Salvador
Dr. M. G. H. Ligda	Stanford Research Institute, Los Altos, Calif.
Dr. D. K. Lilly	USWB, Washington, D. C.
S. Lichtblau	USWB, New Orleans, La.
Prof. E. F. Low, Jr.	University of Miami, Miami, Fla.
B. J. Lund	Eastern Air Lines, Miami, Fla.
R. W. McCaslin	USWB, Miami, Fla.
L. G. McDonald	Headquarters, Air Weather Service, Scott AFB, Ill.
Dr. T. F. Malone	Travelers Research Center, Inc. Hartford, Conn.
A. M. Marshall	USWB, Miami, Fla.
F. Martinez	Servicio Meteorologico Nacional Tegucigalpa, Honduras
N. A. Matson	USWB, Washington, D. C.
B. I. Miller	USWB, Miami, Fla.
H. Mitra	India Meteorological Service, New Delhi, India
E. F. Mitros	USWB, Miami, Fla.
C. P. Mook	USWB, Washington, D. C.
Mrs. M. H. Moore	USWB,Miami, Fla.
P. L. Moore	USWB, Miami, Fla.
Dr. G. Morikawa	New York University, New York, N. Y.
A. L. Morris	Navy Weather Research Facility, USN, Norfolk, Va.
S. Neumán	USWB, Miami, Fla.
C. J. Neumann	USAF, Homestead AFB, Fla.
Prof. J. E. Newman	Purdue University, Lafayette,Ind.
Dr. H. Newstein	USWB, New York, N. Y.
Lt. V. A. Norduane	Fleet Weather Facility, USN, Miami, Fla.
Dr. Y. Ogura	Massachusetts Institute of Technology, Cambridge, Mass.
Lcdr. T.H.R. O'Neill	Navy Weather Research Facility, USN, Norfolk, Va.
Dr. K. Ooyama	New York University, New York, N. Y.
E. M. Page	USWB, Miami, Fla.
L. G. Pardue	USWB, Miami, Fla.
S. C. Pearce	USWB, Miami, Fla.
Capt. R. V. Pereira	Brazilian Air Force, Rio de Janeiro, Brazil
R. G. Plaster	USWB, Jacksonville, Fla.
Prof. G. W. Platzman	University of Chicago, Chicago, Ill.
N. E. Porter, Jr.	USWB, Miami, Fla.
Dr. W. H. Portig	University of Texas, Austin, Tex.
D. V. Rao	India Meteorological Service, Calcutta, India
C. M. Reber	USWB, Miami, Fla.
A. M. Recht	USWB, Miami, Fla.
I. W. Richardson	USWB, Miami, Fla.
Prof. H. Riehl	Colorado State University, Fort Collins, Colo.
Dr. S. L. Rosenthal	USWB, Miami, Fla.
D. T. Rubsam	USWB, Miami, Fla.
A. C. Rudomanski	Barnes Engineering Co., Stamford, Conn.
D. C. Russell	USWB, Daytona Beach, Fla.
Lt.Col. J. Sadler	USAF, Bedford, Mass.
A. Sadowski	USWB, Washington, D. C.
Prof. F. Sanders	Massachusetts Institute of Technology, Cambridge, Mass.
Dr. T. Saville, Jr.	U.S. Beach Erosion Board, Washington, D. C.
J. Schenck	USWB, Miami, Fla.
R. C. Schmidt	USWB, Washington, D. C.
H. V. Senn	University of Miami, Miami,Fla.
Mrs. R. D. Sherrill	USWB, Miami, Fla.
D. H. Shideler	International Cooperation Administration, Port of Spain, Trinidad
W. Shinners	USWB, Washington, D. C.
R. H. Simpson	USWB, Washington, D. C.
C. L. Smith	USWB, Miami, Fla.
J. W. Smith	USWB, Tallahassee, Fla.
R. Smith	USWB, Apalachicola, Fla.
R. H. Sourbeer	USWB, Miami, Fla.
Prof. J. Spar	New York University, New York, N. Y.
D. K. Speed	United Aircraft Corp. Glastonbury, Conn.
K. C. Spengler	American Meteorological Society, Boston, Mass.
A. L. Sugg	USWB, Miami, Fla.
O. Tenenbaum	USWB, Boston, Mass.
W. L. Thompson	USWB, Fort Worth, Tex.
P. D. Thomas	USWB, Miami, Fla.
W. L. Tilson	USWB, Mobile, Ala.
J. D. Tracy	USWB, Miami, Fla.
Mrs. B. R. True	USWB, Miami, Fla.
C. H. True	USWB, Miami, Fla.
P. F. Twitchell	Melpar, Inc., Watertown, Mass.
B. G. Unda	Servicio Meteorologico Mexicano Mexico City, D. F.
J. I. Valera A.	Servicio Meteorologico Mexicano Mexico City, D. F.
Maj. L. W. Vanderman	USAF-USWB, Washington, D. C.
K. Veigas	Travelers Research Center, Inc., Hartford, Conn.
D. O. Vickers	West Indies Meteorological Service, Nassau, Bahamas
R. J. Waite	USWB, Thomasville, Ga.
F. Wells	USWB, Washington, D. C.
F. D. White	National Science Foundation, Washington, D. C.
Dr. R. M. White	Travelers Research Center, Inc., Hartford, Conn.
V. Wiggert	USWB, Miami, Fla.
C. E. Young	Baltimore Gas and Electric Co., Baltimore, Md.
E. J. Zipser	USWB, Miami, Fla.

USCOMM-WB-DC